Technische Universität München
Zentrum Mathematik

MATHEMATICAL MODELS FOR CELL-CELL COMMUNICATION ON DIFFERENT SCALES

Alexandra Elisabeth Hutzenthaler

Vollständiger Abdruck der von der Fakultät für Mathematik der Technischen Universität München zur Erlangung des akademischen Grades eines

Doktors der Naturwissenschaften (Dr. rer. nat.)

genehmigten Dissertation.

TECHNISCHE UNIVERSITÄT MÜNCHEN
Zentrum Mathematik

MATHEMATICAL MODELS FOR CELL-CELL COMMUNICATION ON DIFFERENT SCALES

Alexandra Elisabeth Hutzenthaler

Vollständiger Abdruck der von der Fakultät für Mathematik der Technischen Universität München zur Erlangung des akademischen Grades eines

Doktors der Naturwissenschaften (Dr. rer. nat.)

genehmigten Dissertation.

Vorsitzender:		Univ.-Prof. Dr. Ruppert Lasser
Prüfer der Dissertation:	1.	Univ.-Prof. Dr. Johannes Müller
	2.	Univ.-Prof. Dr. Martin Brokate
	3.	Prof. Dr. Markus Kirkilionis The University of Warwick, Großbritannien (Schriftliche Beurteilung)

Die Dissertation wurde am 14. Juli 2009 bei der Technischen Universität eingereicht und durch die Fakultät für Mathematik am 27. April 2010 angenommen.

Was dem einzelnen nicht möglich ist, das vermögen viele.

Friedrich Wilhelm Raiffeisen (1818 - 1888)

Zusammenfassung

Die interzelluläre Kommunikation spielt eine zentrale Rolle bei der Optimierung der Aktivität verschiedener, zum Beispiel pathogener, Bakterien. Im Rahmen dieser Arbeit entwickeln und untersuchen wir Modelle, die das Quorum Sensing System, einen gängigen Mechanismus der Zell-Zell-Kommunikation, beschreiben. Zunächst betrachten wir ein intrazelluläres regulatorisches Netzwerk um die Signal-Integration zu untersuchen. Anschließend werden Modelle für Populationsdynamik entwickelt, wobei wir zum einen ein stochastisches Modell für kleine, gleichmäßig verteilte Populationen, und zum anderen ein deterministisches Modell für räumlich angeordnete Populationen betrachten.

Abstract

Intercellular communication is a central optimization strategy for activities of, for example, root colonizing bacteria or pathogenic bacteria. In this PhD thesis we develop and analyze different models for the Quorum Sensing system, a common mechanism for cell-cell communication. First, we build up a model for a intracellular regulatory network to understand the information integration. Subsequently, we investigate the mechanism of Quorum Sensing on the population level. Therefore, on the one hand we state a model for small, homogeneously structured populations, based on a stochastic approach, and on the other hand a deterministic model for spatially structured populations is considered.

Acknowledgement

It is my pleasure to acknowledge the support I got from so many people during the last years. Even though I cannot mention all of them here, I want them to know that I am very thankful for all the help and encouragement I received.

This thesis was carried out at the Helmholtz Zentrum München - German Research Center for Environmental Health, Neuherberg. A special thank goes to Prof. Dr. Rupert Lasser, who gave me the possibility to work at the Institute of Biomathematics and Biometry.

I wish to express my deep gratitude to Prof. Dr. Johannes Müller for the kind introduction into the subject, for proposing this research topic, and for many interesting and helpful discussions.

I want to thank Prof. Dr. Hannes Uecker, Universität Oldenburg, and Dr. Robert Schlicht for the collaboration. I am also much obliged to Prof. Dr. Kirsten Jung and Dr. Nina Stambrau, LMU München, for providing the biological data.

Moreover, I am grateful to my colleagues at the Institute of Biomathematics and Biometry for their support and for the enjoyable company during the last years. Among many others, I want to thank Burkhard Hense, Georg Berschneider, Kristine Ey, Moritz Simon, and Wolfgang Castell.

Last but not least, I am indebted to my parents for their understanding, patience and encouragement when it was most required and to Stefan for his patience and support.

Contents

1. Introduction

Cells can be seen as highly sophisticated entities that process and respond on environmental stimuli. Only if a cell has some information about nutrients, temperature, flow, or more refined parameters like crowdedness and the presence of allies or enemies, it is possible for the cell to act successfully in a heterogeneous and complex ecosystem. One method cells utilize to interact with each other is the so-called Quorum Sensing.

1.1. Quorum Sensing

Quorum Sensing is a cell-cell communication system based on small diffusible signaling molecules. An increasing number of bacteria is known to use the Quorum Sensing system to coordinate gene expression patterns in situations where single cells cannot act successfully on their own. Examples are bioluminescence, formation of biofilm or secretion of antibiotics respectively virulence factors [6, 9, 53].

The mechanism of Quorum Sensing enables bacteria to coordinate their behavior. Since the environmental conditions can change, the bacteria need to respond to new situations in order to survive. These responses include adaptation to availability of nutrients, defence against other microorganisms which may compete with the bacteria for the same nutrients, and the avoidance of toxic compounds that are potentially dangerous for the bacteria. It is also very important for pathogenic bacteria during infection of a host to coordinate their virulence, in order to escape the immune response of the host, so that they are able to establish a successful infection.
The regulation by Quorum Sensing was found in Gram-negative as well as Gram-positive bacteria [4]. Common classes of signaling molecules are oligopeptides in Gram-positive bacteria, N-Acyl Homoserine Lactones (AHL) in Gram-negative bacteria and a family of autoinducers known as AI-2 in both Gram-negative and Gram-positive bacteria [31]. Different bacterial species use different signaling molecules to communicate. In many cases a single bacterial species can have more than one Quorum Sensing system and therefore may use more than one kind of signaling molecules [33]. The bacteria may respond to each molecule in a differing or in an interacting manner. In this sense the signaling molecules can be thought of as words within a language, each having a different meaning.

Quorum Sensing is based on the continuous production of usually small amounts of diffusible signaling molecules, also called autoinducers, which are released into the environment. Moreover the cells have the ability to sense the concentration of the signal-

ing molecules in the surrounding environment [8, 37, 53]. The extracellular signaling molecule concentration therefore depends on the cell density, see Figure 1.1.

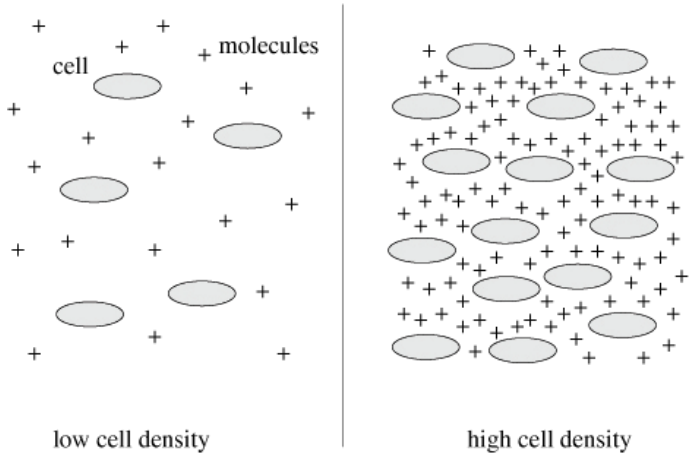

Figure 1.1.: Dependence of the extracellular signaling molecule concentration on the cell density.

If the extracellular concentration exceeds a certain threshold, which correspond to a critical cell density (quorum), the cell initiates a cellular response by gene transcription. In most bacterial taxa this response also includes an increased production of the signaling molecules, which results in a rapid increase of the signaling molecule concentration in the surrounding (positive feedback).

Quorum Sensing was described for the first time about 40 years ago in a bioluminescent bacterium called *Vibrio fischeri* [13, 38]. Due to the historical fact, *Vibrio fischeri* presents the best investigated Quorum Sensing system, so that it can be regarded as model organism for the understanding of Quorum Sensing regulation.
As marine bacteria, *Vibrio fischeri* exist naturally either in a free-living planktonic state or as a symbiont of certain luminescent fishes or squids, where they colonize in specialized light organs. Accumulated in the light organs, the bacteria luminesce as a result of Quorum Sensing. The regulation is based on a member of the AHL family. It turns out that the underlying gene regulation network that implements Quorum Sensing is quite similar across different bacteria taxa. As an example of a Quorum Sensing system, we regard the molecular mechanism of the Lux system in *Vibrio fischeri* (Figure 1.2).

In *Vibrio fischeri* the signaling molecule, AHL, is synthesized by the protein LuxI and sensed by the receptor protein LuxR. At low cell densities, AHL is produced by the bacteria at a low constitutive level. The AHL diffuses out of the bacterial cells and into the surrounding environment and it can diffuse back into the cells. As the cell density increases, AHL accumulates in the surrounding of the bacteria. Within the cell, AHL is able to interact with the LuxR receptor protein. The LuxR/AHL complexes polymerize to higher clusters and are then able to act as a transcription factor. That means they

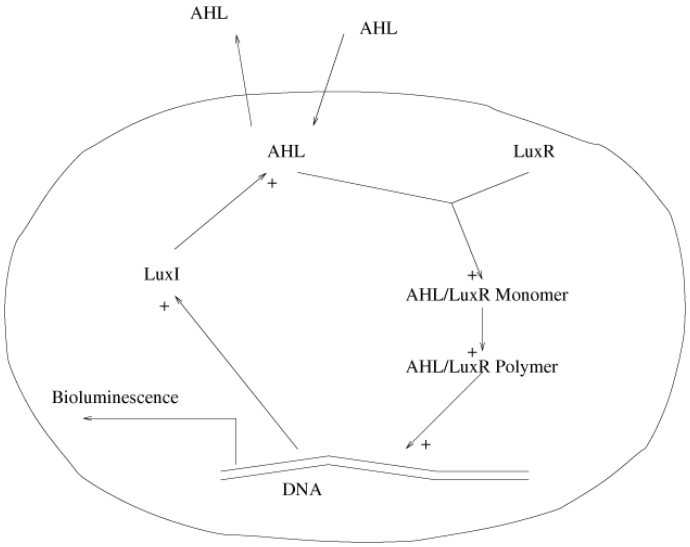

Figure 1.2.: Scheme of the regulatory Lux Quorum Sensing pathway in *Vibrio fischeri*

bind to a region of the DNA called "lux box", causing the expression of the luminescence genes and additionally LuxI, resulting in a high production of AHL. Thus the regulatory pathway contains a positive feedback.

Usually, *Vibrio fischeri* exist at low level densities when free-living and at high cell densities when colonized in the light organs. Therefore Quorum Sensing explains why the bacteria are dark when free-living and luminesce in the light organ.

However, in the literature the mechanism of producing, releasing and sensing signaling molecules is also interpreted as diffusion sensing [42], where the extracellular concentration is determined by the diffusible area around a cell. In this case the critical concentration threshold is exceeded if the diffusible area is sufficiently restricted. In [19] the discussion about quorum or diffusion sensing was united in the more general concept called efficiency sensing. In this concept it makes no difference for the cell if the signaling molecule concentration is high either because of a high cell density or due to limited space. The cell only needs to know that any released substance will accumulate in the exterior, no matter for which reason.

1.2. Mathematical Modeling of Quorum Sensing

Mathematical models for the Quorum Sensing system have only recently been developed. Primarily in the last few years, cell-cell communication has received much attention in the mathematical modeling community. It basically started with nearly simultaneous publications from three different groups, namely James et al. [23], Dockery and Keener [10] and Ward et al. [51].

In the literature one can find two different aspects in modeling the Quorum Sensing system. On the one hand the molecular mechanism of Quorum Sensing is investigated and modeled, on the other hand population dynamical models of bacteria using the Quorums sensing system are developed. The population-based approach can be distinguished between spatially homogeneous and spatially structured models. In general, the mathematical modeling is mainly based on either deterministic or stochastic models.

At the molecular level the Quorum Sensing system was modeled in single cells using the law of mass action. These models consist of a system of ordinary differential equations. For example, in [10] the authors focused on the specific system of *Pseudomonas aeruginosa* and in [23] the molecular Quorum Sensing mechanism in *Vibrio fischeri* was modeled. However, as mentioned above, the mathematical principles are quite similar in most models for Quorum Sensing. The mathematical models of the intracellular pathway reveals bistable behavior as a result of the positive feedback based on the increased production of the autoinducer itself [48]. It is shown that the communication works because of the biochemical switch between two stable steady state solutions, one with low levels of autoinducer and one with high levels of autoinducer. This switch is hysteretic, so that the signaling molecule production switches on and off at different concentrations of the extracellular autoinducer concentration.

The first deterministic population-based model, describing bacterial population growth and Quorum Sensing, was stated in Ward et al [51]. There are several models that assume large homogeneously mixed populations [2, 16, 51], mainly in investigation of biofilm growth. They always consist of a system of ordinary differential equations. Another way to model the dynamics of large homogeneous populations is given in terms of reaction diffusion equations [1, 7]. The population-based models reveals bistable behavior that depends on the population density. Hence, again the models predict the typical hysteretic behavior that is characteristic for the Quorum Sensing system. It turns out that the population switches from a principally down-regulated to an up-regulated population and that there exist bifurcations between the respective steady state solutions.
Improved biological experiments gave the possibility to obtain information about the state and location of single cells within a population. To cope with this new information, spatial structured models for the cell-cell communication were developed [34], described by partial differential equations.

Since the biological measurements on the meantime deal with smallest entities like single cells or even single molecules, the mathematical modeling is forced to acknowledge discreteness and stochasticity. Therefore stochastic models for the Quorum Sensing system have been developed [15, 28], concerning intra- and extracellular noise. For instance, in [28] a stochastic model for a single cell is stated, where a system of first-order partial differential equations describes the probability density function for the cell to be in down- or up-regulated state. Goryachev et al. [15] presented a population model where the intracellular model is incorporated into an agent-based stochastic model.

1.3. Overview

In this PhD thesis we derive and study models for the communication system of cells. To this end, we focus on different levels of the Quorum Sensing system, starting with a biochemical intracellular pathway, next considering a stochastic model for small population sizes and finally describing a deterministic model suitable for large populations.

In Chapter 2 we consider the biochemical information integration pathway in the marine bacterium *Vibrio harveyi*. *Vibrio harveyi* employs different parallel, seemingly redundant, Quorum Sensing systems which govern the same cellular response. The aim is to understand how cells integrate different information channels into one decision process. We first determine a model for one Quorum Sensing system and show that this model meets the experimental data quite nicely. Furthermore it turns out that the straight combination of two systems does not yield an adequate description of the data for the complete system. In contrast to the experimental findings, where the different autoinducer behave in a synergistic manner, the combined model behaves in a non-synergistic manner. Both the experimental and the theoretical results indicate that an additional mechanism is essential in this pathway.

The goal of the third chapter is to develop and analyze a stochastic model for bacterial populations of small and medium size. The question arises if the communication is still effective or if the intracellular noise destroys the possibility of the cells in the population to understand each other. An example for this setting are micro-colonies on roots of plants.
In the case of small population sizes we may assume that the number of cells within the population is small, whereas the number of signaling molecules is large in comparison. Based on the Lux-system of Quorum Sensing in *Vibrio fischeri* we develop a stochastic model where the population is associated with a probability density function that depends on the number of activated cells within the population and the number of signaling molecules at a given time. This approach yields a velocity jump process. To determine the asymptotic behavior of the population, we utilize the idea that the processes governing the population dynamics respectively the production of signaling molecules live on different time scales. However, the analysis allows to derive a closed equation for the marginal distribution of the signaling molecule density only.
During the analysis of the marginal distribution it turns out that even small populations act in a synchronized way. The bistability found in deterministic models now translates into bimodality of the AHL density. When analyzing the long term behavior of small populations, we get an idea of the implications of stochastic effects and we see that for large populations the long time behavior of the system returns to the behavior of corresponding deterministic models. Furthermore, the results suggest that stochasticity in the system may be used as a sophisticated mechanism to filter stochasticity in the signal.

In the fourth chapter we study a dynamical population model that is based on single cell models, where the cells are spatially structured. In order to understand the mechanism

of Quorum Sensing in a better way, experiments on single cell level are performed, where information of the state and location of single cells can be obtained. Classical spatially structured population models usually describe cell densities and do not consider the state of single cells.
In Müller et. al. [34] another approach was chosen, where the single cells are modeled as extended objects in the three dimensional space with a spatially homogeneous interior, and the cells communicate with the exterior by a spatially extended surface. The production of signaling molecules within each cell is formulated as an ordinary differential equation, while dispersion and absorption of the signaling molecules in the exterior are described by a linear partial differential equation. Renormalization of the parameters and shrinking the cell radius to zero, the authors found an approximation theorem for the stationary case, which leads to a homogeneous equation for the signaling molecules. We take up the findings of [34] and present a solution to the following problem: how to handle individual-based models of cell communication in non-equilibrium situations? Therefore, we first investigate the case of a single cell thoroughly, present an approximative model and an approximation theorem that shows that for long times the solutions of original and approximative model are close to each other. Eventually, we consider the interaction of several cells. The resulting approximative model assumes the form of a delay equation, where the delay represents the time needed for a molecule to bridge the space between two cells by diffusive processes.

2. Information Integration by Vibrio harveyi

In this chapter we investigate a new aspect of the internal information processing of the Quorum sensing system in *Vibrio harveyi*. The question is how do cells integrate different information channels into one decision process. Boolean algebra shows that combinations of inverter and AND gate are able to realize any logical function. It is thus intriguing to study both aspects in biochemical pathways. As in literature the inverter is well studied [36], we focus in the present work on the AND gate, which is less frequently investigated. To be more precise: how does *Vibrio harveyi* build the biochemical equivalent of an AND gate?

Experiments showed that in *Vibrio harveyi* multiple signals are integrated in the autoinducer signalling pathway in a synergistic manner. I.e. each signal, even at high concentration, evokes only a limited effect, whereas only the concurrent presence of all signals results in the full response, which is substantially stronger than the sum of each [33, 45]. This behavior can be interpreted as an AND gate.

However, we do not claim that a cell can be understood as a Boolean network - this simplification is useful in some settings, but the biochemistry is much more sophisticated and built on continuous variables. In comparison with a Boolean logic, a continuous approach allows to process more information with very few elementary circuits. Also in this study we will see that signals are not processed in a qualitative but in a quantitative way. To understand the mechanism and full functionality of the biochemical circuit it is essential to account for this fact.

The picture developed in literature up to now focussed on phosphotransfer as the central way to integrate the information of the corresponding signals. The analysis of a rather general model formulating this picture reveals that the experimentally observed data cannot be explained in this way.

2.1. Biological Pathway

The marine bacterium *Vibrio harveyi*, a model organism for autoinducer analysis, employs three autoinducers, HAI-1, a N-acyl-homoserine lactone, AI-2, a furanosyl-borate-diesther and CAI-1, a (S)-3-hydroxytridecan-4-one. These autoinducers bind to specific, membrane bound receptors, LuxN, LuxP/Q and CqsS, which convey the information via LuxU, LuxO, and five small RNAs to the transcription regulator LuxR [47, 52]. Note that the AI-2 receptor is composed of two proteins, LuxQ and LuxP. For simplicity we will term it just LuxQ. The relative effect of the signal input on LuxR differs

and varies dependent on the environmental conditions (HAI-1>AI-2>CAI-1 in liquid medium) [17]. The interesting fact is that the information of all three autoinducers is integrated in LuxU.

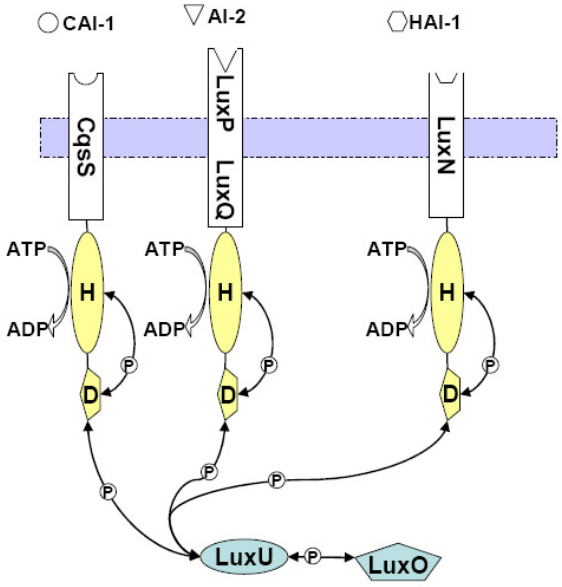

Figure 2.1.: Phosphorylation/dephosphorylation cascade in *Vibrio harveyi.*

The picture of the pathway developed so far is as follows: between the receptors and LuxO, the information is transduced by a phosphorylation/dephosphorylation cascade (Figure 2.1). The receptors act as two-component sensor kinases, but additionally carry phosphatase properties. In the absence of its cognate autoinducer, kinase activity of each receptor strongly dominates. After autophosporylation of a histidine residue (H), the phosphate is transferred to an aspartate (D) in the sensor kinase. Binding of cognate autoinducers decreases the kinase/phosphatase activity relation of the sensor kinases, at least for LuxN and LuxQ by decreasing the kinase activity. This results in a lower degree of phosphorylation for LuxU and LuxO. The strength of the decrease depends on the sensor kinase [46, 45].

The function of the three parallel, seemingly redundant autoinducer systems for *Vibrio harveyi* is not well understood. Several hypothesis have been suggested, e.g. use for coincidence detection [33] or as a gauge for the genetic relatedness in the vicinity of the receptor cell [52].

Beside the general aspect of understanding biological information processing, this specific structure of autoinducer information integration is of interest as it has been found similarly in related pathogens, e.g. *Vibrio cholerae* [18, 32]. Crucial for an interpretation is the qualitative and quantitative analysis of information processing by the sensor

kinases and the integration by LuxU. Therefore, experimental studies for the HAI-1 and AI-2 signalling pathway down to LuxU have been conducted [45, 46]. Generally, the signal integration is assumed to be able to act as a kind of AND gate [33, 45], although it apparently does not adequately describe the response on gene expression level for all regulated genes [52].

The introduced picture assumes that the sensor kinases independently process the different input channels (autoinducers), and translate the autoinducer density in a normed signal - a certain phosphorylation rate towards LuxU. Consequently, LuxU collects the different signals and integrates them in a rather additive way. From a theoretical point of view, it is intriguing that a system with only a low degree of interaction between the channels should be able to build a function that is as nonlinear as an AND gate.

One main aspect of this chapter is to clarify the validity of this picture. This will be done by developing a mathematical model, based on the biological pathway as depicted in Figure 2.1. The amount of phosphorylated LuxU is responsible for the information integration respectively for the decision process. We thus concentrate on the description of the density of phosphorylated LuxU in dependence on the densities of the autoinducers HAI-1 and AI-2. The model investigates the single branches of the processing and, in a second step, a combination of both branches. The predictions of the model are compared with experimental data. Finally, we will show that contradictions between the model prediction and experimental data require the assumption of an additional biological process, for which we make a proposal.

2.2. Model for one sensor kinase

We start off with the investigation of the system that processes HAI-1 in absence of the system that processes AI-2 and vice versa. The biochemical structure of these two systems is quite similar. Thus, we develop a general model where we use $SensK$ to indicate either the sensor kinase LuxQ or the sensor kinase LuxN. The autoincucers HAI-1, respectively AI-2, are denoted by AI. The reactions are sketched in Figure 2.2 and the names used are explained in Table 2.1.

Basically, there are three processes

(1) the sensor kinase exchanges phosphor with ATP/ADP,

(2) it exchanges phosphor with LuxU/LuxUP, and

(3) the autoinducer may associate/dissociate with the sensor kinase.

To understand the reaction scheme completely, it is necessary to remark that different amino acid residues within the sensor kinase are responsible for the phosphotransfer between the sensor kinase and ATP/ADP resp. LuxU/LuxUP. A histidine residue is responsible for the phosphor exchange with ATP/ADP, while an aspartate residue moves phosphor from LuxUP and to LuxU. I.e., within the sensor kinases, phosphor is moved between H and D.

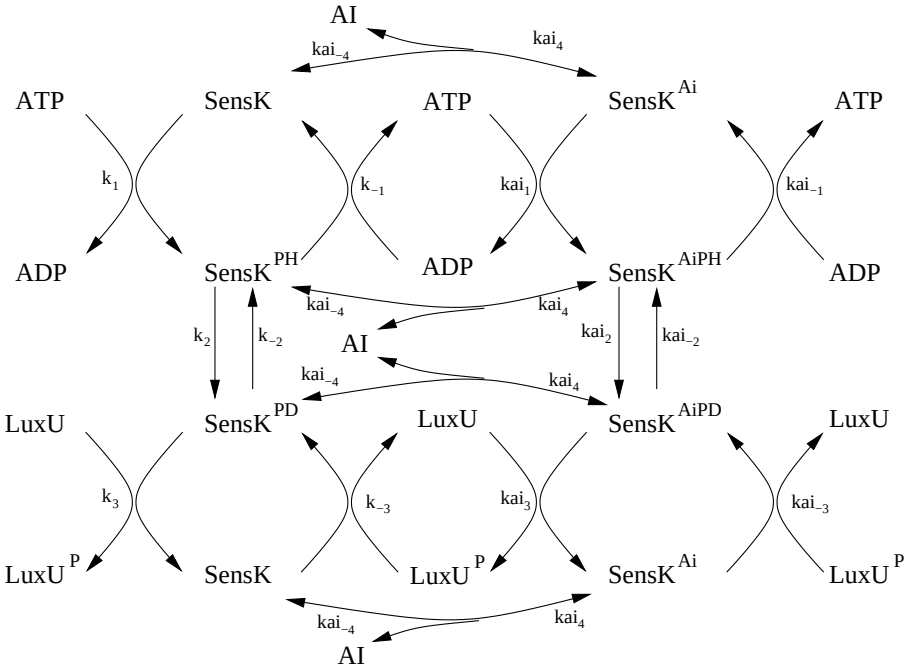

Figure 2.2.: Reaction scheme of one sensor kinase only.

Name	Meaning	Model
$SensK$	Sensor kinase (LuxQ or LuxN)	section 2.2
$SensKPH$	Sensor kinase with phosphorylated histidine	section 2.2
$SensKPD$	Sensor kinase with phosphorylated aspartate	section 2.2
$SensKAi$	Sensor kinase with autoinducer	section 2.2
$SensKAiPH$	Sensor kinase with autoinducer and phosphorylated histidine	section 2.2
$SensKAiPD$	Sensor kinase with autoinducer and phosphorylated aspartate	section 2.2
Ai	Autoinducer (either AI-2 or HAI-1)	section 2.2
$LuxU$	LuxU	all models
$LuxU^*$	LuxU in second (hypothetical) conformation	section 2.4
$LuxUP$	Phosphorylated LuxU	all models
$LuxU^*P$	Phosphorylated LuxU in second conformation	section 2.4
ATP	ATP	all models
ADP	ADP	all models

Table 2.1.: Names of all state variables in the models.

2.2.1. Reactions

The chemical reactions for one sensor kinase read

$$\begin{aligned}
SensK + ATP &\rightleftharpoons SensKPH + ADP && \text{rate } \text{“}\rightarrow\text{”} k_1, \text{ rate } \text{“}\leftarrow\text{”} k_{-1},\\
SensKAi + ATP &\rightleftharpoons SensKAiPH + ADP && \text{rate } \text{“}\rightarrow\text{”} kai_1, \text{ rate } \text{“}\leftarrow\text{”} kai_{-1},\\
SensKPH &\rightleftharpoons SensKPD && \text{rate } \text{“}\rightarrow\text{”} k_2, \text{ rate } \text{“}\leftarrow\text{”} k_{-2},\\
SensKAiPH &\rightleftharpoons SensKAiPD && \text{rate } \text{“}\rightarrow\text{”} k_2, \text{ rate } \text{“}\leftarrow\text{”} k_{-2},\\
SensKPD + LuxU &\rightleftharpoons SensK + LuxUP && \text{rate } \text{“}\rightarrow\text{”} k_3, \text{ rate } \text{“}\leftarrow\text{”} k_{-3},\\
SensKAiPD + LuxU &\rightleftharpoons SensKAi + LuxUP && \text{rate } \text{“}\rightarrow\text{”} kai_3, \text{ rate } \text{“}\leftarrow\text{”} kai_{-3}\\
SensK + Ai &\rightleftharpoons SensKAi && \text{rate } \text{“}\rightarrow\text{”} kai_4, \text{ rate } \text{“}\leftarrow\text{”} kai_{-4},\\
SensKPH + Ai &\rightleftharpoons SensKAiPH && \text{rate } \text{“}\rightarrow\text{”} kai_4, \text{ rate } \text{“}\leftarrow\text{”} kai_{-4},\\
SensKPD + Ai &\rightleftharpoons SensKAiPD && \text{rate } \text{“}\rightarrow\text{”} kai_4, \text{ rate } \text{“}\leftarrow\text{”} kai_{-4}.
\end{aligned}$$

It is possible to use data about phosphorylation of LuxU, dephosphorylation of LuxUP and the initial rates of phosphorylation in dependence on the amount of autoinducer to determine most of the rates, see Appendix A.2. The complete identifiability of all rates is not given, some rate constants can be only determined in combinations.

2.2.2. Time scales for one sensor kinase

To better understand the underlying mechanism, and to reduce the rather complex reaction scheme above, we use singular perturbation theory and develop a small working model. This small model will be important when we re-consider this model in the context of interacting sensor kinases.

We describe the assumption and the process used to extract the toy model verbally at this point. The first assumption is that binding and dissociation of autoinducers are fast since we do not see hints in the data that the autoinducers bind slowly [46]. Furthermore, Figure 2.3 (e) and (f) show that the phosphorylation rate still declines in the amount of autoinducer, even if we consider densities of autoinducer that are ten fold and more in comparison with the sensor kinase. If the autoinducers bind fast but dissociate slow, the sensor kinases should be almost completely bound to autoinducer at much less autoinducer concentrations, and the phosphorylation degree of LuxU would not change any more. Thus, the sensor kinases bind and dissociate quite fast. This is the first time scale we will work with.

Our parameter estimation done in Appendix A.2 reveals that the phosphotransfer within the sensor kinases between D and H is slower than the binding of the autoinducers, but much faster than the phosphotransfer between sensor kinases and LuxU respectively sensor kinases and ATP/ADP. This is the second time scale we use.

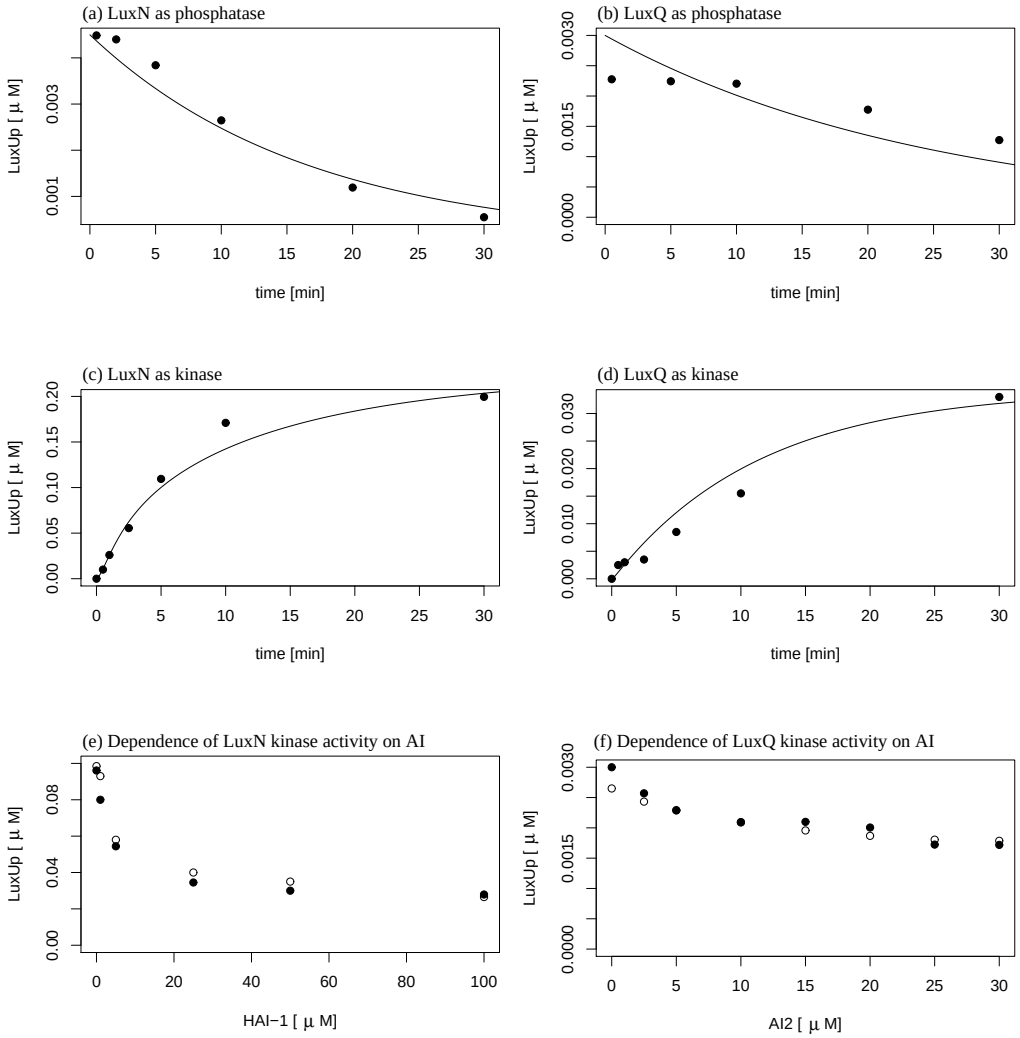

Figure 2.3.: Simulation and experimental data [45, 46] for the kinase and phosphatase activities of LuxN and LuxQ, represented by the turnover of LuxUP. Closed circles always indicate the experimental data, lines resp. open circles the results of simulation. For information about the experimental procedures see Appendix A.1.

The third assumption we use is that the autoinducers only affect the phosphotransfer from ATP to the sensor kinases, i.e. the kinase activity of the sensor kinases. This assumption is supported by the data presented in [45, 46]. These data show that the dephosphorylation of LuxUP, i.e. the phosphatase activity, is not affected by the autoinducers.

The last assumption is clearly met by the experiments as well as in the cell: the amount of sensor kinases is low in comparison with the amount of LuxU and ATP.

We show that these time scale arguments and a reasoning similar to that used to derive the Michaelis-Menten kinetics yield a considerable reduction of the model.

Starting point are two time scales, corresponding to the first and second assumption,

$$\begin{aligned}
SensK + ATP &\rightleftharpoons SensKPH + ADP && \text{rate } \text{“}\rightarrow\text{”} k_1, \text{ rate } \text{“}\leftarrow\text{”} k_{-1},\\
SensKAi + ATP &\rightleftharpoons SensKAiPH + ADP && \text{rate } \text{“}\rightarrow\text{”} kai_1, \text{ rate } \text{“}\leftarrow\text{”} kai_{-1},\\
\\
SensKPH &\rightleftharpoons SensKPD && \text{rate } \text{“}\rightarrow\text{”} \frac{k_2}{\varepsilon_2}, \text{ rate } \text{“}\leftarrow\text{”} \frac{k_{-2}}{\varepsilon_2},\\
SensKAiPH &\rightleftharpoons SensKAiPD && \text{rate } \text{“}\rightarrow\text{”} \frac{k_2}{\varepsilon_2}, \text{ rate } \text{“}\leftarrow\text{”} \frac{k_{-2}}{\varepsilon_2},\\
\\
SensKPD + LuxU &\rightleftharpoons SensK + LuxUP && \text{rate } \text{“}\rightarrow\text{”} k_3, \text{ rate } \text{“}\leftarrow\text{”} k_{-3},\\
SensKAiPD + LuxU &\rightleftharpoons SensKAi + LuxUP && \text{rate } \text{“}\rightarrow\text{”} kai_3, \text{ rate } \text{“}\leftarrow\text{”} kai_{-3}\\
\\
SensK + Ai &\rightleftharpoons SensKAi && \text{rate } \text{“}\rightarrow\text{”} \frac{kai_4}{\varepsilon_1}, \text{ rate } \text{“}\leftarrow\text{”} \frac{kai_{-4}}{\varepsilon_1},\\
SensKPH + Ai &\rightleftharpoons SensKAiPH && \text{rate } \text{“}\rightarrow\text{”} \frac{kai_4}{\varepsilon_1}, \text{ rate } \text{“}\leftarrow\text{”} \frac{kai_{-4}}{\varepsilon_1},\\
SensKPD + Ai &\rightleftharpoons SensKAiPD && \text{rate } \text{“}\rightarrow\text{”} \frac{kai_4}{\varepsilon_1}, \text{ rate } \text{“}\leftarrow\text{”} \frac{kai_{-4}}{\varepsilon_1},
\end{aligned}$$

where $\varepsilon_1 \ll \varepsilon_2 \ll 1$. Thus, the last three reactions can be assumed to be in quasi-steady-state. For $SensK$ and $SensKAi$ we then obtain

$$SensK\ Ai\ kai_4 = kai_{-4}\ SensKAi.$$

Defining $SensK_0 = SensK + SensKAi$, where $SensK_0 \equiv \text{const}$, we obtain

$$SensK = \tau\ SensK_0, \quad SensKAi = (1-\tau)\ SensK_0, \tag{2.1}$$

with $\tau := \frac{\widehat{ai}}{(\widehat{ai}+Ai)}$, and $\widehat{ai} := \frac{kai_{-4}}{kai_4}$. The parameter $\widehat{ai}$ denotes the amount of autoinducer for half-activation.

Similarly, with

$$\begin{aligned}
SensKPH_0 &= SensKPH + SensKAiPH,\\
SensKPD_0 &= SensKPD + SensKAiPD,
\end{aligned}$$

where $SensKPH_0$ and $SensKPD_0$ are assumed to be constant and τ defined as before, we obtain

$$\begin{aligned} SensKPH &= \tau\ SensKPH_0, \quad SensKAiPH = (1-\tau)\ SensKPH_0, \\ SensKPD &= \tau\ SensKPD_0, \quad SensKAiPD = (1-\tau)\ SensKPD_0. \end{aligned}$$

Now we introduce the second time scale, and thus also the amount of $SensKPD_0$ and $SensKPH_0$ are in quasi-equilibrium. Let

$$SensKP_0 = SensKPH_0 + SensKPD_0$$

denote the constant total amount of phosphorylated sensor kinase. Then we obtain

$$SensKPH = \tau\,\rho\,SensKP_0, \qquad SensKAiPH = (1-\tau)\,\rho\,SensKP_0, \tag{2.2}$$

$$SensKPD = \tau\,(1-\rho)\,SensKP_0, \qquad SensKAiPD = (1-\tau)\,(1-\rho)\,SensKP_0, \tag{2.3}$$

where the parameter $\rho := \frac{k_{-2}}{(k_2+k_{-2})} \in (0,1)$ indicates the ratio of the kinase density with phosphotransfer at H resp. D.

At this point, we rewrite the equations governing the slow dynamics of ATP/ADP and LuxU/LuxUP,

$$\begin{aligned} \frac{d}{dt}ATP &= -k_1 SensK\ ATP + k_{-1} SensKPH\ ADP - kai_1 SensKAi\ ATP \\ &\quad + kai_{-1} SensKAiPH\ ADP, \\ \frac{d}{dt}LuxUP &= -k_{-3} SensK\ LuxUP + k_3 SensKPD\ LuxU - kai_{-3} SensKAi\ LuxUP \\ &\quad + kai_3 SensKAiPD\ LuxU, \\ ADP &= ATP_0 - ATP, \\ LuxU &= LuxU_0 - LuxUP, \end{aligned}$$

where $LuxU_0$ denotes the amount of LuxU and LuxUP, and ATP_0 denotes the total amount of ATP and ADP.

The last assumption is that only the rate k_1 is affected by the autoinducer, i.e. $k_1 \gg kai_1$, but $k_{-1} = kai_{-1}$, and $k_{\pm 3} = kai_{\pm 3}$. Furthermore, we are able to rewrite the amounts of the different states of the sensor kinase in terms of $SensK_0$ and $SensKP_0$ only. Substituting (2.1), (2.2) and (2.3), we obtain

$$\frac{d}{dt}ATP = -(k_1\tau + kai_1(1-\tau))\ SensK_0\ ATP + k_{-1}\rho SensKP_0\ (ATP_0 - ATP), \tag{2.4}$$

$$\frac{d}{dt}LuxUP = -k_{-3} SensK_0\ LuxUP + k_3(1-\rho) SensKP_0\ (LuxU_0 - LuxUP). \tag{2.5}$$

These two equations, (2.4), (2.5), are sufficient to describe the time course of the six substances $LuxU$, $LuxUP$, ATP, ADP, $SensK_0$ and $SensKP_0$, as we have four conservation laws, i.e. $LuxU_0$, ATP_0, $S_0 = SensK_0 + SensKP_0$, and P_0 are constant.

To be complete, we give the equation for $SensKP_0$. As the amount of phosphor in the system is constant, we know

$$LuxUP + SensKP_0 + ATP = P_0. \tag{2.6}$$

Thus,

$$\begin{aligned}\frac{d}{dt}SensKP_0 =&(k_1\tau + kai_1(1-\tau))\, SensK_0\ ATP - k_{-1}\rho SensKP_0\ (ATP_0 - ATP)\\ &+ k_{-3}SensK_0\ LuxUP - k_3(1-\rho)SensKP_0\ (LuxU_0 - LuxUP).\end{aligned} \tag{2.7}$$

Due to the time scale arguments up to now it turns out that the complete system can be replaced by one sensor kinase accepting phosphor from and transferring to ATP and LuxU, where only one rate is affected by the presence of the autoinducer.

In the last step, we use the fact that the amount of sensor kinase is much less than that of LuxU and ATP, i.e.

$$SensK_0 = \varepsilon\, s, \quad SensKP_0 = \varepsilon\, sp, \quad S_0 = \varepsilon\, s_0, = \varepsilon(s + sp) \tag{2.8}$$

where S_0 denotes the constant total amount of the respective sensor kinase. The procedure resembles the approach to derive the Michaelis-Menten kinetics, where the enzyme has a low density. The rescaled equations for our system now read

$$\begin{aligned}\frac{d}{dt}ATP &= \varepsilon\left[-(k_1\tau + kai_1(1-\tau))\, s\ ATP + k_{-1}\rho\ sp\ (ATP_0 - ATP)\right],\\ \varepsilon\frac{d}{dt}sp &= \varepsilon\big[(k_1\tau + kai_1(1-\tau))\, s\ ATP - k_{-1}\rho\ sp\ (ATP_0 - ATP),\\ &\quad + k_{-3}s\ LuxUP - k_3(1-\rho)sp\ (LuxU_0 - LuxUP)\big]\\ \frac{d}{dt}LuxUP &= \varepsilon\left[-k_{-3}s\ LuxUP + k_3(1-\rho)sp\ (LuxU_0 - LuxUP)\right].\end{aligned}$$

If we now use the slow time scale $\sigma = \varepsilon t$, we obtain

$$\frac{d}{d\sigma}ATP = -(k_1\tau + kai_1(1-\tau))\, s\ ATP + k_{-1}\rho\ sp\ (ATP_0 - ATP), \tag{2.9}$$

$$\begin{aligned}\varepsilon\frac{d}{d\sigma}sp &= (k_1\tau + kai_1(1-\tau))\, s\ ATP - k_{-1}\rho\ sp\ (ATP_0 - ATP),\\ &\quad + k_{-3}s\ LuxUP - k_3(1-\rho)sp\ (LuxU_0 - LuxUP)\end{aligned} \tag{2.10}$$

$$\frac{d}{d\sigma}LuxUP = -k_{-3}s\ LuxUP + k_3(1-\rho)sp\ (LuxU_0 - LuxUP), \tag{2.11}$$

and in the singular limit (2.10) can be rewritten as

$$[(k_1\tau + kai_1(1-\tau))\ ATP + k_{-3}\ LuxUP]s = [k_3(1-\rho)\ LuxU + k_{-1}\rho\ ADP]sp.$$

With $s + sp = s_0$ we know

$$\begin{aligned}sp &= \frac{[(k_1\tau + kai_1(1-\tau))\ ATP + k_{-3}\ LuxUP\,]s_0}{k_3(1-\rho)\ LuxU + k_{-1}\rho\ ADP + [k_1\tau + kai_1(1-\tau)]\ ATP + k_{-3}\ LuxUP}\\ s &= \frac{k_3(1-\rho)\ LuxU + k_{-1}\rho\ ADP]s_0}{k_3(1-\rho)\ LuxU + k_{-1}\rho\ ADP + [k_1\tau + kai_1(1-\tau)]\ ATP + k_{-3}\ LuxUP}\end{aligned}$$

If we plug these terms in equation (2.11) it results

$$\begin{aligned}
&\frac{d}{d\sigma}LuxUP = \\
= &-\frac{k_{-3}LuxUP[k_3(1-\rho)\ LuxU + k_{-1}\rho\ ADP]s_0}{k_3(1-\rho)\ LuxU + k_{-1}\rho\ ADP + [k_1\tau + kai_1(1-\tau)]\ ATP + k_{-3}\ LuxUP} \\
&+\frac{k_3(1-\rho)\ LuxU[(k_1\tau + kai_1(1-\tau))\ ATP + k_{-3}\ LuxUP]s_0}{k_3(1-\rho)\ LuxU + k_{-1}\rho\ ADP + [k_1\tau + kai_1(1-\tau)]\ ATP + k_{-3}\ LuxUP} \\
= &-\frac{k_{-3}k_{-1}\rho\ s_0\ ADPLuxUP}{k_3(1-\rho)\ LuxU + k_{-1}\rho\ ADP + [k_1\tau + kai_1(1-\tau)]\ ATP + k_{-3}\ LuxUP} \\
&+\frac{k_3(1-\rho)\ (k_1\tau + kai_1(1-\tau))\ s_0\ LuxUATP}{k_3(1-\rho)\ LuxU + k_{-1}\rho\ ADP + [k_1\tau + kai_1(1-\tau)]\ ATP + k_{-3}\ LuxUP}.
\end{aligned}$$

In the singular limit, $\varepsilon \to 0$, the conservation law for phosphor (2.6) yields

$$P_0 = LuxUP + ATP,$$

which is constant. Thus, the system reduces to two reactions,

$$\begin{aligned}
LuxU + ATP &\to LuxUP + ADP \qquad \text{at rate } K_+ \\
LuxUP + ADP &\to LuxU + ATP \qquad \text{at rate } K_-
\end{aligned}$$

where the rates $K_\pm$ are not constants, but given by

$$K_+ = \frac{k_3(1-\rho)\ (k_1\tau + kai_1(1-\tau))\ s_0}{k_3(1-\rho)\ LuxU + k_{-1}\rho\ ADP + [k_1\tau + kai_1(1-\tau)]\ ATP + k_{-3}\,LuxUP} \quad (2.12)$$

$$K_- = \frac{k_{-3}k_{-1}\rho\ s_0}{k_3(1-\rho)\ LuxU + k_{-1}\rho\ ADP + [k_1\tau + kai_1(1-\tau)]\ ATP + k_{-3}\,LuxUP}. \quad (2.13)$$

From this result it is clear that only parameter combinations can be estimated, and not each single rate constant.

2.3. Combination of the two pathways without further interaction

The next step is to combine the two pathways in a straight manner. The first model for the effect of combined sensor kinases is a straight summation of the chemical reactions for one kinase.

Notation 2.1 To differ the parameters of the two systems we precede each parameter with n or q, corresponding to the $LuxN$, resp. $LuxQ$ pathway, e.g. nk_1, qk_1.

Hence, the chemical reactions for the combined model read

$$\begin{aligned}
LuxN + ATP &\rightleftharpoons LuxNPH + ADP && \text{rate } \text{“}\rightarrow\text{”} nk_1, \text{ rate } \text{“}\leftarrow\text{”} nk_{-1},\\
LuxNAi + ATP &\rightleftharpoons LuxNAiPH + ADP && \text{rate } \text{“}\rightarrow\text{”} nkai_1, \text{ rate } \text{“}\leftarrow\text{”} nkai_{-1},\\
\\
LuxNPH &\rightleftharpoons LuxNPD && \text{rate } \text{“}\rightarrow\text{”} nk_2, \text{ rate } \text{“}\leftarrow\text{”} nk_{-2},\\
LuxNAiPH &\rightleftharpoons LuxNAiPD && \text{rate } \text{“}\rightarrow\text{”} nk_2, \text{ rate } \text{“}\leftarrow\text{”} nk_{-2},\\
\\
LuxNPD + LuxU &\rightleftharpoons LuxN + LuxUP && \text{rate } \text{“}\rightarrow\text{”} nk_3, \text{ rate } \text{“}\leftarrow\text{”} nk_{-3},\\
LuxNAiPD + LuxU &\rightleftharpoons LuxNAi + LuxUP && \text{rate } \text{“}\rightarrow\text{”} nkai_3, \text{ rate } \text{“}\leftarrow\text{”} nkai_{-3}\\
\\
LuxN + Ai &\rightleftharpoons LuxNAi && \text{rate } \text{“}\rightarrow\text{”} nkai_4, \text{ rate } \text{“}\leftarrow\text{”} nkai_{-4},\\
LuxNPH + Ai &\rightleftharpoons LuxNAiPH && \text{rate } \text{“}\rightarrow\text{”} nkai_4, \text{ rate } \text{“}\leftarrow\text{”} nkai_{-4},\\
LuxNPD + Ai &\rightleftharpoons LuxNAiPD && \text{rate } \text{“}\rightarrow\text{”} nkai_4, \text{ rate } \text{“}\leftarrow\text{”} nkai_{-4}.\\
\\
LuxQ + ATP &\rightleftharpoons LuxQPH + ADP && \text{rate } \text{“}\rightarrow\text{”} qk_1, \text{ rate } \text{“}\leftarrow\text{”} qk_{-1},\\
LuxQAi + ATP &\rightleftharpoons LuxQAiPH + ADP && \text{rate } \text{“}\rightarrow\text{”} qkai_1, \text{ rate } \text{“}\leftarrow\text{”} qkai_{-1},\\
\\
LuxQPH &\rightleftharpoons LuxQPD && \text{rate } \text{“}\rightarrow\text{”} qk_2, \text{ rate } \text{“}\leftarrow\text{”} qk_{-2},\\
LuxQAiPH &\rightleftharpoons LuxQAiPD && \text{rate } \text{“}\rightarrow\text{”} qk_2, \text{ rate } \text{“}\leftarrow\text{”} qk_{-2},\\
\\
LuxQPD + LuxU &\rightleftharpoons LuxQ + LuxUP && \text{rate } \text{“}\rightarrow\text{”} qk_3, \text{ rate } \text{“}\leftarrow\text{”} qk_{-3},\\
LuxQAiPD + LuxU &\rightleftharpoons LuxQAi + LuxUP && \text{rate } \text{“}\rightarrow\text{”} qkai_3, \text{ rate } \text{“}\leftarrow\text{”} qkai_{-3}\\
\\
LuxQ + Ai &\rightleftharpoons LuxQAi && \text{rate } \text{“}\rightarrow\text{”} qkai_4, \text{ rate } \text{“}\leftarrow\text{”} qkai_{-4},\\
LuxQPH + Ai &\rightleftharpoons LuxQAiPH && \text{rate } \text{“}\rightarrow\text{”} qkai_4, \text{ rate } \text{“}\leftarrow\text{”} qkai_{-4},\\
LuxQPD + Ai &\rightleftharpoons LuxQAiPD && \text{rate } \text{“}\rightarrow\text{”} qkai_4, \text{ rate } \text{“}\leftarrow\text{”} qkai_{-4}.
\end{aligned}$$

The first check is for sure the measurement of LuxUP development in presence of LuxN and LuxQ without any autoinducer. The result (dotted line in Figure 2.4, left panel) seems acceptable, although not perfect. For sure, tuning the parameters could improve this picture.

However, if we also add autoinducer, the picture changes completely: in Figure 2.6 the total kinase activity, presented as the phosphorylation rate of LuxU (in percent of that for LuxN as the only present kinase) obtained by an experiment with AI-2 and an experiment with AI-2 and HAI-1 is shown.

We find almost no phosphorylated LuxU in the experiment. While this is in agreement with the synergism reported *in vivo* for the bioluminescence induction by Mok [33], the model still predicts a considerable amount of LuxUP. This is not only a quantitative disagreement of model and data, but a qualitative difference. With the parameters chosen above, the model is not able to realize an AND gate, while the data indicate that the biochemical system shows the behavior of an AND gate, indeed.

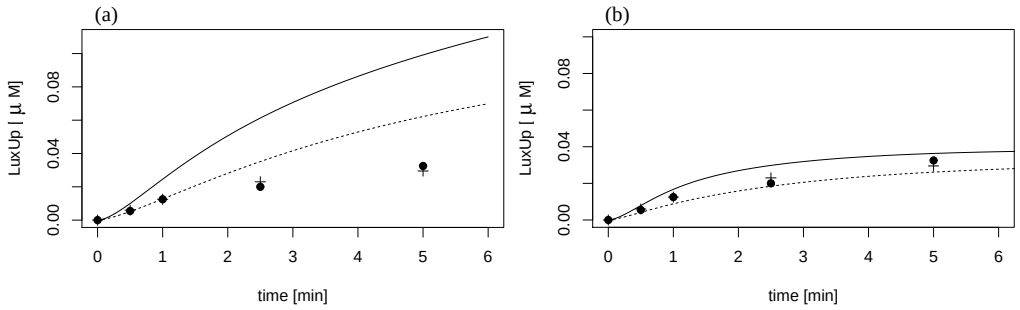

Figure 2.4.: Kinase activity of LuxN and LuxQ (without autoinducer). The experimental data, which are identical in both panels, are represented by solid dots (LuxN + LuxQ) and crosses (LuxN + LuxQ-). Simulation results are given as solid curve (LuxN + LuxQ-) and dotted curve (LuxN + LuxQ). Left panel: no further interaction, right panel: LuxU*-model.

The first thought may be that the model structure is appropriate, but that the fit is bad. We already discussed that only parameter combinations can be identified, but not each single parameter. With an approximative model we will answer the question if there are other parameter combinations that allow to explain the data.

2.3.1. Approximate model with two sensor kinases

Let us consider this problem. Under weak assumptions, met by the experimental system, we are especially able to show that the combination of two sensor kinases (with or without autoinducer) cannot decrease the amount of LuxUP below the lowest value that can be obtained with one single sensor kinase (with the given amount of autoinducer).

We have seen that the system with one sensor kinase can be approximated by

$$\begin{aligned} LuxU + ATP &\rightarrow LuxUP + ADP \qquad \text{at rate } K_+ \\ LuxUP + ADP &\rightarrow LuxU + ATP \qquad \text{at rate } K_- \end{aligned}$$

If we have two sensor kinases, we find

$$\begin{aligned} LuxU + ATP &\rightarrow LuxUP + ADP \qquad \text{at rate } nK_+ + qK_+ \\ LuxUP + ADP &\rightarrow LuxU + ATP \qquad \text{at rate } nK_- + qK_- \end{aligned}$$

where the rates $nK_\pm$, $qK_\pm$ assume the form (2.12) and (2.13).

Hence, in equilibrium, we obtain

$$LuxU\ ATP\ (nK_+ + qK_+) \;=\; LuxUP\ ADP\ (nK_- + qK_-).$$

We furthermore know, as in the model with one sensor kinase, $LuxU+LuxUP = LuxU_0$, $ADP+ATP = ATP_0$ and $LuxUP+ATP = P_0$. From these conservation laws, we find

$$\begin{aligned} LuxU &= LuxU_0 - LuxUP \\ ATP &= P_0 - LuxUP \\ ADP &= ATP_0 - ATP = ATP_0 - P_0 + LuxU_p \end{aligned}$$

and thus

$$\begin{aligned} (LuxU_0 - LuxUP)\ (P_0 - LuxUP)\ (nK_+ + qK_+) = \\ = LuxUP\ (ATP_0 - P_0 + LuxU_p)\ (nK_- + qK_-) \end{aligned}$$

This yields

$$\begin{aligned} 0 = LuxUP^2[nK_+ + qK_+ - (nK_- + qK_-)] - LuxUP[(P_0 + LuxU_0)(qK_+ + nK_+) \\ + ATP_0(nK_- + qK_-)] + [LuxU_0P_0(nK_+ + qK_+)]. \quad (2.14) \end{aligned}$$

Note that the rates $nK_\pm$ and $qK_\pm$ both depend on LuxUP. Let us consider the structure of these rates. The rates have a similar shape for both sensor kinases. For nK_+ we obtain

$$\begin{aligned} nK_+ &= \frac{nk_3(1-\rho)\ (nk_1\tau + nkai_1(1-\tau))\, s_0}{nk_3(1-\rho)LuxU + nk_{-1}\rho ADP + [nk_1\tau + nkai_1(1-\tau)]ATP + nk_{-3}LuxUP} \\ &= \frac{nk_3(1-\rho)\ (nk_1\tau + nkai_1(1-\tau))\ s_0}{nA + nBLuxUP} = \frac{nC_+}{nA + nBLuxUP}, \end{aligned}$$

where

$$\begin{aligned} nC_+ &= nk_3(1-\rho)\ (nk_1\tau + nkai_1(1-\tau))\ s_0 > 0, \\ nA &= nk_3(1-\rho)\ LuxU_0 + nk_{-1}\rho\ (ATP_0 - P_0) + [(nk_1\tau + nkai_1(1-\tau)]\ P_0, \\ nB &= nk_{-3} + nk_{-1}\rho - nk_3(1-\rho) - [nk_1\tau + nkai_1(1-\tau)]. \end{aligned}$$

We find $nA > 0$ as we have $ATP_0 - P_0 = 0$ in the experiments. It is of crucial importance to know the sign of nB (and also of qB). Inspecting the estimations, we find that $nB \gg 0$. As $nk_{-1} \approx 10^5$ is magnitudes larger than all other rates, and $\rho \approx 10^{-2}$, this inequality does not depend on the special parameter estimation, but is given for all parameter sets that reproduce the data in a reasonable way. We are allowed to take this inequality for granted. Thus we obtain $nK_+ > 0$ and because of the similar shape we also know $qK_+ > 0$.

Similarly, we are interested in the coefficient of the quadratic term of (2.14). If we consider $nK_+ - nK_-$, we find

$$\begin{aligned} nK_+ - nK_- &= \frac{nk_3(1-\rho)\ (nk_1\tau + nkai_1(1-\tau))\ s_0}{nA + nBLuxUP} - \frac{nk_{-3}nk_{-1}\rho\ s_0}{nA + nBLuxUP} \\ &= \frac{nC_+ - nC_-}{nA + nBLuxUP} \end{aligned}$$

where

$$nC_- = nk_{-3}nk_{-1}\rho\ s_0 > 0$$

Again, we are interested in the sign of $nC_+ - nC_-$ (and $qC_+ - qC_-$). As nk_{-3} dominates nk_3, k_{-1} dominates k_1 as well as kai_1, we find $nC_+ - nC_- \ll 0$ though $\rho \approx 10^{-2}$. This inequality is again a structural inequality and does not depend on the special fit. Hence

$$nK_+ - nK_- < 0, \qquad\qquad qK_+ - qK_- < 0.$$

Notation 2.2 All in all we find the equation

$$nP(LuxUP) + qP(LuxUP) = 0$$

where

$$P(x) \;=\; \frac{C_- - C_+}{A + Bx}x^2 \;+\; \left(\frac{C_+(LuxU_0 + P_0)}{A + Bx} + \frac{C_-\,ATP_0}{A + Bx}\right)x \;-\; LuxU_0\,P_0\,\frac{C_+}{A + Bx}.$$

We obtain $nP(x)$ and $qP(x)$ by attaching n resp. q at the constants A, B, $C_\pm$ that are positive, according to Notation 2.1.

Let us identify roots of the equations $nP(x) = 0$, $qP(x) = 0$ and $nP(x) + qP(x) = 0$.

Lemma 2.3
There is at least one root of $nP(x) = 0$, $qP(x) = 0$ *and* $nP(x) + qP(x) = 0$ *in the interval* $(0, LuxU_0)$.

Proof. First, we find $P(0) < 0$ and

$$\begin{aligned} P(LuxU_0) \;&=\; \frac{C_- - C_+}{A + BLuxU_0}LuxU_0^2 - LuxU_0P_0\,\frac{C_+}{A + B\,LuxU_0} \\ &\quad + \left((LuxU_0 + P_0)\frac{C_+}{A + B\,LuxU_0} + ATP_0\;\frac{C_-}{A + B\,LuxU_0}\right)LuxU_0 = \\ &=\; \frac{C_-}{A + BLuxU_0}LuxU_0^2 + ATP_0\;\frac{C_-}{A + B\,LuxU_0}LuxU_0 > 0 \end{aligned}$$

□

Now let us determine the number of roots in the interval $(0, LuxU_0)$.

Lemma 2.4
There is a unique root of $nP(x) = 0$, $qP(x) = 0$ *and* $nP(x) + qP(x) = 0$ *in the interval* $(0, LuxU_0)$.

Proof. The equation $nP(x) = 0$ can be multiplied by $nA + nB\,x$, and we are left with a quadratic polynomial

$$0 = (nC_- - nC_+)x^2 + \big(nC_+(LuxU_0 + P_0) + nC_-\,ATP_0\big)x - LuxU_0\,P_0\,nC_+.$$

We calculated $nC_+ - nC_- \ll 0$ and thus the quadratic term is multiplied by a positive constant and this polynomial tends to infinity for $x \to \pm\infty$. As $nP(0) < 0$, there is,

apart of the root in $(0, LuxU_0)$, a further, negative root. Hence, the root in $(0, LuxU_0)$ is unique. Similarly, the root of $qP(x) = 0$ is unique.

Now let us investigate $nP(x) + qP(x) = 0$. All terms

$$\frac{(C_- - C_+)x^2}{A + Bx}, \quad (LuxU_0 + P_0)\frac{C_+ x}{A + Bx}, \quad ATP_0 \frac{C_- x}{A + Bx}, \quad -LuxU_0P_0 \frac{C_+}{A + Bx}.$$

are monotonously increasing in $(0, LuxU_0)$. Thus, there is only one single root in $(0, LuxU_0)$. □

Moreover we investigate the root of $nP(x) + qP(x) = 0$.

Lemma 2.5
The root of $nP(x) + qP(x) = 0$ *is between the roots of* $nP(x) = 0$ *and* $qP(x) = 0$.

Proof. Let x_n be the root of $nP(x) = 0$, x_q the root of $qP(x) = 0$, and $\hat{x}$ the root of $nP(x) + qP(x) = 0$. From Lemma 2.4 we know that $x_n, x_q, \hat{x} \in (0, LuxU_0)$. If $x_n = x_q$ then we find immediately $\hat{x} = x_n = x_q$.

Now let us assume $x_q < x_n$. From $nP(x_n) = 0$ and the monotonicity of $nP(x)$ we find $nP(x_q) < 0$. Consequently $nP(x_q) + qP(x_q) < 0$, since $qP(x_q) = 0$. Similarly we find, $qP(x_n) > 0$ and also $qP(x_n) + nP(x_n) > 0$. Therefore,

$$nP(x_q) + qP(x_q) < 0 < qP(x_n) + nP(x_n).$$

For $x_n < x_q$ we can use parallel arguments and obtain

$$qP(x_n) + nP(x_n) < 0 < nP(x_p) + qP(x_q)$$

Hence, we find $\hat{x} \in (x_q, x_n)$. □

Intuitively, this result can be understood as follows. One may view the situation as two basins or reservoirs of phosphor (ATP and LuxUP), connected by two pipes with pumps, LuxN and LuxQ. If the pipe LuxN achieves a certain equilibrium, and LuxQ another, the combined pipes will archive an equilibrium between the two: if the stronger pump LuxN tries to force LuxUP at a higher equilibrium than the weaker pump LuxQ will start to reverse the phosphor flow and pumps phosphor back into the ATP reservoir. The autoinducers change the efficiency of the pumps LuxN and LuxQ, and, in this way, modify the equilibrium concentration of LuxUP.

These theoretical findings give a first hint that our picture is not complete. A further, strong hint is an experiment using LuxN and a mutant of LuxQ, where the phosphor binding aspartate residue of LuxQ has been exchanged. In the following we denote the mutant of LuxQ by LuxQ-. I.e., LuxQ- is not able to exchange phosphor with LuxU. One thus expects that the experimental system with respect to LuxUP behaves like the system with LuxN only. Nevertheless, the data look quite similar to that of the combination between LuxQ and LuxN, and not at all like the data for LuxN alone. The

data are given in Figure 2.4 (right panel,crosses), the prediction of the model developed so far is shown in Figure 2.4 (left panel, solid curve). This result is an experimental proof that an additional interaction between LuxN and LuxQ is going on. The observations are in line with the fact that an AND gate is a highly nonlinear function.

An OR gate may be considered as a linear superposition of signals, followed by a downstream threshold element, whereas the AND gate involves some kind of multiplication. A multiplication necessarily implies a close interaction of both channels. The point of view present in the literature about *Vibrio harveyi* up to now, and mapped into a mathematical model in the previous sections, is seemingly not sufficient to implement dependencies of the two input channels strong enough to represent the biochemical system.

2.4. Additional component: conformational change of LuxU

Our analysis revealed that necessarily an additional assumption is required to understand the experimental findings. One could think especially of the following possibilities:

1. *Direct interaction of LuxQ and LuxN.* If LuxQ and LuxN interact directly, the rates of phosphotransfer can be arbitrarily altered for one sensor kinase in the presence of the other sensor kinase. This additional degree of freedom in the choice of parameters is sufficient to explain the data. However, the experimental setup separates the sensor kinases spatially. There is no reasonable chance for LuxN to get in the spatial vicinity of LuxQ and vice versa. This fact rules out this explanation.
2. *Changed LuxU conformation.* The only known protein that is in contact with both LuxN and LuxQ and that – at the same time – plays a central role in the signaling cascade of *Vibrio harveyi* is LuxU. Especially the experiments with the phosphatase negative mutant LuxQ- strongly indicate that the information of the presence of both sensor kinases is somehow spread over the complete system. As LuxU plays a central role, it is natural to assume that LuxU itself codes this information. One can conjecture that the sensor kinases have two functions on LuxU. One is responsible for the phosphotransfer, while the second leads to a conformational change of LuxU.

We thus assume that LuxU may be present in two different forms, see Figure 2.5. On the one hand LuxU is present as native LuxU and on the other side as modified form of LuxU, that we call LuxU*. We further assume that both forms of LuxU can be phosphorylated, i.e. we find LuxUP and LuxU*P. The experiments, however, cannot distinguish between LuxU and LuxU* respectively LuxUP and LuxU*P. These assumptions are, of course, highly speculative. However, as we will see, this simple assumption is sufficient to explain all shortcomings of the previous model. Furthermore, there are biochemical indications that LuxU may have second active histidine residue with unknown functionality [12, 49]. This observation is in line with the present hypothesis. In order to meet the present data, we assume that only the LuxQ(AI-2) (i.e. LuxQ with or without bound AI-2) complex has

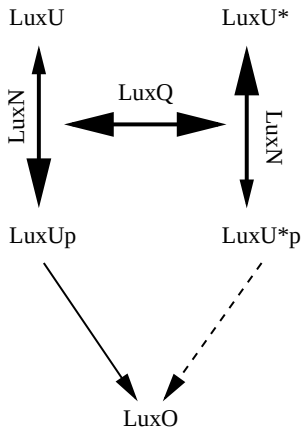

Figure 2.5.: Idea of mechanism developed in this work. While LuxN basically (de)phosphorylate LuxU, LuxQ influences mainly the equilibrium between LuxU and LuxU*.

the ability to transform LuxU to LuxU*. Furthermore, we assume that LuxU* switches back to LuxU spontaneously. Last, the rates of phosphotransfer between LuxQ(AI-2) and LuxU resp. LuxU* do not differ, while the rates of phosphotransfer from the LuxN(HAI-1) (i.e. LuxN with or without bound HAI-1) complex to LuxU are much higher than from LuxN(HAI-1) to LuxU*. Whereas, the reverse direction is much more efficient between LuxU*P and LuxN(HAI-1) than between LuxUP and LuxN(HAI-1). We will see that this rather simple version of the extended model is sufficient to meet the data.

I.e., without LuxQ(AI-2) there is no LuxU*, and LuxQ(AI-2) does not discriminate between LuxU and LuxU*. This allows us to keep the satisfying results for the single pathays. The trajectories shown in Figure 2.3 do not differ for both models. We only find an effect for the combined pathways. LuxQ(AI-2) creates LuxU*, and LuxN(HAI-1) performs less efficient as a kinase on a mixture of LuxU and LuxU*. In this situation we find parameters that very nicely reproduce the dynamics for the combination of LuxQ and LuxN, and also for the combination of LuxQ- and LuxN (Figure 2.4 (b)). Furthermore, the presented model is able to reproduce the results in the presence of LuxQ, LuxN and autoinducers (Figure 2.6).

Of course, even if we accept this hypothesis, we expect the reality to be more complex: LuxN(HAI-1) as well as LuxQ(AI-2) are able to transfer phosphor between ATP/ADP and LuxU/LuxUP. Most likely, LuxN(HAI-1) as well as LuxQ(AI-2) will be also able to transform LuxU to LuxU* and *vice versa*. However, while LuxN(HAI-1) dominates the phosphotransfer, LuxQ(AI-2) dominates the transition between LuxU(P) and LuxU*(P). The two kinases basically modify different parts of the pathway.

Summarized, the autoinducer signalling in *V. harveyi* (and probably in related species) allows a sophisticated signal integration, reminding of an AND gate, which probably enables the bacteria to process information of different quality in a highly adaptive manner.

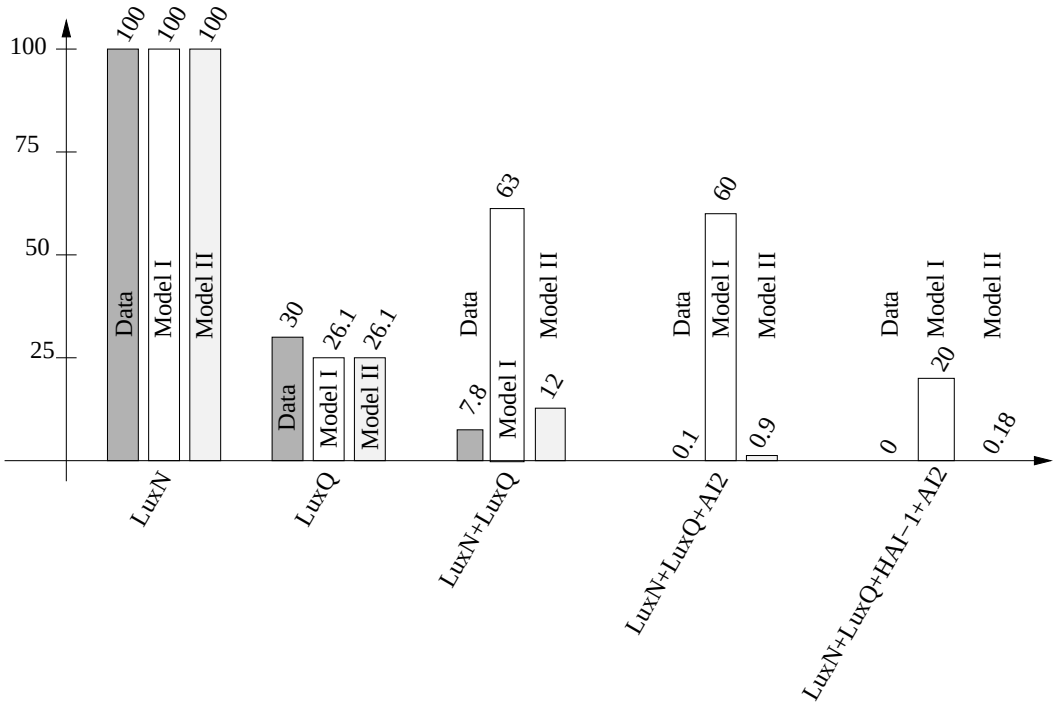

Figure 2.6.: Effect of different combinations of LuxN, LuxQ, and autoinducers. Dark grey are experimental data, white the model predictions without LuxU* (model I), light grey the model predictions with LuxU* (model II). The amount of LuxUP in the experiment without any autoinducer is taken as reference value, i.e. 100%.

For the sake of completeness we list the equations for the complete model with two different states of LuxU:

$$
\begin{aligned}
LuxN + ATP &\rightleftharpoons LuxNPH + ADP && \text{rate}\text{“} \rightarrow \text{”}nk_1,\ \text{rate}\text{“} \leftarrow \text{”}nk_{-1},\\
LuxNAi + ATP &\rightleftharpoons LuxNAiPH + ADP && \text{rate}\text{“} \rightarrow \text{”}nkai_1,\ \text{rate}\text{“} \leftarrow \text{”}nkai_{-1},\\
\\
LuxNPH &\rightleftharpoons LuxNPD && \text{rate}\text{“} \rightarrow \text{”}nk_2,\ \text{rate}\text{“} \leftarrow \text{”}nk_{-2},\\
LuxNAiPH &\rightleftharpoons LuxNAiPD && \text{rate}\text{“} \rightarrow \text{”}nk_2,\ \text{rate}\text{“} \leftarrow \text{”}nk_{-2},\\
\\
LuxNPD + LuxU &\rightleftharpoons LuxN + LuxUP && \text{rate}\text{“} \rightarrow \text{”}nk_3,\ \text{rate}\text{“} \leftarrow \text{”}nk_{-3},\\
LuxNAiPD + LuxU &\rightleftharpoons LuxNAi + LuxUP && \text{rate}\text{“} \rightarrow \text{”}nkai_3,\ \text{rate}\text{“} \leftarrow \text{”}nkai_{-3}\\
\\
LuxNPD + LuxU^* &\rightleftharpoons LuxN + LuxU^*P && \text{rate}\text{“} \rightarrow \text{”}nks_3,\ \text{rate}\text{“} \leftarrow \text{”}nks_{-3},\\
LuxNAiPD + LuxU^* &\rightleftharpoons LuxNAi + LuxU^*P && \text{rate}\text{“} \rightarrow \text{”}nksai_3,\ \text{rate}\text{“} \leftarrow \text{”}nksai_{-3}\\
\\
LuxN + Ai &\rightleftharpoons LuxNAi && \text{rate}\text{“} \rightarrow \text{”}nkai_4,\ \text{rate}\text{“} \leftarrow \text{”}nkai_{-4},\\
LuxNPH + Ai &\rightleftharpoons LuxNAiPH && \text{rate}\text{“} \rightarrow \text{”}nkai_4,\ \text{rate}\text{“} \leftarrow \text{”}nkai_{-4},\\
LuxNPD + Ai &\rightleftharpoons LuxNAiPD && \text{rate}\text{“} \rightarrow \text{”}nkai_4,\ \text{rate}\text{“} \leftarrow \text{”}nkai_{-4}.\\
\\
LuxQ + ATP &\rightleftharpoons LuxQPH + ADP && \text{rate}\text{“} \rightarrow \text{”}qk_1,\ \text{rate}\text{“} \leftarrow \text{”}qk_{-1},\\
LuxQAi + ATP &\rightleftharpoons LuxQAiPH + ADP && \text{rate}\text{“} \rightarrow \text{”}qkai_1,\ \text{rate}\text{“} \leftarrow \text{”}qkai_{-1},\\
\\
LuxQPH &\rightleftharpoons LuxQPD && \text{rate}\text{“} \rightarrow \text{”}qk_2,\ \text{rate}\text{“} \leftarrow \text{”}qk_{-2},\\
LuxQAiPH &\rightleftharpoons LuxQAiPD && \text{rate}\text{“} \rightarrow \text{”}qk_2,\ \text{rate}\text{“} \leftarrow \text{”}qk_{-2},\\
\\
LuxQPD + LuxU &\rightleftharpoons LuxQ + LuxUP && \text{rate}\text{“} \rightarrow \text{”}qk_3,\ \text{rate}\text{“} \leftarrow \text{”}qk_{-3},\\
LuxQAiPD + LuxU &\rightleftharpoons LuxQAi + LuxUP && \text{rate}\text{“} \rightarrow \text{”}qkai_3,\ \text{rate}\text{“} \leftarrow \text{”}qkai_{-3}\\
\\
LuxQPD + LuxU^* &\rightleftharpoons LuxQ + LuxU^*P && \text{rate}\text{“} \rightarrow \text{”}qk_3,\ \text{rate}\text{“} \leftarrow \text{”}qks_{-3},\\
LuxQAiPD + LuxU^* &\rightleftharpoons LuxQAi + LuxU^*P && \text{rate}\text{“} \rightarrow \text{”}qkai_3,\ \text{rate}\text{“} \leftarrow \text{”}qksai_{-3}\\
\\
LuxQ + Ai &\rightleftharpoons LuxQAi && \text{rate}\text{“} \rightarrow \text{”}qkai_4,\ \text{rate}\text{“} \leftarrow \text{”}qkai_{-4},\\
LuxQPH + Ai &\rightleftharpoons LuxQAiPH && \text{rate}\text{“} \rightarrow \text{”}qkai_4,\ \text{rate}\text{“} \leftarrow \text{”}qkai_{-4},\\
LuxQPD + Ai &\rightleftharpoons LuxQAiPD && \text{rate}\text{“} \rightarrow \text{”}qkai_4,\ \text{rate}\text{“} \leftarrow \text{”}qkai_{-4}.\\
\\
LuxU + LuxQ &\rightarrow LuxU^* + LuxQ && \text{rate } k_5,\\
LuxU + LuxQPD &\rightarrow LuxU^* + LuxQPD && \text{rate } k_5,\\
LuxU + LuxQPH &\rightarrow LuxU^* + LuxQPH && \text{rate } k_5,\\
\\
LuxU + LuxQAi &\rightarrow LuxU^* + LuxQAi && \text{rate } kai_5,\\
LuxU + LuxQAiDpai &\rightarrow LuxU^* + LuxQAiPD && \text{rate } kai_5,\\
LuxU + LuxQAiHp &\rightarrow LuxU^* + LuxQAiPH && \text{rate } kai_5,\\
\\
LuxU^* &\rightarrow LuxU && \text{rate } k_6.
\end{aligned}
$$

3. Communication in Small Bacterial Population

In this chapter we investigate the mechanism of Quorum Sensing at the population level. Our aim in this chapter is to develop and analyze a model for the dynamics of small bacterial populations that communicate with each other via the Quorum sensing system, for example micro-colonies on roots of plants in the rhizosphere. The dynamics of the population is driven by the behavior of the cells within the population. Since we are interested in small cell numbers we take into account the effect of intracellular noise. A cell is allowed to switch back and forth between low and high level of signaling molecule production. For large population sizes, the dynamics of the cells can be assumed to be averaged. In the case of small population sizes the state of each cell can influence the dynamics of the population strongly. Thus the question arises, whether the communication in small populations is still effective or if the impact of noise is extensive so that the bacteria cannot understand each other.

For this reason we establish a stochastic model for the population dynamics. Since the underlying mechanism of Quorum sensing is quite similar in most bacteria taxa, we apply the Lux system of *Vibrio fischeri* as the underlying communication system (described in Section 1.1). We associate the population with a probability density function $p(n, x, t)$ where the number of activated cells within the population, $n \in \{0, .., N\}$, is a discrete random variable, while the corresponding AHL molecule concentration $x \in \mathbb{R}_+$ can be treated as a continuous variable. It will be shown that the time evolution of the probability density function is determined by a transport equation.

We analyze the asymptotic behavior of this transport equation. In order to achieve this description, we study the diffusion approximation for a slightly extended transport equation, utilizing the idea that the population dynamics and the signaling live on different time scales. The analysis allows to derive a closed equation for the signaling molecule density only, being of parabolic type.

In addition, we analyze the long time behavior of the AHL distribution for small populations in order to get an idea of the implication of stochasticity, and moreover the long time behavior for large populations will be investigated.

3.1. Stochastic Model

The goal of this section is to derive a probabilistic description of the dynamics of a bacterial population. One can see in Figure 3.1 that the dynamics of the population is driven on the one hand by the behavior of the cells, namely AHL production at high or low level, and on the other hand by the AHL molecule concentration. Because of the small population size we assume to encounter a high stochasticity concerning the behavior of the cells, whereas the dynamics of the AHL concentration is assumed to be deterministic.

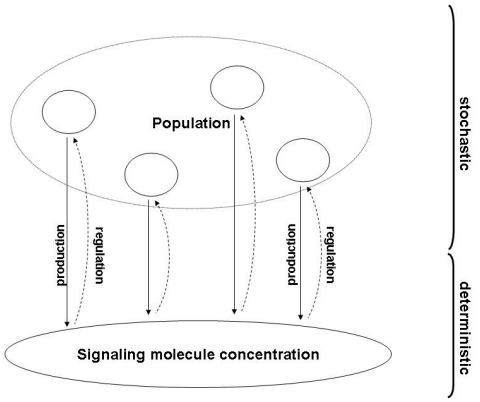

Figure 3.1.: Sketch of the dynamics of a population.

In the first part of this section, we give a probabilistic description of the dynamics of one single cell. The molecular mechanism of Quorum sensing involves several steps, as seen in Figure 1.2. For our model we focus on the stochastic process that governs the binding and dissociation of the AHL/LuxR complex [35].

We regard the cell as a system consisting of a constant number of independently acting LuxR receptor molecules. Then the dynamics of the cell is driven by the dynamics of the LuxR receptor molecules. As a first step, we derive a discrete valued random walk model in one dimension where the state of the cell is defined by the number of LuxR/AHL complexes. Based on this model, we determine a simplified model for one cell where the state of the cell is characterized as "activated" or "resting". Activated cells are cells with a supercritical number of LuxR/AHL complexes, while the number of these complexes is subcritical for resting cells. It turns out that this simplified model approximates the random walk model quite well in the long run.

Our aim of the second part is to describe the behavior of a population consisting of a given number of cells. In addition to the dynamics of the cells we take into account the change of AHL concentration, since cells within the population produce AHL molecules depending on their state. Recently, the investigation of stochastic dynamics of regulatory

pathways attracted an increased attention [21, 25, 26, 43, 50].

We propose a velocity jump model [20] where the continuous variable corresponds to the AHL molecule concentration, whereas the discrete variable describes the different states of the population, determined by the number of activated cells. The model can be written in terms of a transport equation, where the velocity depends on the AHL concentration.

In the final part we prove the existence and uniqueness of solutions for the transport equation.

3.1.1. Dynamics of One Cell

This section is dedicated to the derivation of a model describing the dynamics of one single cell. In a first model we characterize the cell by the number of AHL/LuxR complexes. Furthermore, we simplify the model by assuming that the cell is described as binary random variable that tells us if the cell is activated or resting otherwise. The models are stated under the assumption of independence of the receptor molecules. However, we show that for large cell numbers the mean number of activated cells is essentially equal in both models.

For simplicity the AHL concentration is assumed to be constant during this subsection.

Dynamics of the LuxR Receptor

A main aspect in developing the mathematical model is the fact that the LuxR receptors are independently acting entities that form complexes with AHL molecules, which may dissociate again. The corresponding reaction kinetics is given by

$$\text{AHL} + \text{LuxR} \quad \underset{\gamma_1}{\overset{\kappa}{\rightleftarrows}} \quad \text{AHL/LuxR} \, . \tag{3.1}$$

Here $\kappa \geq 0$ is the association rate of LuxR receptors and AHL molecules, and $\gamma_1 \geq 0$ is the dissociation rate of the AHL/LuxR complex. We are interested in the states of the LuxR receptors within the cell, i.e. we ask whether one receptor is bound to AHL and thus activated or if it is free.

Definition 3.1 In the following we identify LuxR_b as the LuxR/AHL complex respectively bounded LuxR receptor and LuxR_f as the free LuxR receptor. Furthermore, $x \in \mathbb{R}_+$ denotes the density of AHL molecules.

Rewriting the reaction kinetics we obtain the following transition rates describing the change of state for one receptor

$$\begin{array}{rcll} \text{LuxR}_f & \to & \text{LuxR}_b : & \kappa x, \\ \text{LuxR}_b & \to & \text{LuxR}_f : & \gamma_1. \end{array} \tag{3.2}$$

Hence $1/\kappa x$, respectively $1/\gamma_1$ is the mean time between the state transition.

Model for One Cell Based on the Number of LuxR$_b$

To derive a probabilistic description of the dynamics of one cell, based on the number of LuxR$_b$, we use a random walk model with constant transition rates where we consider the number $M \in \mathbb{N}$ of LuxR receptors within a cell to be constant. The transitions are limited to binding and dissociation.

Let $\{m_t, t \geq 0\}$ be a stochastic process where $m_t \in \{0, ..., M\}$ is the number of LuxR$_b$ within the cell at time t. We define

$$p(m,t) := P(\text{state } m \text{ at time } t) = P(m_t = m)$$

as the probability to find the cell in the state $m \in \{0, ..., M\}$ at time $t \in \mathbb{R}_+$. To determine the probabilistic transition laws we define the infinitesimal transition probability per unit time as [14]

$$\lim_{\Delta t \to 0} \frac{1}{\Delta t}\, p(m^*, t + \Delta t | m, t) = P(m^*|m,t) \qquad \text{for } m^* \neq m.$$

If the cell is in state m at a time t, it can either jump to state $m+1$ or to $m-1$. Since the receptors are independently acting entities, the transition $m \to m+1$ implies that one of the $M - m$ free LuxR receptors binds to x with rate κx. To change the state from $m \to m-1$ implies that one of the m bounded LuxR receptors dissociates with rate γ_1.

$$0 \underset{\leftarrow}{\rightarrow} \cdots \underset{\leftarrow}{\rightarrow} m-1 \underset{m\gamma_1}{\overset{(M-(m-1))\kappa x}{\rightleftarrows}} m \underset{(m+1)\gamma_1}{\overset{(M-m)\kappa x}{\rightleftarrows}} m+1 \underset{\leftarrow}{\rightarrow} \cdots \underset{\leftarrow}{\rightarrow} M$$

Thus the transition probabilities from state m to state m^* are

$$\begin{aligned} P(m+1|m,t) &= \kappa x(M-m) && m = 0, ..., M \\ P(m-1|m,t) &= \gamma_1 m && m = 0, ...M. \end{aligned}$$

We have $P(m^*|m,t) = 0 \quad \forall\ m^* \in [0, M] \setminus \{m-1, m, m+1\}$. The states $m = 0$ and $m = M$, where only transition in one direction is possible, ($0 \to 1$ respectively $M \to M-1$), are also covered by this definition.

Kolmogorov's forward equation describes the time evolution of the probability density function $p(m,t)$ for all $m \in \{0, ..., M\}$ at given x as

$$\begin{aligned} \frac{d}{dt}p(m,t) &= \lim_{\Delta t \to 0} \frac{1}{\Delta t}[p(m, t+\Delta t) - p(m,t)] \\ &= \lim_{\Delta t \to 0} \frac{1}{\Delta t} \left[\sum_{i=m-1}^{m+1} p(m, t+\Delta t|i,t)p(i,t) - \sum_{i=m-1}^{m+1} p(i, t+\Delta t|m,t)p(m,t) \right] \\ &= \lim_{\Delta t \to 0} \frac{1}{\Delta t} \big[p(m, t+\Delta t|m-1,t)p(m-1,t) \\ &\qquad + p(m, t+\Delta t|m+1,t)p(m+1,t) - \\ &\qquad - (p(m-1, t+\Delta t|m,t) + p(m+1, t+\Delta t|m,t))p(m,t) \big]. \end{aligned}$$

Substitution of the transition probabilities brings the master equation to the form

$$\begin{aligned}\frac{d}{dt}p(m,t) &= p(m,t)(-\gamma_1 m - \kappa x(M-m)) + p(m+1,t)\gamma_1(m+1) \\ &\quad + p(m-1,t)\kappa x(M-(m-1)).\end{aligned} \tag{3.3}$$

Since the random walk has the finite state space $\{0,...,M\}$, it is necessary to define boundary conditions. The probability to be in state -1 or in state $M+1$ is zero, so we formally agree on

$$p(-1,t) = p(M+1,t) = 0.$$

Let us investigate the stationary solution $p_s(m)$ of (3.3)

$$0 = p_s(m)(-\gamma_1 m - \kappa x(M-m)) + p_s(m+1)\gamma_1(m+1) + p_s(m-1)\kappa x(M-(m-1)).$$

Proposition 3.2
The stationary solution $p_s(m)$ of (3.3) follows a binomial distribution Binom(M,p), where $\mathsf{p} = \frac{\kappa x}{\kappa x+\gamma_1}$.

Proof. The stationary solution can be rewritten as

$$0 = J(m+1) - J(m) \tag{3.4}$$

with

$$J(m) = P(m-1|m,t)p_s(m) - P(m|m-1,t)p_s(m-1).$$

$J(m)$ can be interpreted as the probabilistic flux from state m to state $m-1$. It has to be recognized that m only assumes the values $\{0,...,M\}$. Therefore the transition probability $P(-1|0)$ is equal to zero and with $p_s(-1) = 0$ we find

$$J(0) = P(-1|0)p_s(0) - P(0|-1)p_s(-1) = 0. \tag{3.5}$$

From (3.4) we find $J(m+1) = J(m)$ and together with (3.5) we obtain the detailed balance condition $J(m) \equiv 0$, which implies that there is no net flow of probability in the stationary state and thus

$$p_s(m) = \frac{\kappa x(M-(m-1))}{\gamma_1 m} p_s(m-1),$$

so that

$$p_s(m) = p_s(0)\prod_{l=1}^{m}\frac{\kappa x(M-(l-1))}{\gamma_1 x} = p_s(0)\left(\frac{\kappa x}{\gamma_1}\right)^m \binom{M}{m}.$$

It remains to show that

$$p_s(0) = \left(\frac{\gamma_1}{\kappa x+\gamma_1}\right)^M.$$

As this constant is uniquely defined by

$$\sum_{m=0}^{M} p_s(m) = 1,$$

being indeed true for our choice of $p_s(0)$, the result follows. □

Simplified Model for One Cell

Now we derive a simplified model for one cell, where the state of the cell is characterized as "activated" or "resting".

Definition 3.3 Given a certain threshold $m_0 \in \{0, ..., M\}$. A cell is in the activated state if the number of LuxR_b within the cell exceeds the threshold m_0. If the number of LuxR_b is below this threshold, the cell is in the resting or inactivated state.

The intracellular noise allows the cell to switch back and forth between the two states, defined in Definition 3.3. The model we develop here, describes the transition between these states and does not count the exact number of LuxR_b within the cell. As before we assume that $x \in \mathbb{R}_+$ is constant.

We introduce the time dependent, binary random variable $C(t)$ describing the state of one cell at time t. As before, the receptors are independently acting entities, and thus the dynamics of the cell is driven by the dynamics of the receptors. We define the transition probabilities for the cell to change from the activated state to the inactivated state and vice versa, depending on x, as follows

$$\text{(resting state)} \quad 0 \quad \underset{\mu(x)}{\overset{\nu(x)}{\rightleftarrows}} \quad 1 \quad \text{(activated state)}.$$

$\nu(x)$ is the activation probability per unit time and $\mu(x)$ is the deactivation probability. Notice that this process is a special case of the stochastic process determined in the previous paragraph. The stochastic process of the simplified model, is therefore determined by the infinitesimal transition probabilities per unit time

$$\begin{aligned} P(0|1,t) &= \mu(x), \\ P(1|0,t) &= \nu(x). \end{aligned}$$

Considering $p(c,t)$ as the probability density to find the cell in state $c \in \{0,1\}$ at a time $t \geq 0$ we get the time evolution

$$\begin{aligned} \tfrac{d}{dt}p(0,t) &= -p(0,t)\nu(x) + p(1,t)\mu(x), \\ \tfrac{d}{dt}p(1,t) &= p(0,t)\nu(x) - p(1,t)\mu(x). \end{aligned} \tag{3.6}$$

Again, we emphasize that this is a simplification of the receptor based model. However, as we aim to describe a population of cells, the conclusions we will draw do not depend on the detailed intra cellular dynamics. These observations after all allows us to use this more simple setting for one cell.

Analysis of the stationary solution p_s of (3.6),

$$\begin{aligned} 0 &= -p_s(0)\nu(x) + p_s(1)\mu(x) \\ 0 &= p_s(0)\nu(x) - p_s(1)\mu(x), \end{aligned}$$

results in the following, similar to Proposition 3.2.

Proposition 3.4
The stationary solution $p_s(m)$ *of* (3.6) *follows a binomial distribution Binom*$(1, \mathrm{q})$*, where* $\mathrm{q} = \frac{\nu(x)}{\mu(x)+\nu(x)}$.

Transition Probabilities $\mu(x)$ and $\nu(x)$

To approximate the activation and deactivation rates of one cell for the simplified model we determine the mean waiting time between the jumps from activated to resting state, respectively vice versa, in the full model.

Consider a cell in state m of the full model. We derive a formula for the expected waiting time, T_m, that passes between the transition from m LuxR$_b$ to $m+1$ LuxR$_b$ within one cell. Note, that there may be an excursion to the states $\{0, .., m-1\}$ before the jump to state $m+1$ takes place. We need to take this fact into account. Similarly we define $\widetilde{T}_m$ as the expected waiting time of a cell that is in state m before it jumps to state $m-1$.

To determine T_m we assume a cell with m LuxR$_b$. Because of the dynamics of the cell there are only two possibilities for the next transition

$$m-1 \quad \overset{m\gamma_1}{\longleftarrow} \quad m \quad \overset{(M-m)\kappa x}{\longrightarrow} \quad m+1;$$

one more LuxR$_b$ is formed or one LuxR$_b$ dissociates. The transition probability that a jump occurs, in whatever direction, is determined by

$$P(m^*|m,t) = P(m+1|m,t) + P(m-1|m,t) = m\gamma_1 + (M-m)\kappa x$$

with $m^* = m-1, m+1$. Thus the waiting time within state m before the next jumps occurs, is given by

$$\frac{1}{P(m^*|m,t)} = \frac{1}{m\gamma_1 + (M-m)\kappa x}.$$

The probability to jump from m to $m+1$ is determined by $\frac{(M-m)\kappa x}{m\gamma_1+(M-m)\kappa x}$ while the probability for the jump from m to $m-1$ is $\frac{m\gamma_1}{m\gamma_1+(M-m)\kappa x}$.

Investigating the expected waiting time T_m that elapses between the transition from m to $m+1$, we consider two possible ways. The first possibility is that the cell stays in the current state m and then jumps to $m+1$ immediately. The second possibility is that the cell first jumps back to $m-1$. If the cell is in state $m-1$ there are again two possibilities. To take into account that the cell can jump back to any of the states $\{0, ..., m-1\}$ before it jumps to state $m+1$ we define the formula for the expected waiting time recursively.

Therefore the expected waiting time T_m is composed of the waiting time before a jump occurs and additionally, if the cell jumps back to $m-1$, the expected waiting time for

the jump from $m-1$ to m and m to $m+1$. We obtain

$$\begin{aligned} T_m &= \frac{1}{m\gamma_1+(M-m)\kappa x} + \frac{(M-m)\kappa x\ 0}{m\gamma_1+(M-m)\kappa x} + \frac{m\gamma_1}{m\gamma_1+(M-m)\kappa x}(T_{m-1}+T_m) \\ &= \frac{1}{m\gamma_1+(M-m)\kappa x}(1+m\gamma_1(T_{m-1}+T_m)). \end{aligned} \tag{3.7}$$

We can rewrite this equation as

$$T_m\left(1-\frac{\gamma_1 m}{\gamma_1 m+(M-m)\kappa x}\right) = \frac{1}{(m\gamma_1+(M-m)\kappa x)} + \frac{m\gamma_1}{\gamma_1 m+(M-m)\kappa x}T_{m-1},$$

so that we finally get

$$T_m = A_m + B_m T_{m-1}, \qquad A_m := \frac{1}{(M-m)\kappa x}, \quad B_m := \frac{m\gamma_1}{(M-m)\kappa x}. \tag{3.8}$$

We know the waiting time T_0 to jump from state 0 to state 1, since there is only one possibility

$$T_0 = \frac{1}{P(1|0,t)} = \frac{1}{M\kappa x}.$$

Iteration of (3.8) thus results in

$$T_m = A_m + \sum_{k=1}^{m-1}\left(A_k\prod_{j=k+1}^{m}B_j\right) + T_0\prod_{k=1}^{m}B_k = \sum_{k=0}^{m}\left(A_k\prod_{j=k+1}^{m}B_j\right).$$

Similar arguments can be used to determine $\widetilde{T}_m$, which describes the expected waiting time between the jump from m to $m-1$

$$\widetilde{T}_m := \frac{1}{\gamma_1 m+(M-m)\kappa x}(1+(M-m)\kappa x(\widetilde{T}_{m+1}+\widetilde{T}_m)).$$

And inserting iteratively results in

$$\widetilde{T}_m = \sum_{k=m}^{M}\left(C_k\prod_{j=m}^{k-1}D_j\right),$$

where

$$C_m := \frac{1}{m\gamma_1}, \qquad D_m := \frac{(M-m)\kappa x}{m\gamma_1}.$$

To approximate the transition rate $\nu(x)$, we assume that the cell has just changed state from activated to resting. That means the state of the cell at that time is m_0-1. We need to investigate the mean time T_{m_0-1} of staying in the resting state, before the cell jumps back to the activated state. With the same argumentation we obtain the

deactivation rate $\nu(x)$ which is determined by the mean time $\widetilde{T}_{m_0}$. Hence the transition rates should be defined as

$$\nu(x) := \frac{1}{T_{m_0-1}}, \qquad \mu(x) := \frac{1}{\widetilde{T}_{m_0}}. \tag{3.9}$$

where

$$\begin{aligned} T_{m_0-1} &= \sum_{k=0}^{m_0-1} \left[\frac{1}{\gamma_1 m_0} \left(\frac{\gamma_1}{\kappa x}\right)^{m_0-k} \binom{M}{k} \binom{M}{m_0}^{-1} \right], \\ \widetilde{T}_{m_0} &= \sum_{k=m_0}^{M} \left[\frac{1}{\gamma_1 m_0} \left(\frac{\kappa x}{\gamma_1}\right)^{k-m_0} \binom{M}{k} \binom{M}{m_0}^{-1} \right]. \end{aligned}$$

Notice that for $x \in \mathbb{R}_+$ the activation rate $\nu(x)$ is a monotonously increasing and the deactivation rate $\mu(x)$ is a monotonously decreasing function. Both transition rates are furthermore strictly positive functions.

Let us define two modes of measurement, where we obtain sample values of the random variable describing the state of a cell, also denoted as random characteristics [22]. The random variable for the state of a cell in the first mode is given by the number of LuxR_b. In the second mode the random variable is the state of the cell based on activation and resting. The aim is to justify our above choice of the transition rates. We show that for large cell numbers the mean number of activated cells is essentially equal in both models.

Based on the stochastic process $\{m_t, t \geq 0\}$, where $m_t \in \{0, ..., M\}$ describes the number of LuxR_b within one cell, we define the random variable

$$\chi_{\{m_t \geq m_0\}} = \begin{cases} 1 & \text{if } m_t \geq m_0, \\ 0 & \text{otherwise} \end{cases}$$

The first measurement mode for the full sample of N cells is constructed as

$$X_{1,t}^N := \frac{1}{N} \sum_{i=0}^{N} \chi_{\{m_t^i \geq m_0\}}$$

where m_t^i are i.i.d. describing the number of LuxR_b in the i-th cell.
The second mode of measurement for the simplified model is determined by the stochastic process $\{C_t, t \geq 0\}$, where C_t describes whether the cell is activated or resting. Hence we define

$$X_{2,t}^N := \frac{1}{N} \sum_{i=0}^{N} C_t^i.$$

The family $(C_t^i)_{t\geq 0}$ as well as the family $(\chi_{\{m_t^i \geq m_0\}})_{t\geq 0}$ are i.i.d and as a consequence of the law of large numbers we obtain

$$\begin{aligned} X_{1,t}^N &\to \mu_1 \quad \text{for} \quad N \to \infty \\ X_{2,t}^N &\to \mu_2 \quad \text{for} \quad N \to \infty \end{aligned}$$

with finite expectation values $\mu_1 = E(\chi_{\{m_t \geq m_0\}})$ and $\mu_2 = E(C_t)$. By investigation of the expectation values $E(\chi_{\{m_t \geq m_0\}})$ and $E(C_t)$ we obtain

$$\begin{aligned} E(C_t) &= 0 \cdot P(C_t = 0) + 1 \cdot P(C_t = 1) = \frac{\nu(x)}{\mu(x) + \nu(x)} = \frac{\widetilde{T}_{m_0}}{\widetilde{T}_{m_0} + T_{m_0 - 1}} \\ &= \frac{\sum_{k=m_0}^{M} \left[\left(\frac{\kappa x}{\gamma_1} \right)^k \binom{M}{k} \right]}{\sum_{k=m_0}^{M} \left[\left(\frac{\kappa x}{\gamma_1} \right)^k \binom{M}{k} \right] + \sum_{k=0}^{m_0 - 1} \left[\left(\frac{\gamma_1}{\kappa x} \right)^{-k} \binom{M}{k} \right]} = \frac{\sum_{k=m_0}^{M} \left[\left(\frac{\kappa x}{\gamma_1} \right)^k \binom{M}{k} \right]}{\sum_{k=0}^{M} \left[\left(\frac{\kappa x}{\gamma_1} \right)^k \binom{M}{k} \right]} \\ &= \left(\frac{\gamma_1}{\kappa x + \gamma_1} \right)^M \sum_{k=m_0}^{M} \left[\left(\frac{\kappa x}{\gamma_1} \right)^k \binom{M}{k} \right], \end{aligned}$$

furthermore,

$$\begin{aligned} E(\chi_{\{m_t \geq m_0\}}) &= 0 \cdot P(m_t < m_0) + 1 \cdot P(m_t \geq m_0) = \sum_{i=m_0}^{M} P(m_t = i) \\ &= \sum_{i=m_0}^{M} \binom{M}{i} \mathrm{p}^i (1 - \mathrm{p})^{M-i} = \left(\frac{\gamma_1}{\kappa x + \gamma_1} \right)^M \sum_{i=m_0}^{M} \left[\binom{M}{i} \left(\frac{\kappa x}{\gamma_1} \right)^i \right], \end{aligned}$$

where $\mathrm{p} = \frac{\kappa x}{\kappa x + \gamma_1}$.
Thus we find $E(C_t) = E(\chi_{\{m_t \geq m_0\}})$ so that both models have essentially the same mean number of activated cells for large enough cell numbers, respectively samples.

3.1.2. Mathematical Model for the Complete System

Based on the simplified model for one cell we establish a model for the whole population in this section. For the description of the dynamics of the population we have to take into account that the cells within the population produce AHL molecules at different levels and therefore x is not constant. So let us propose a velocity jump model [39] where the continuous variable corresponds to the AHL concentration whereas the discrete variable describes different states of the population, which determine the number of activated cells.

For the mathematical setting we adopt a constant population of $N \in \mathbb{N}$, $N < \infty$, cells. The state of the population is characterized by the number of activated cells. We define $n \in I := \{0, ..., N\} \subset \mathbb{N}$, $|I| = N + 1$, as the state space of the population. Conditioned on the AHL concentration, the cells are independently acting entities and follow the dynamics derived in the previous section. In contrast to the afore discussed model, we have to introduce $x \in \mathbb{R}$ as a second, continuous variable, to characterize the complete state of the system. This second variable bears some similarities with a spatial structure.

Additionally we define the velocity $v_n(x) : I \times \mathbb{R}_+ \to \mathbb{R}$ which describes the change of the AHL concentration over time. The velocity depends upon the number of activated cells within the population and is defined for all $n \in I$ as follows

$$v_n(x) \quad := \quad \frac{d}{dt}x(t)\Big|_n = \alpha N + \beta n - \gamma x. \tag{3.10}$$

Here $\alpha > 0$ denotes the small constitutive production of AHL of the resting cells, $\beta > \alpha$ is the increased AHL production of activated cells and $\gamma > 0$ is the degradation rate of the AHL molecules.

For arbitrary $n \in I$ the stationary solution of (3.10) is $x_s \equiv x_s(n) = \frac{\alpha N + \beta n}{\gamma}$. We see that $x_s(n)$ increases with n. Thus we find

$$x_{min} := x_s(0) = \frac{\alpha N}{\gamma} \qquad \text{and} \qquad x_{max} := x_s(N) = \frac{(\alpha+\beta)N}{\gamma}. \tag{3.11}$$

As $\alpha, \gamma, N > 0$ clearly we have $x_{min} > 0$. Moreover we find that x is bounded on an invariant interval $\Omega := (x_{min}, x_{max})$ since $v_n(x)$ is a monotone function in x and for all $n \in I$

$$v_n(x_{min}) = \beta n \geq 0 \qquad \text{and} \qquad v_n(x_{max}) = \beta(n - N) \leq 0.$$

The monotonicity of the velocity also implies

$$\|v_n(\cdot)\|_\infty := \max_{x \in \overline{\Omega}} |v_n(\cdot)| = \max\{|\beta n|, |\beta(n-N)|\} < \infty \qquad \forall\, n \in I.$$

Define $p_n(x,t)$ as the probability to find $n \in I$ activated cells within the population at signaling molecule concentration $x \in \overline{\Omega}$ at time $t \geq 0$. To obtain the time evolution of $p_n(x,t)$ for given $n \in I$, we decompose

$$\partial_t p_n(x,t) = \big(\partial_t p_n(x,t)\big)_{drift} + \big(\partial_t p_n(x,t)\big)_{sp}$$

where $\big(\partial_t p\big)_{drift}$ denotes the change of the AHL density over time and $\big(\partial_t p\big)_{sp}$ constitutes the change of the number of activated cells within the population over time. These two terms can be investigated separately, since there is no direct dependence in the change of the two random variables. Note that $x(t)$ is continuous in time and a jump in n does not imply an instantaneous change in x. Also the transition rates $\mu(x)$ and $\nu(x)$ are continuous in x and therefore a change in x does not imply a immediate state change.

First of all, we model the state change of the population, $\big(\partial_t p\big)_{sp}$, where we assume the production of x to be constant once more, so that the population only senses a constant AHL molecule density $\tilde{x}$. The cells are independently acting entities and thus the dynamics of the population is driven by the dynamics of the N cells. A scheme of the transition graph is given below.

$$0 \underset{\leftarrow}{\rightarrow} \cdots \underset{\leftarrow}{\rightarrow} n-1 \underset{n\mu(\tilde{x})}{\overset{(N-(n-1))\nu(\tilde{x})}{\rightleftarrows}} n \underset{(n+1)\mu(\tilde{x})}{\overset{(N-n)\nu(\tilde{x})}{\rightleftarrows}} n+1 \underset{\leftarrow}{\rightarrow} \cdots \underset{\leftarrow}{\rightarrow} N$$

Define the transition probabilities per unit time as done in Section 3.1.1.

$$\begin{aligned} P(n+1|n,\tilde{x},t) &= (N-n)\nu(\tilde{x}) && n=0,...,N-1, \\ P(n-1|n,\tilde{x},t) &= n\mu(\tilde{x}) && n=1,...,N \end{aligned}$$

Hence we derive the time evolution for the population to be in state n at time t with constant signaling molecule concentration $\tilde{x}$, analogous to the receptor based model in Section 3.1.1 as

$$\begin{aligned} \big(\partial_t p_n(\tilde{x},t)\big)_{sp} &= -(n\mu+(N-n)\nu)p_n(\tilde{x},t)+(N-(n-1))\nu p_{n-1}(\tilde{x},t)+ \\ &\quad +(n+1)\mu p_{n+1}(\tilde{x},t). \end{aligned}$$

Next we encounter $\big(\partial_t p\big)_{drift}$. Consider an interval $\omega := [\omega_1,\omega_2]$ in the x-space Ω. As we are interested in the change of x over time, we assume that there is a given constant number n^* of activated cells within the population. The flux $J(x,t)$ of the system, which measures the amount x that will flow through a small area during a small time interval, is given by

$$J(x,t) = -v_{n^*}(x)p_{n^*}(x,t).$$

Hence the rate of change of x inside the interval ω is given by the relation

$$\partial_t \int_\omega p_{n^*}(x,t)dx = J(\omega_1,t) - J(\omega_2,t) = \int_\omega \partial_x J\, dx.$$

In the limit, where ω becomes small we get

$$\partial_t p_{n^*}(x,t) - \partial_x J(x,t) = 0,$$

where we assume p to be C^1 both on x and t, so that

$$\big(\partial_t p_{n^*}(x,t)\big)_{drift} = -\partial_x(v_{n^*}(x)p_{n^*}(x,t)).$$

We obtain the time evolution of the density function $p_n(x,t)$ of the complete model by adding up $\big(\partial_t p\big)_{drift}$ and $\big(\partial_t p\big)_{sp}$. This results in a transport equation, that describes the velocity jump process governing the population dynamics, for all $n \in I$,

$$\begin{aligned} \partial_t p_n(x,t) + \partial_x(v_n(x)p_n(x,t)) &= -(n\mu(x)+(N-n)\nu(x))p_n(x,t) \\ &\quad +(N-(n-1))\nu(x)p(n-1,x,t)+(n+1)\mu(x)p(n+1,x,t). \end{aligned} \tag{3.12}$$

Eventually, we show that there exists a unique solution of the transport equation (3.12) describing the population dynamics. In this sense our model is well-posed.

Definition 3.5 We define

$$\mathbf{p}(x,t) := \begin{pmatrix} p_0(x,t) \\ p_1(x,t) \\ \vdots \\ p_N(x,t) \end{pmatrix}, \qquad \mathbf{v}(x) := \begin{pmatrix} v_0(x) \\ v_1(x) \\ \vdots \\ v_N(x) \end{pmatrix}, \qquad \mathbf{n} := \begin{pmatrix} 0 \\ 1 \\ \vdots \\ N \end{pmatrix}$$

with $\mathbf{p}(x,t) : I \times \Omega \times [0,\infty) \to \mathbb{R}^{N+1}$ and $\mathbf{v}(x) : I \times \Omega \to \mathbb{R}^{N+1}$.
Additionally we define a elementwise product, for $\phi, \psi \in \mathbb{R}^{M+1}$

$$\psi \odot \phi := \begin{pmatrix} \psi_0\phi_0 \\ \psi_1\phi_1 \\ \vdots \\ \psi_M\phi_M \end{pmatrix} \in \mathbb{R}^{M+1}. \tag{3.13}$$

With these definitions the transport equation (3.12) can be written as

$$\partial_t \mathbf{p}(x,t) + \partial_x(\mathbf{v}(x) \odot \mathbf{p}(x,t)) = \mathcal{L}_x[\mathbf{p}(x,t)]. \tag{3.14}$$

Additionally we determine the boundary conditions as we assume that the flux on $\partial\Omega$ is equal to zero. Thus we get

$$\mathbf{v}(x) \odot \mathbf{p}(x,t) = 0 \qquad \forall\, x \in \partial\Omega.$$

The transition operator $\mathcal{L}_x : L^2(\Omega) \to L^2(\Omega)$ is determined pointwise by the transition matrix $L_x \in \mathbb{R}^{(N+1)\times(N+1)}$

$$\mathcal{L}_x[\mathbf{p}(x,t)] = L_x \mathbf{p}(x,t).$$

The transition matrix is the infinitesimal generator of the random walk on I and is defined as

$$L_x := \begin{pmatrix} l_0(x) & l_0^+(x) & 0 & & & \cdots & 0 \\ l_1^-(x) & l_1(x) & l_1^+(x) & 0 & & & \\ 0 & l_2^-(x) & l_2(x) & l_2^+(x) & 0 & & \\ \vdots & \ddots & \ddots & \ddots & \ddots & \ddots & \vdots \\ & & 0 & l_{N-2}^-(x) & l_{N-2}(x) & l_{N-2}^+(x) & 0 \\ & & & 0 & l_{N-1}^-(x) & l_{N-1}(x) & l_{N-1}^+(x) \\ 0 & \cdots & & & 0 & l_N^-(x) & l_N(x) \end{pmatrix}. \tag{3.15}$$

where

$$\begin{array}{rcll} l_i(x) & := & -\big(P(n+1|n,x,t) + P(n-1|n,x,t)\big), & i = 0,...,N, \\ l_i^-(x) & := & P(n|n-1,x,t), & i = 1,...,N, \\ l_i^+(x) & := & P(n|n+1,x,t), & i = 0,...,N-1. \end{array} \tag{3.16}$$

The transition rates l_i depend on the number of activated cells within the population and on the AHL concentration. Moreover $1/l_i$ is a measure of the expected waiting time between the state jumps.

Since the number of cells within the population is constant (conservation law), we have, for all $i = 0...N$,

$$l_i(x) = -(l_{i-1}^+(x) + l_{i+1}^-(x))$$

where $l^+_{-1}(x) = l^-_{M+1}(x) = 0$ so that

$$\mathbf{e}^T L_x = \mathbf{0}$$

with $\mathbf{e} = (1, ..., 1)^T \in \mathbb{R}^{N+1}$. For the transition operator we find

$$\sum_{n=0}^{N} \mathcal{L}_x p_n(x,t) = 0.$$

Therefore the operator has a zero left-eigenvalue. In Appendix B.1.2 we show that this left-eigenvalue is simple and we can find a unique right-eigenvector (Perron theory)

$$\mathbf{Y}(x) := \begin{pmatrix} y_0 \\ y_1 \\ \vdots \\ y_N \end{pmatrix} \quad \text{where} \quad y_i := \binom{N}{i} \frac{\mu(x)^{N-i}\nu(x)^i}{(\mu(x)+\nu(x))^N}, \quad i = 0, ..., N. \tag{3.17}$$

As the transition matrix L_x governs the continuous time Markov process, we find that $\mathbf{Y}(x)$ is the stationary probability distribution of the Markov process as

$$\mathbf{Y}(x)^T\ L_x = \mathbf{0} \qquad \text{and} \qquad \mathbf{Y}(x)^T\ \mathbf{e} = 1.$$

For more information about the transition matrix see Appendix B.1.1, where we investigated the structure of the transition matrix and calculated especially its eigenvalues and eigenvectors as we need this information later during the diffusion limit.

Existence of the Solution

Eventually, we prove the existence of the solution of the transport equation (3.14), which can be rewritten in the form

$$\partial_t \mathbf{p}(x,t) \quad = \quad \mathcal{A}\mathbf{p}(x,t) + \mathcal{L}_x \mathbf{p}(x,t) \tag{3.18}$$

where the operator $\mathcal{A}$ is defined by

$$\mathcal{A}\phi(x) \quad := \quad -\partial_x(\mathbf{v}(x) \odot \phi(x))$$

with domain $D(\mathcal{A}) = \{\phi \in L^2(\Omega)^{N+1} : \phi_n(\cdot) \in H^1(\Omega) \quad \forall\ n \in I\}$.
Notice that $L^2(\Omega)^{N+1}$ is a Hilbert space with the scalar procuct

$$\langle \phi, \psi \rangle_{L^2(\Omega)^{N+1}} = \sum_{i \in I} \langle \phi_i(\cdot), \psi_i(\cdot) \rangle_{L^2(\Omega)}.$$

Theorem 3.6 (Existence and uniqueness of the transport equation)
For each $\phi(x) \in D(\mathcal{A})$ there exists a unique solution of the initial value problem

$$\begin{array}{rcll} \partial_t \mathbf{p}(x,t) & = & \mathcal{A}\mathbf{p}(x,t) + \mathcal{L}_x \mathbf{p}(x,t) & \text{for } x \in \Omega, \\ 0 & = & \mathbf{v}(x) \odot \mathbf{p}(x,t) & \text{for } x \in \partial\Omega, \\ \mathbf{p}(x,0) & = & \phi(x). & \end{array} \tag{3.19}$$

To prove Theorem 3.6 we need the following auxiliary result.

Lemma 3.7
Let $\phi \in L^2(\Omega)$, and $\varphi_t : \overline{\Omega} \to \overline{\Omega}$ a family of C^1 functions with

$$\lim_{t\to 0} \|\varphi_t(x) - x\|_{C^0(\Omega)} = 0$$

and $\varphi_t'(x) \geq \mu > 0$ for all $x \in \overline{\Omega}$, $t \leq t_0$ (for some positive t_0). Then

$$\lim_{t\to 0} \|\phi \circ \varphi_t - \phi\|_{L^2(\Omega)} = 0.$$

Proof. Choose $\varepsilon > 0$. As $C^1(\overline{\Omega})$ is dense in $L^2(\Omega)$, we find $\psi \in C^1(\overline{\Omega})$ s.t.

$$\|\phi - \psi\|_{L^2(\Omega)} \leq \min\{\varepsilon/3, \sqrt{\mu}\varepsilon/3\}.$$

Furthermore, as $\psi \in C^1(\overline{\Omega})$, we find $t_1 = t_1(\varepsilon) > 0$ such that $t_1 \leq t_0$ and

$$\forall t \in [0, t_1) : \ \|\psi \circ \varphi_t - \psi\|_{L^2(\Omega)} \leq \varepsilon/3.$$

Now, with substituting $z = \varphi_t(x)$,

$$\begin{aligned}\left(\int_{x_{min}}^{x_{max}} (\phi \circ \varphi_t(x) - \psi \circ \varphi_t(x))^2 \, dx\right)^{1/2} &= \left(\int_{\varphi_t(x_{min})}^{\varphi_t(x_{max})} (\phi(z) - \psi(z))^2 \frac{1}{\varphi_t'(\varphi_t^{-1}(z))} \, dz\right)^{1/2} \\ &\leq \frac{1}{\sqrt{\mu}} \, \|\phi - \psi\|_{L^2(\Omega)} \leq \varepsilon/3.\end{aligned}$$

Thus, for $0 \leq t < t_1 = t_1(\varepsilon) \leq t_0$, we find

$$\|\phi \circ \varphi_t - \phi\|_{L^2(\Omega)} \leq \|\phi \circ \varphi_t - \psi \circ \varphi_t\|_{L^2(\Omega)} + \|\psi \circ \varphi_t - \psi\|_{L^2(\Omega)} + \|\psi - \phi\|_{L^2(\Omega)} \leq \varepsilon.$$

Hence, for each $\varepsilon > 0$ we find $t_1(\varepsilon) > 0$ s.t. for all $0 \leq t < t_1(\varepsilon)$ it is true that

$$\|\phi \circ \varphi_t - \phi\|_{L^2(\Omega)} \leq \varepsilon.$$

Therefore, the limit $t \to 0$ exists and

$$\lim_{t\to 0} \|\phi \circ \varphi_t - \phi\|_{L^2(\Omega)} = 0. \qquad \square$$

Proof. (Theorem 3.6) The proof is based on semigroup theory [3, 5, 24, 41]. We first show that $\mathcal{A}$ is the infinitesimal generator of a C_0 semigroup of bounded linear operators. Indeed, let $\pi_{n,t}x_0$ denote the solution of the equation

$$\frac{d}{dt}x(t)\big|_n = v_n(x(t))$$

for $n \in I$, with $x(0) = x_0$, i.e.

$$x(t)|_n = \pi_{n,t}x_0 = \frac{1}{\gamma}(\alpha N + \beta n - e^{-\gamma t}(\alpha N + \beta n - \gamma x_0)).$$

Note, that $\Omega = (x_{min}, x_{max})$ is an invariant region under this flow. We define

$$\pi_t(x) := (\pi_{0,t}, \pi_{1,t}, ..., \pi_{N,t})^T : \Omega^{N+1} \to \Omega^{N+1}.$$

If $\phi : \Omega^{N+1} \to \Omega^{N+1}$ is a differentiable function, then the initial value problem

$$\partial_t \mathbf{p}(x,t) = -\partial_x(\mathbf{v}(x) \odot \mathbf{p}(x,t)), \qquad \mathbf{p}(x,0) = \phi(x)$$

has a unique classical solution of the form

$$\mathbf{p}(x,t) = \phi(\pi_{-t}x)\partial_x(\pi_{-t}x) = \phi(\pi_{-t}x)e^{\gamma t}.$$

Otherwise we define the solution operator

$$P_t\phi(x) := \phi(\pi_{-t}x)e^{\gamma t}, \qquad \phi \in D(\mathcal{A}).$$

Observe that $\{P_t\}_{t\geq 0}$ is a semigroup of linear bounded operators on $D(\mathcal{A})$. Indeed for $\phi \in D(\mathcal{A})$ we have, for all $n \in I$,

$$\begin{aligned} P_0\phi(x) &= \phi(\pi_0 x) = \phi(x) \\ P_{t+s}\phi(x) &= \phi(\pi_{t+s}x)e^{\gamma(t+s)} = \phi(\pi_t\pi_s x)e^{\gamma s}e^{\gamma t} = P_t\phi(\pi_s x)e^{\gamma s} = P_tP_s\phi(x) \end{aligned}$$

Moreover, for $n \in I$,

$$\begin{aligned} \|P_t\phi_n(x)\|_{L^2(\Omega)} &= \left(\int_\Omega |P_t\phi_n(x)|^2 dx\right)^{1/2} = \left(\int_\Omega \phi_n^2(\pi_{n,-t}x)e^{2\gamma t}dx\right)^{1/2} = \\ &= \left(\int_\Omega \phi_n^2(y)e^{\gamma t}dy\right)^{1/2} = e^{\gamma t/2}\|\phi(y)\|_{L^2(\Omega)} \end{aligned}$$

and consequently we obtain

$$\begin{aligned} \|P_t\phi\|^2_{L^2(\Omega)^{N+1}} &= \sum_{i\in I}\|P_t\phi_i(x)\|^2_{L^2(\Omega)} = e^{\gamma t}\sum_{i\in I}\|\phi_i(y)\|^2_{L^2(\Omega)} = e^{\gamma t}\|\phi\|^2_{L^2(\Omega)^{N+1}}, \\ \|P_t\phi\|_{L^2(\Omega)^{N+1}} &= e^{\gamma t/2}\|\phi\|_{L^2(\Omega)^{N+1}}. \end{aligned} \tag{3.20}$$

Since $H^1(\Omega)^{N+1}$ is dense in $L^2(\Omega)^{N+1}$ we find $\psi_s \in H^1(\Omega)^{N+1}$ and $\psi \in L^2(\Omega)^{N+1}$ with $\psi_s \to \psi$ so that

$$\|P_t\psi_s - P_t\psi\|_{L^2(\Omega)^{N+1}} = \|P_t(\psi_s - \psi)\|_{L^2(\Omega)^{N+1}} \leq e^{1/2\gamma t}\|\psi_s - \psi\|_{L^2(\Omega)^{N+1}} \to 0$$

We showed that P_t is a continuous extension of the solution operator from $H^1(\Omega)^{N+1}$ to $L^2(\Omega)^{N+1}$.
Finally, one has to show the strong continuity of P_t.

$$\begin{aligned} \lim_{t\to 0}\|P_t\phi - \phi\|_{L^2(\Omega)^{N+1}} &= \lim_{t\to 0}\|\phi(\pi_{-t}x)e^{\gamma t} - \phi(x)\|_{L^2(\Omega)^{N+1}} \\ &\leq \lim_{t\to 0}\|\phi(\pi_{-t}x)e^{\gamma t} - \phi(\pi_{-t}x)\|_{L^2(\Omega)^{N+1}} + \lim_{t\to 0}\|\phi(\pi_{-t}x) - \phi(x)\|_{L^2(\Omega)^{N+1}} \end{aligned}$$

As consequence of (3.20) we immediately find

$$\lim_{t\to 0}\|\phi(\pi_{-t}x)e^{\gamma t} - \phi(\pi_{-t}x)\|_{L^2(\Omega)^{N+1}} = 0.$$

Still, it remains to show that $\lim_{t\to 0}\|\phi(\pi_{-t}x) - \phi(x)\|_{L^2(\Omega)^{N+1}} = 0$. Since $\pi_{n,t}(x)$ is a family of C^1-functions that satisfy the conditions of Lemma 3.7 we obtain for $\phi \in L^2(\Omega)$

$$\lim_{t\to 0}\|\phi(\pi_{n,t}(x)) - \phi(x)\|_{L^2(\Omega)} = 0$$

and for $\phi \in D(\mathcal{A})$

$$\lim_{t\to 0}\|\phi(\pi_t(x)) - \phi(x)\|_{L^2(\Omega)^{N+1}} \leq \sum_{i\in I}\lim_{t\to 0}\|\phi_i(\pi_{i,t}(x)) - \phi_i(x)\|_{L^2(\Omega)} = 0$$

Now it follows from the semigroup theory [3, 24, 41] that the operator $\mathcal{A}$ with domain $D(\mathcal{A})$ is the infinitesimal generator of the C^0 semigroup $\{P_t\}_{t\geq 0}$.

$\mathcal{L}_x$ is a bounded linear operator with domain

$$\mathcal{D}(\mathcal{L}_x) = C(\Omega)^{N+1} \supset D(\mathcal{A}).$$

From the perturbation theory of linear operators we can conclude that the operator $\mathcal{A}+\mathcal{L}_x$ with domain $D(\mathcal{A}+\mathcal{L}_x) = D(\mathcal{A})$ is the infinitesimal generator of a C_0 semigroup $\{S_t\}_{t\geq 0}$ of linear bounded operators on $L^2(\Omega)^{N+1}$, see e.g. [24, Chapter 3, Theorem 1.1].

Once again semigroup theory, e.g. [41, Chapter 4, Theorem 1.3] then garantees that the initial value problem has a unique solution, which is continuously differentiable on $[0,\infty)$, for every initial value $\mathbf{p}_0(x) \in D(\mathcal{A})$. □

3.2. Formal Diffusion Approximation

In this section we want to approximate the asymptotic behavior of the transport equation. Therefore we have to expand the transport equation by adopting a modified velocity $\tilde{\mathbf{v}}(x)$, where we introduce the deviation of the expectation of the underlying stochastic process, to obtain the modified transport equation

$$\partial_t\mathbf{p}(x,t) + \partial_x(\tilde{\mathbf{v}}(x)\odot\mathbf{p}(x,t)) = \mathcal{L}_x[\mathbf{p}(x,t)]. \tag{3.21}$$

The idea we utilize is that the processes that govern the system live on different time scales. We assume that the stochastic process is fast in comparison to the other processes and thus already in equilibrium, so that the asymptotic behavior of the solution of (3.21) can be approximated by

$$\mathbf{p}(x,t) \approx h(x,t)\mathbf{Y}(x) \tag{3.22}$$

where $\mathbf{Y}(x)$ is the stationary probability distribution of the stochastic process and $h(x,t) : \Omega \times [0,\infty) \to \mathbb{R}_+$ is a scalar function, describing the marginal distribution of the AHL concentration.

We study two different scaling arguments, hyperbolic and parabolic scaling, to find interesting relations and differences between the scalings. Via regular perturbation expansion, as done in [20, 40], we derive a partial differential equation determining the marginal distribution $h(x,t)$. After all the parabolic scaling will turn out to be the most suitable scaling for our purpose.

3.2.1. Expansion of the Transport Equation

To apply the diffusion approximation we expand the transport equation (3.14) by adopting a modified velocity. In the expanded transport equation we distinguish between the mean AHL production of the system, determined by the mean number of activated cells within the population, and the variability due to stochasticity.

In the formal approximation we concentrate on the interior of Ω and we denote the mean number of activated cells of the underlying stochastic process, which depends on x, by $E(n|x) \in \mathbb{R}_+$. Consequently the expectation $E(n|x)$ is independent of n.
Thus, we define the modified velocity $\tilde{\mathbf{v}}(x)$ of our expanded system as

$$\tilde{\mathbf{v}}(x) = (\tilde{v}_0, \tilde{v}_1, ...\tilde{v}_N)^T := \tilde{\mathbf{v}}_1(x) + \tilde{\mathbf{v}}_2(x) \tag{3.23}$$

where $\tilde{\mathbf{v}}_1(x) := \tilde{v}_1(x)\mathbf{e}$, since $\mathbf{e} := (1,1,...,1) \in \mathbb{R}^{N+1}$, with

$$\tilde{v}_1(x) := \alpha N - \gamma x + \beta_1 E(n|x),$$

determining the mean drift of the system, while

$$\tilde{\mathbf{v}}_2(x) = (\tilde{v}_{2,0}(x), \tilde{v}_{2,1}(x), ..., \tilde{v}_{2,N}(x))^T,$$

with

$$\tilde{v}_{2,n}(x) := \beta_2(n - E(n|x)),$$

expressing the variability due to the stochasticity within the system.
Note, that we introduced two different production rates β_1 and β_2. As we will see, appropriate scaling requires a difference in magnitude of the parameters β_1 and β_2, so we must extend our model. Let us agree on $\beta_1 \geq \beta_2$, in order to emphasize the mean AHL production rate versus the variability. One can see that for $\beta_1 = \beta_2 = \beta$ we recover the original velocity (3.10) derived in the previous section. In this sense, the original model is embedded into this model.

To part it in a nutshell, the extended transport equation now reads

$$\partial_t \mathbf{p}(x,t) + \partial_x\big((\tilde{\mathbf{v}}_1(x) + \tilde{\mathbf{v}}_2(x)) \odot \mathbf{p}(x,t)\big) = \mathcal{L}_x[\mathbf{p}(x,t)]. \tag{3.24}$$

As before the n-th component $p_n(x,t)$ of $\mathbf{p}(x,t)$ denotes the density of the population to be in state $n \in I := \{0,...,N\}$ at $x \in \Omega$ and $t \geq 0$. The scaling is not given a priori, but there is a degree of freedom. In order to find an appropriate scaling, we discuss in the following three different cases.

3.2.2. Hyperbolic Scaling

We conjecture that the stochastic process in (3.24) is very fast, i.e the transition between different states of the population is very fast. Thus, we assume that the time scale of the transition operator is of order $\mathcal{O}(\varepsilon^2)$ and we substitute

$$\mu(x) \to \frac{1}{\varepsilon^2}\tilde{\mu}(x) \quad \text{and} \quad \nu(x) \to \frac{1}{\varepsilon^2}\tilde{\nu}(x).$$

Let $\tilde{\mathcal{L}_x}$ be the transition operator which depends on the scaled transition rates $\tilde{\nu}(x)$ and $\tilde{\mu}(x)$, then (3.24) can be written

$$\partial_t \mathbf{p}(x,t) + \partial_x(\tilde{\mathbf{v}}(x) \odot \mathbf{p}(x,t)) = \frac{1}{\varepsilon^2}\tilde{\mathcal{L}_x}[\mathbf{p}(x,t)]. \tag{3.25}$$

As we rescale this equation we obtain the singularly perturbed transport equation

$$\varepsilon^2\partial_t \mathbf{p}(x,t) + \varepsilon^2\partial_x(\tilde{\mathbf{v}}(x) \odot \mathbf{p}(x,t)) = \tilde{\mathcal{L}_x}[\mathbf{p}(x,t)]. \tag{3.26}$$

Hereafter we drop the tilde on the transition operator and the transition rates.

Since we are interested in the solution of (3.26) on the fast time scale we consider the regular perturbation expansion

$$\mathbf{p}(x,t) = \mathbf{p}_0(x,t) + \varepsilon\mathbf{p}_1(x,t) + \varepsilon^2\mathbf{p}_2(x,t) + \mathcal{O}(\varepsilon^3)$$

This ansatz gives the outer solution in the sense of singular perturbations. By equating terms of equal order in ε we obtain the following equations:

$$\begin{array}{lrcl} \varepsilon^0: & \mathcal{L}_x[\mathbf{p}_0(x,t)] &=& 0, \\ \varepsilon^1: & \mathcal{L}_x[\mathbf{p}_1(x,t)] &=& 0, \\ \varepsilon^2: & \mathcal{L}_x[\mathbf{p}_2(x,t)] &=& \partial_t\mathbf{p}_0(x,t) + \partial_x\left(\tilde{\mathbf{v}}(x) \odot \mathbf{p}_0(x,t)\right). \end{array} \tag{3.27}$$

Concerning the first equation, ε^0, we find that $\mathbf{p}_0(x,t)$ is proportional to the zero-eigenvector of the transition matrix L_x, hence

$$\mathbf{p}_0(x,t) = h_1(x,t)\mathbf{Y}(x) \tag{3.28}$$

with some scalar function $h_1(x,t) : \Omega \times [0,\infty) \to \mathbb{R}_+$. The function $h_1(x,t)$ denotes the marginal probability density of x, as we find

$$1 = \int_\Omega \sum_{n=0}^{N} h_1(x,t)y_n(x)dx = \int_\Omega h_1(x,t)\sum_{n=0}^{N} y_n(x)dx = \int_\Omega h_1(x,t)dx. \tag{3.29}$$

The transition matrix L_x is singular (see Appendix B.1) and thus the right-hand sides must satisfy the solvability condition

$$\sum_{n=0}^{N}(L_x f)_n = 0 \quad \text{for all } f : I \times \Omega \to \mathbb{R}_+^{N+1}. \tag{3.30}$$

As the right-hand side of the equation of order ε^1 is equal to zero the solvability condition is fulfilled. It remains to solve the equation for order ε^2 subject to (3.28). Again the solvability condition has to be satisfied, so that

$$\sum_{n=0}^{N} \left[\partial_t p_{0,n}(x,t) + \partial_x \left(\tilde{v}_n(x) p_{0,n}(x,t)\right)\right] \;=\; 0.$$

Accordingly, we get the evolution equation for $\mathbf{p}_0(x,t)$ as a result of the solvability condition, which results in

$$\begin{aligned}\sum_{n=0}^{N}(\partial_t p_{0,n}(x,t) + \partial_x(\tilde{v}_n(x)p_{0,n}(x,t))) &= \sum_{n=0}^{N}\Big(\partial_t h_1(x,t)y_n(x) + \partial_x\big(\tilde{v}_n(x)h_1(x,t)y_n(x)\big)\Big) \\ &= \partial_t\left(h_1(x,t)\sum_{n=0}^{N} y_n(x)\right) + \partial_x\left(h_1(x,t)\sum_{n=0}^{N}\tilde{v}_n(x)y_n(x)\right) \qquad (3.31)\end{aligned}$$

We know that $\mathbf{Y}(x)$ is the normalized Perron-eigenvector (see Lemma B.4). Hence $\sum_{n=0}^{N} y_n(x) = 1$. Further we obtain

$$\begin{aligned}\sum_{n=0}^{N}\tilde{v}_n(x)y_n(x) &= \sum_{n=0}^{N}\big[(\alpha N - \gamma x + \beta_1 E(n|x) + \beta_2(n - E(n|x)))y_n(x)\big] \\ &= \alpha N - \gamma x + \beta_1 E(n|x) - \beta_2 E(n|x) + \beta_2\sum_{n=0}^{N} n y_n(x) \\ &= \alpha N - \gamma x + \beta_1 E(n|x) = \tilde{v}_1(x)\end{aligned}$$

as $\sum_{n=0}^{N} n y_n(x) = E(n|x)$. When we insert the above relation into (3.31), a transport equation is produced describing the scalar function $h_1(x,t)$ as

$$\partial_t h_1(x,t) + \partial_x(\tilde{v}_1(x)h_1(x,t)) = 0.$$

Thus, with these scaling assumptions we obtain a drift model describing the pure transport of the signaling molecule concentration. The drift velocity is determined by the mean drift of the system, whereas the variability due to stochasticity within the system is completely ignored. As we are interested in the influence of the stochasticity to our model, this scaling seems to be a bit harsh.

3.2.3. Parabolic Scaling

To derive a parabolic partial differential equation as an approximation for the modified transport equation (3.24) we now study the parabolic scaling. This is done for two different settings of the transport equation, (1) a simplified version of the transport equation with constant transition rates and (2) $x-$dependent transition rates as in the original transport equation. Investigation of both settings can only be understood if the details of the approximations are given. Our goal is to compare the results and explain differences and similarities.

Parabolic Scaling for Constant Transition Rates

In this part we assume that the activation and deactivation rates, ν and μ, are constant and do not depend on x. Although we know that this restriction does not achieve the requirements of our model, this scaling will at least give us some useful information for the x-dependent case.

As a consequence of this assumption the transition operator $\mathcal{L}$ is independent of x. Furthermore, the Perron eigenvector of L, denoted by $\mathbf{Y}$ here, does not depend on x. The simplified transport equation thus reads

$$\partial_t \mathbf{p}(x,t) + \partial_x(\tilde{\mathbf{v}}(x) \odot \mathbf{p}(x,t)) = \mathcal{L}[\mathbf{p}(x,t)]. \tag{3.32}$$

Same as in the previous section, we assume that the stochastic process is very fast and thus the time scale is of order $\mathcal{O}(\varepsilon^2)$. Therefore we define

$$\mu \to \frac{1}{\varepsilon^2}\hat{\mu} \quad \text{and} \quad \nu \to \frac{1}{\varepsilon^2}\hat{\nu}.$$

As further assumption we suppose the variation due to stochasticity to be fast, but not as fast as the transition, whereas the mean drift itself is bounded. Thus we assume the time scale of $\tilde{\mathbf{v}}_2(x)$ to be of order $\mathcal{O}(\varepsilon^1)$ and the time scale for $\tilde{v}_1(x)$ to be of order $\mathcal{O}(\varepsilon^0)$ so that we substitute

$$\beta_2 \to \frac{1}{\varepsilon}\hat{\beta}_2.$$

Let $\hat{\mathcal{L}}$ be the transition operator depending on the scaled transition rates $\hat{\nu}$ and $\hat{\mu}$ and let $\hat{\tilde{\mathbf{v}}}_2(x)$ depend on $\hat{\beta}_2$. Introducing the scaling to the simplified transport equation, we obtain

$$\partial_t \mathbf{p}(x,t) + \partial_x(\tilde{v}_1(x)\mathbf{p}(x,t)) + \frac{1}{\varepsilon^1}\partial_x(\tilde{\mathbf{v}}_2(x) \odot \mathbf{p}(x,t)) = \frac{1}{\varepsilon^2}\mathcal{L}[\mathbf{p}(x,t)]$$

Here and hereafter we drop the hat on the scaled expressions.
The above equation is equivalent to the singularly perturbed transport equation

$$\varepsilon^2\partial_t \mathbf{p}(x,t) + \varepsilon^2\partial_x(\tilde{v}_1(x)\mathbf{p}(x,t)) + \varepsilon\partial_x(\tilde{\mathbf{v}}_2(x) \odot \mathbf{p}(x,t)) = \mathcal{L}\mathbf{p}(x,t). \tag{3.33}$$

As before we encounter the regular perturbation expansion

$$\mathbf{p}(x,t) = \mathbf{p}_0(x,t) + \varepsilon\mathbf{p}_1(x,t) + \varepsilon^2\mathbf{p}_2(x,t) + \mathcal{O}(\varepsilon^3)$$

and by equating terms of equal order in ε we get:

$$\begin{array}{lrcl} \varepsilon^0: & \mathcal{L}[\mathbf{p}_0(x,t)] & = & 0, \\ \varepsilon^1: & \mathcal{L}[\mathbf{p}_1(x,t)] & = & \partial_x\left(\tilde{v}_{2,n}(x)\mathbf{p}_0(x,t)\right), \\ \varepsilon^2: & \mathcal{L}[\mathbf{p}_2(x,t)] & = & \partial_t\mathbf{p}_0(x,t) + \partial_x\left(\tilde{v}_1(x)\mathbf{p}_0(x,t)\right) + \partial_x\left(\tilde{\mathbf{v}}_2(x) \odot \mathbf{p}_1(x,t)\right). \end{array} \tag{3.34}$$

From the first equation (order ε^0) we obtain that $\mathbf{p}_0(x,t)$ is proportional to the zero-eigenvector of the transition operator $\mathcal{L}$ and so we get

$$\mathbf{p}_0(x,t) \;=\; h_2(x,t)\mathbf{Y}$$

where $h_2(x,t) : \Omega \times [0,\infty] \to \mathbb{R}$ is a scalar function that describs the marginal distribution of x, see (3.29).
Next we consider the order ε^1: if this equation should allow a solution, the right hand side has to fulfill the solvability condition (3.30). If we multiply the right-hand side with the left-eigenvector, the resulting sum has to be equal to zero. Thus,

$$\begin{aligned}\sum_{n=0}^{N} \partial_x \left(\tilde{v}_{2,n}(x) p_{0,n}(x,t)\right) &= \partial_x \sum_{n=0}^{N} \left(\tilde{v}_{2,n}(x) h_2(x,t) y_n\right) \\ &= \partial_x \left(h_2(x,t)\beta_2 \left(\sum_{n=0}^{N} n y_n - E(n|x) \sum_{n=0}^{N} y_n \right) \right) = 0\end{aligned}$$

which is indeed true as $\sum_{n=0}^{N} y_n = 1$ and $\sum_{n=0}^{N} n y_n = E(n|x)$.
Hence there is a solution of the equation for order (ε^1). Since $\mathcal{L}$ is linear and bounded the equation can be solved via a generalized or pseudo inverse (see Appendix B.1.3). We denote the generalized inverse of $\mathcal{L}$ with $\mathcal{L}^+$. Then the solution can be written as

$$\mathbf{p}_1(x,t) = \mathcal{L}^+ \left[\partial_x \left(\tilde{\mathbf{v}}_2(x) \odot \mathbf{p}_0(x,t)\right)\right] = \mathcal{L}^+ \left[\partial_x \left(h(x,t)\tilde{\mathbf{v}}_2(x) \odot (\mathbf{Y})\right)\right].$$

Since the generalized inverse is a linear operator and does not depend on x in this setting, we can rewrite it in the form

$$\mathbf{p}_1(x,t) = \partial_x \left(h_2(x,t)\beta_2 (\mathcal{L}^+[\mathbf{n} \odot \mathbf{Y}] - E(n|x)\mathcal{L}^+[\mathbf{Y}]) \right)$$

In Lemma B.11 we show that

$$\mathcal{L}_x^+[\mathbf{Y}] = 0 \qquad \text{and} \qquad \mathcal{L}_x^+[\mathbf{n} \odot \mathbf{Y}] = \frac{N\nu\mu}{(\mu+\nu)^{N+2}} \mathbf{w}_1,$$

where $\mathbf{w}_1$ is the eigenvector of the transition matrix L corresponding to the eigenvalue $\lambda_1 = -(\mu+\nu)$. These evaluations results in

$$\mathbf{p}_1(x,t) = \frac{\beta_2 N \nu \mu}{(\mu+\nu)^{N+2}} \, \partial_x h(x,t) \, \mathbf{w}_1. \tag{3.35}$$

Next we consider the term of order $\mathcal{O}(\varepsilon^2)$. This equation is solvable if the solvability condition

$$\begin{aligned} 0 &= \sum_{n=0}^{N} (\partial_t p_{0,n}(x,t) + \partial_x \left(\tilde{v}_1(x) p_{0,n}(x,t)\right) + \partial_x \left(\tilde{v}_{2,n}(x) p_{1,n}(x,t)\right)) \\ &= \partial_t \sum_{n=0}^{N} (h_2(x,t) y_n) + \partial_x \sum_{n=0}^{N} (\tilde{v}_1(x) h_2(x,t) y_n) + \partial_x \sum_{n=0}^{N} (\tilde{v}_{2,n}(x) p_{1,n}(x,t)) \end{aligned}$$

is satisfied, which is true if $h_2(x,t)$ solves the following equation

$$\partial_t h_2(x,t) = -\partial_x (\tilde{v}_1(x) h_2(x,t)) - \partial_x \sum_{n=0}^{N} (\tilde{v}_{2,n}(x) p_{1,n}(x,t)). \tag{3.36}$$

Analyzing the sum in (3.36) we obtain

$$\sum_{n=0}^{N}(\tilde{v}_{2,n}(x)p_{1,n}(x,t)) \quad = \quad \beta_2^2\frac{N\nu\mu}{(\mu+\nu)^{N+2}}\partial_x h_2(x,t)\sum_{n=0}^{N}\left((n-E(n|x))\mathbf{w}_1\right).$$

In Proposition B.3 we calculate $\sum_{n=0}^{N}\mathbf{w}_1 = 0$ and $\sum_{n=0}^{N} n\mathbf{w}_1 = -(\mu+\nu)^{N-1}$ which leads to

$$\sum_{n=0}^{N}\tilde{v}_{2,n}(x)p_{1,n}(x,t) \quad = \quad -D\partial_x h_2(x,t)$$

where $D := \beta_2^2\frac{N\nu\mu}{(\mu+\nu)^3}$. Hence we can rewrite (3.36) and obtain a parabolic differential equation for the scalar function as

$$\partial_t h_2(x,t) \quad = \quad -\partial_x(\tilde{v}_1(x)h_2(x,t)) + D\partial_x^2 h_2(x,t). \tag{3.37}$$

The diffusion tensor of the resulting limit equation is given by

$$D = \beta_2^2\frac{N\nu\mu}{(\mu+\nu)^3} = \frac{\beta_2^2}{\mu+\nu}\mathrm{Var}(n|x)$$

so that the diffusion term is determined by the variance of the underlying jump process, whereas the drift term is governed by the mean drift of the model. In contrast to the hyperbolic scaling, we find that the stochasticity affects the equation.

Parabolic scaling for $x-$dependent Transition Rates

We use the same scaling arguments as in the previous section, but now we study the original expanded transport equation (3.24) where the transition rates and therefore the transition operator depends on x. As before we scale

$$\mu(x) \to \frac{1}{\varepsilon^2}\hat{\mu}(x), \qquad \nu(x) \to \frac{1}{\varepsilon^2}\hat{\nu}(x) \qquad \text{and} \qquad \beta_2 \to \frac{1}{\varepsilon}\hat{\beta}_2.$$

Let $\hat{\mathcal{L}}_x$ be the transition operator depending on the scaled transition rates $\hat{\nu}(x)$ and $\hat{\mu}(x)$ and let $\hat{\tilde{v}}_2(n,x)$ depend on $\hat{\beta}_2$. Introducing the scaling to the transport equation (3.24) we maintain

$$\partial_t\mathbf{p}(x,t) + \partial_x(\tilde{v}_1(x)\mathbf{p}(x,t)) + \frac{1}{\varepsilon^1}\partial_x(\tilde{\mathbf{v}}_2(x)\odot\mathbf{p}(x,t)) = \frac{1}{\varepsilon^2}\mathcal{L}_x[\mathbf{p}(x,t)].$$

Here and hereafter we drop the hat on the scaled expressions.
The rescaled equation results in the singularly perturbed transport equation

$$\varepsilon^2\partial_t\mathbf{p}(x,t) + \varepsilon^2\partial_x(\tilde{v}_1(x)\mathbf{p}(x,t)) + \varepsilon\partial_x(\tilde{\mathbf{v}}_2(x)\odot\mathbf{p}(x,t)) = \mathcal{L}_x[\mathbf{p}(x,t)]. \tag{3.38}$$

Since we are interested in the solution of (3.38) on the diffusion time scale, we consider the regular perturbation expansion

$$\mathbf{p}(x,t) = \mathbf{p}_0(x,t) + \varepsilon\mathbf{p}_1(x,t) + \varepsilon^2\mathbf{p}_2(x,t) + \mathcal{O}(\varepsilon^3).$$

Equating terms of equal order in ε, we obtain the following system of equations

$$\begin{aligned}
\varepsilon^0: \quad & \mathcal{L}_x[\mathbf{p}_0(x,t)] &&= 0,\\
\varepsilon^1: \quad & \mathcal{L}_x[\mathbf{p}_1(x,t)] &&= \partial_x(\tilde{\mathbf{v}}_2(x) \odot \mathbf{p}_0(x,t)),\\
\varepsilon^2: \quad & \mathcal{L}_x[\mathbf{p}_2(x,t)] &&= \partial_t\mathbf{p}_0(x,t) + \partial_x(\tilde{v}_1(x)\mathbf{p}_0(x,t)) + \partial_x(\tilde{\mathbf{v}}_2(x) \odot \mathbf{p}_1(x,t)).
\end{aligned}$$

From the first equation we get, that $\mathbf{p}_0(x,t)$ is proportional to the zero-eigenvector of the transition operator matrix L_x,

$$\mathbf{p}_0(x,t) = h(x,t)\mathbf{Y}(x)$$

where $h(x,t) : \Omega \times [0,\infty) \to \mathbb{R}$ is the marginal distribution of the AHL molecule concentration x, see (3.29).

Since the transition operator $\mathcal{L}_x$ is singular, the right-hand side of the second equation (ε^1) has to satisfy the solvability condition (3.30), that is

$$\begin{aligned}
\sum_{n=0}^{N} \partial_x(\tilde{v}_{2,n}(x)p_0) &= \partial_x \sum_{n=0}^{N} \left(\tilde{\beta}_2(n - E(n|x)))h(x,t)y_n(x)\right) =\\
&= \partial_x \left(h(x,t)\beta_2 \left(\sum_{n=0}^{N} n y_n(x) - E(n|x)\sum_{n=0}^{N} y_n(x)\right)\right) =\\
&= \partial_x \left(h(x,t)\beta_2(E(n|x) - E(n|x))\right) = 0.
\end{aligned}$$

The solvability condition is satisfied. Thus equation (ε^1) can be solved via the generalized inverse of $\mathcal{L}_x$, which is denoted by $\mathcal{L}_x^+$ (see Appendix B.1). Then the solution can be written in the form

$$\mathbf{p}_1(x,t) \;=\; \mathcal{L}_x^+[\partial_x(h(x,t)\tilde{\mathbf{v}}_2(x) \odot \mathbf{Y}(x))].$$

Please note that ∂_x and $\mathcal{L}_x^+$ do not commutate, as a new ingredient of the $x-$dependence. In comparison to the case of constant rates, we obtain an additional term that is caused by the interaction of the jump process and the AHL production.

As the generalized inverse $\mathcal{L}_x^+$ is a linear functional we can rewrite

$$\begin{aligned}
\mathbf{p}_1(x,t) \;&= \mathcal{L}_x^+[h(x,t)\tilde{\mathbf{v}}_2(x) \odot \partial_x\mathbf{Y}(x)]\\
&\quad + \mathcal{L}_x^+[\tilde{\mathbf{v}}_2(x) \odot \mathbf{Y}(x)\partial_x h(x,t)] + \mathcal{L}_x^+[h(x,t)\mathbf{Y}(x) \odot \partial_x\tilde{\mathbf{v}}_2(x)]. \qquad (3.39)
\end{aligned}$$

In our case it is not possible to calculate the generalized inverse $\mathcal{L}_x^+$ explicitly. However, due to the structure of the eigenvalues and eigenvectors, we could analyze the generalized

inverse applied to this terms (Appendix B.1.3). Calculations that are needed here are derived in Lemma B.11 and Lemma B.12. We just summarize the results here

$$\begin{aligned}
\mathcal{L}_x^+[\mathbf{Y}(x)] &= 0, && (3.40)\\
\mathcal{L}_x^+\left[\left(\mathbf{n}\odot\mathbf{Y}(x)\right)\right] &= \frac{N\nu(x)\mu(x)}{(\mu(x)+\nu(x))^{N+2}}\mathbf{w}_1, && (3.41)\\
\mathcal{L}_x^+[\partial_x\mathbf{Y}(x)] &= -b_1(x)\mathbf{w}_1, && (3.42)\\
\mathcal{L}_x^+\left[\left(\mathbf{n}\odot\partial_x\mathbf{Y}(x)\right)\right] &= b_2(x)\mathbf{w}_1^N + b_3(x)\mathbf{w}_2, && (3.43)
\end{aligned}$$

with

$$\begin{aligned}
b_1(x) &:= \frac{N(\nu(x)\partial_x\mu(x)-\mu(x)\partial_x\nu(x))}{(\mu+\nu)^{N+2}},\\
b_2(x) &= \frac{N(\nu(x)\partial_x\mu(x)-\mu(x)\partial_x\nu(x))}{(\mu+\nu)^{N+3}}\left(N\nu-(\mu(x)+\nu(x)(2N-1))\right),\\
b_3(x) &:= \frac{N(N-1)\nu(x)\mu(x)(\nu(x)\partial_x\mu(x)-\mu(x)\partial_x\nu(x))}{2(\mu+\nu)^{N+3}}.
\end{aligned}$$

Notice, that $\mathbf{w}_k$ denotes the eigenvector of the transition matrix L_x corresponding to the eigenvalue $\lambda_k = -k(\mu(x)+\nu(x))$.

Let us consider equation (3.39). Investigation of its third term leads to

$$\partial_x\tilde{\mathbf{v}}_2(x) = -\tilde{\beta}_2\partial_x E(n|x)\mathbf{e}, \qquad \mathbf{e} := (1,1,...,1)^T$$

which does not depend on n any more. Together with (3.40) we find

$$\mathcal{L}_x^+[h(x,t)\partial_x\tilde{\mathbf{v}}_2(x)\odot\mathbf{Y}(x)] = h(x,t)\partial_x\tilde{\mathbf{v}}_2(x)\mathcal{L}_x^+[\mathbf{Y}(x)] = 0. \tag{3.44}$$

Concerning the first expression of (3.39), we obtain

$$\begin{aligned}
\mathcal{L}_x^+[\tilde{\mathbf{v}}_2(x)\odot\mathbf{Y}(x)\partial_x h(x,t)] &= \partial_x h(x,t)\mathcal{L}_x^+[(\tilde{\beta}_2(\mathbf{n}-E(n|x)\,\mathbf{e}))\odot\mathbf{Y}(x)]\\
&= \partial_x h(x,t)\left(\tilde{\beta}_2\mathcal{L}_x^+\left[\left(\mathbf{n}\odot\mathbf{Y}(x)\right)\right]-\tilde{\beta}_2 E(n|x)\mathcal{L}_x^+[\mathbf{Y}(x)]\right)
\end{aligned}$$

Subject to (3.41) and (3.40) this can be rewritten as

$$\mathcal{L}_x^+[\tilde{\mathbf{v}}_2(x)\odot\mathbf{Y}(x)\partial_x h(x,t)] = \tilde{\beta}_2\partial_x h(x,t)\frac{N\nu(x)\mu(x)}{(\mu(x)+\nu(x))^{N+2}}\mathbf{w}_1. \tag{3.45}$$

The same calculations can be done for the first term of (3.39). With (3.42) and (3.43) we get

$$\begin{aligned}
&\mathcal{L}_x^+[h(x,t)\tilde{\mathbf{v}}_2(x)\odot\partial_x\mathbf{Y}(x)] =\\
&\quad = h(x,t)\tilde{\beta}_2\mathcal{L}_x^+\left[\left(\mathbf{n}\odot\partial_x\mathbf{Y}(x)\right)\right]-h(x,t)E(n|x)\tilde{\beta}_2\mathcal{L}_x^+\left[\partial_x\mathbf{Y}(x)\right] \qquad (3.46)\\
&\quad = h(x,t)\tilde{\beta}_2\left((b_2(x)\mathbf{w}_1+b_3(x)\mathbf{w}_2)+E(n|x)b_1(x)\mathbf{w}_1\right).
\end{aligned}$$

Composing (3.45), (3.46) and (3.44) we end up with

$$\begin{aligned}\mathbf{p}_1(x,t) = \tilde{\beta}_2 \partial_x h(x,t) \frac{N\nu(x)\mu(x)}{(\mu(x)+\nu(x))^{N+2}} \mathbf{w}_1 \\ + h(x,t)\tilde{\beta}_2 \left((b_2(x)\mathbf{w}_1 + b_3(x)\mathbf{w}_2) + E(n|x) b_1(x)\mathbf{w}_1 \right) \end{aligned} \tag{3.47}$$

Eventually we consider the condition corresponding to the (ε^2) equation. The following solvability condition has to be satisfied

$$\begin{aligned} 0 &= \sum_{n=0}^{N} (\partial_t p_{0,n}(x,t) + \partial_x(\tilde{v}_1(x) p_{0,n}(x,t)) + \partial_x(\tilde{v}_{2,n}(x) p_{1,n}(x,t))) = \\ &= \partial_t h(x,t) \sum_{n=0}^{N} y_n(x) + \partial_x \left(h(x,t)\tilde{v}_1(x) \sum_{n=0}^{N} y_n(x) \right) + \partial_x \left(\sum_{n=0}^{N} (\tilde{v}_{2,n}(x) p_{1,n}(x,t)) \right). \end{aligned}$$

From this solvability condition we obtain the evolution equation for $h(x,t)$

$$\partial_t h(x,t) = -\partial_x \left(h(x,t)\tilde{v}_1(x) \right) - \partial_x \left(\sum_{n=0}^{N} (\tilde{v}_{2,n}(x) p_{1,n}(x,t)) \right). \tag{3.48}$$

We analyze the expression $\sum_{n=0}^{N} (\tilde{v}_{2,n}(x) p_{1,n}(x,t))$ which corresponds to the investigation of the terms $\sum_{n=0}^{N} (n p_{1,n}(x,t))$ and $\sum_{n=0}^{N} p_{1,n}(x,t)$ as follows

$$\sum_{n=0}^{N} (\tilde{v}_{2,n}(x) p_{1,n}(x,t)) = \beta_2 \left(\sum_{n=0}^{N} n p_{1,n}(x,t) - E(n|x) \sum_{n=0}^{N} p_{1,n}(x,t) \right).$$

The sum $\sum_{n=0}^{N} p_{1,n}(x,t)$ bores down to

$$\begin{aligned} \sum_{n=0}^{N} p_{1,n}(x,t) &= \beta_2 \partial_x h(x,t) \frac{N\nu(x)\mu(x)}{(\mu(x)+\nu(x))^{N+2}} \sum_{n=0}^{N} \mathbf{w}_1 \\ &\quad + h(x,t)\beta_2 \left(\left(b_2(x) \sum_{n=0}^{N} \mathbf{w}_1 + b_3(x) \sum_{n=0}^{N} \mathbf{w}_2 \right) + E(n|x) b_1(x) \sum_{n=0}^{N} \mathbf{w}_1 \right). \end{aligned}$$

In Proposition B.3 we calculate

$$\sum_{n=0}^{N} \mathbf{w}_0 = (\mu+\nu)^N, \ \sum_{n=0}^{N} \mathbf{w}_1 = \sum_{n=0}^{N} \mathbf{w}_2 = \sum_{n=0}^{N} n w_{2,n} = 0 \ \text{ and } \ \sum_{n=0}^{N} n w_{1,n} = -(\mu+\nu)^{N-1}.$$

Hence, we obtain

$$\sum_{n=0}^{N} p_{1,n}(x,t) = 0.$$

A similar procedure for $\sum_{n=0}^{N} np_{1,n}(x,t)$ leads to

$$\begin{aligned}\sum_{n=0}^{N} np_{1,n}(x,t) &= \beta_2 \partial_x h(x,t) \frac{N\nu(x)\mu(x)}{(\mu(x)+\nu(x))^{N+2}} \sum_{n=0}^{N} nw_{1,n} \\ &\quad + h(x,t)\beta_2 \left((b_2(x) \sum_{n=0}^{N} nw_{1,n} + b_3(x) \sum_{n=0}^{N} nw_{2,n} + E(n|x) b_1(x) \sum_{n=0}^{N} nw_{1,n} \right) \\ &= -\beta_2 \partial_x h(x,t) \frac{N\nu(x)\mu(x)}{(\mu(x)+\nu(x))^3} - h(x,t)\beta_2 \frac{N(\nu(x)\partial_x\mu(x) - \mu(x)\partial_x\nu(x))}{(\mu(x)+\nu(x))^4} \\ &\qquad \cdot (N\nu(x) - (\mu(x)+\nu(x)(2N-1)) + N\nu(x)) .\end{aligned}$$

Thus, we rewrite

$$\begin{aligned}\sum_{n=0}^{N} np_{1,n}(x,t) &= -\partial_x h(x,t) \frac{\beta_2 N\nu(x)\mu(x)}{(\mu(x)+\nu(x))^3} \\ &\quad + h(x,t) \frac{\beta_2 N(\nu(x)\partial_x\mu(x) - \mu(x)\partial_x\nu(x))}{(\mu(x)+\nu(x))^4} (\nu(x) - \mu(x)).\end{aligned}$$

All in all we obtain

$$\begin{aligned}\partial_x \left(\sum_{n=0}^{N} (\tilde{v}_{2,n}(x) p_{1,n}(x,t)) \right) &= \partial_x \left(\beta_2 \sum_{n=0}^{N} np_1 - \beta_2 E(n|x) \sum_{n=0}^{N} p_1 \right) \\ &= \partial_x \left(-a(x)\partial_x h(x,t) + g(x) h(x,t) \right)\end{aligned}$$

where

$$\begin{aligned} g(x) &:= \frac{\beta_2^2 N(\nu(x)\partial_x\mu(x) - \mu(x)\partial_x\nu(x))}{(\mu(x)+\nu(x))^4} (\nu(x) - \mu(x)), \\ a(x) &:= \frac{\beta_2^2 N\nu(x)\mu(x)}{(\mu(x)+\nu(x))^3}. \end{aligned} \tag{3.49}$$

In view of (3.48), we finally end up with a partial differential equation

$$\partial_t h(x,t) = -\partial_x \left(h(x,t)(\tilde{v}_1(x) - g(x)) \right) + \partial_x \left(a(x)\partial_x h(x,t) \right) \tag{3.50}$$

where $g(x), a(x)$ defined in (3.49).

As $a(x) = \frac{\beta_2^2}{\mu(x)+\nu(x)} \mathrm{Var}(n|x)$, the diffusion is caused by the variance of the stationary distribution of the jump process, whereas the drift term is determined by the mean drift of the system plus some additional factor $g(x)$. This factor is caused by an interaction term of both the AHL production and the jump process. We will see below that this term does not play a role for population of large or moderate population sizes, only for small populations this interaction may have an effect.

3.3. The Parabolic Limit Equation

In this final section we are going to investigate the asymptotic behavior of the limit equation (3.50) of the parabolic scaling. We return to the original model with $\beta_1 = \beta_2 = \beta$. For $x \in \Omega = (x_{min}, x_{max}) \subset \mathbb{R}$, with x_{min} and x_{max} defined as in (3.11), and $t \geq 0$ we consider

$$\partial_t h(x,t) \quad = \quad -\partial_x \left(\tilde{g}(x) h(x,t)\right) + \partial_x \left(a(x) \partial_x h(x,t)\right) \tag{3.51}$$

where $\tilde{g}(x) := (\tilde{v}_1(x) - g(x))$ and $a(x), g(x)$ defined in the previous section.

This second order parabolic equation describes the time evolution of the AHL distribution. We introduce below boundary conditions that lead to mass conservation.

We rather focus on AHL per volume than on the total AHL mass per cell. In case of a given cell number N and a given volume V, there is no difference. However, if we consider experiments that take place in different volumina, the density is more appropriate to use than the total mass of AHL, since the cells senses the density and not the mass.

We are interested in the long term behavior for small populations, in order to obtain an idea of the implication of stochasticity, as well as for large populations, to recognize how the system returns to a deterministic behavior. It turns out that the probability density converges to stationary states at large time. If we moreover regard large population sizes, we consider two limits: the limit $t \to \infty$ as well as the limit $V \to \infty$. Surprisingly, the outcome depends on the order of the two limits.

As we ask for conservation of probability mass in our model, let us define appropriate boundary conditions. We know that x is defined within a bounded interval. To consider conservation of probability mass, we require, that the flux of the model, which is defined as

$$j(x,t) := \tilde{g}(x) h(x,t) - a(x) \partial_x h(x,t),$$

is equal to zero at the boundary of Ω, so that $j(x_{min}, t) = j(x_{max}, t) = 0$. Therefore the boundary conditions read

$$\tilde{g}(x) h(x,t) - a(x) \partial_x h(x,t) \quad = \quad 0 \qquad\qquad \text{for } x \in \partial\Omega. \tag{3.52}$$

Properties of the functions $a(x)$, $g(x)$ and $\tilde{g}(x)$ are summarized in the following.

Lemma 3.8
The functions $a(x)$, $g(x)$ and $\tilde{g}(x) := \tilde{v}_1(x) - g(x)$ have the following properties.

1. $a(x), g(x), \tilde{g}(x) \in C^\infty(\overline{\Omega})$
2. $\|a\|_\infty < \infty$ *and* $\|\tilde{g}\|_\infty < \infty$
3. $a(x)$ *is strictly positive with* $0 < a \leq a(x) \leq \bar{a} < \infty$

Proof. We find $\nu(x), \mu(x) \in C^\infty(\overline{\Omega})$, defined in (3.9), with $\|\mu\|_\infty < \infty$, $\|\nu\|_\infty < \infty$. It follows

$$a(x), g(x) \in C^\infty(\overline{\Omega}) \quad \text{ and } \quad \|a\|_\infty < \infty, \|g\|_\infty < \infty.$$

Since $\tilde{v}_1(x) = \alpha N - \gamma x + \beta_1 E(n|x)$ is a C^∞-function and within the bounded interval $\overline{\Omega}$ $\|\tilde{v}_1\|_\infty < \infty$ we also have

$$\tilde{g}(x) \in C^\infty(\overline{\Omega}) \quad \text{and} \quad \|\tilde{g}\|_\infty < \infty.$$

Furthermore, as $\mu(x)$ and $\nu(x)$ are strictly positive functions with $\mu(x), \nu(x) > 0$ for $x \in \overline{\Omega}$ and $\beta_2, N > 0$ we obtain that $a(x)$ is a strictly positive function as claimed. □

Finally, notice that the initial value problem

$$\begin{aligned} \partial_t h(x,t) &= -\partial_x\left(h(x,t)\hat{g}(x)\right) + \partial_x\left(a(x)\partial_x h(x,t)\right) && x \in \Omega, \\ 0 &= \hat{g}(x)h(x,t) - a(x)\partial_x h(x,t) && x \in \partial\Omega, \\ h(x,0) &= h_0(x) \end{aligned} \tag{3.53}$$

has a unique solution for each $h_0(x) \in H^3(\overline{\Omega})$ that satisfies the compatibility conditions of order 1, i.e the derivatives $\frac{\partial^k h}{\partial t^k}\Big|_{t=0}$, $k = \{0, 1\}$, must satisfy the boundary conditions for $x \in \partial\Omega$. The statement can be found in [29, Chapter 5, Theorem 5.3].

3.3.1. Scaling of the Limit Equation

Up to now our model bears no information about space, since we only measured the number of AHL molecules and the number of cells in the population. To assign the space where the population lives or how much space the population occupies, we introduce the volume $V \in \mathbb{R}$ and rewrite AHL mass as AHL concentration

$$z := \frac{x}{V}, \qquad z \in \Omega/V := \Omega_z,$$

i.e. we measure the number of AHL molecules per volume. Furthermore we introduce the density ρ, that is the number of cells N per volume V, as

$$\rho := \frac{N}{V}, \qquad \rho \in \mathbb{R}_+,$$

thus we can rewrite $\Omega_z = (z_{min}, z_{max}) = \left(\frac{\alpha\rho}{\gamma}, \frac{(\alpha+\beta)\rho}{\gamma}\right)$. Moreover let us define

$$\hat{h}(z,t) := h(Vz,t), \quad \hat{\mu}(z) = \mu(Vz) \text{ and } \hat{\nu}(z) = \nu(Vz). \tag{3.54}$$

Then (3.51) can be written in the form

$$\partial_t \hat{h}(z,t) = -\frac{1}{V}\partial_z(\hat{h}(z,t)(\tilde{v}_1(Vz) - g(Vz))) + \frac{1}{V^2}\partial_z(a(Vz)\partial_z\hat{h}(z,t)). \tag{3.55}$$

Investigating the right hand side we obtain, due to $E(n|Vz) = \frac{N\hat{\nu}(z)}{\hat{\mu}(z)+\hat{\nu}(z)}$,

$$\begin{aligned} &\frac{1}{V}(\tilde{v}_1(Vz) - g(Vz)) = \\ &= \frac{1}{V}\left[\alpha N - \gamma V z + \beta E(n|Vz) - \frac{\beta^2 \frac{N}{V}(\hat{\nu}(z)\partial_z\hat{\mu}(z) - \hat{\mu}(z)\partial_z\hat{\nu}(z))(\hat{\nu}(z) - \hat{\mu}(z))}{(\hat{\mu}(z)+\hat{\nu}(z))^4}\right] \\ &= \alpha\rho - \gamma z + \beta\rho\frac{\hat{\nu}(z)}{(\hat{\mu}(z)+\hat{\nu}(z))} - \frac{1}{V}\,\frac{\beta^2\rho(\hat{\nu}(z)\partial_z\hat{\mu}(z) - \hat{\mu}(z)\partial_z\hat{\nu}(z))(\hat{\nu}(z) - \hat{\mu}(z))}{(\hat{\mu}(z)+\hat{\nu}(z))^4} \end{aligned}$$

and

$$\frac{1}{V^2}a(Vz) \quad = \quad \frac{\beta^2\rho}{V}\,\frac{\hat{\nu}(z)\hat{\mu}(z)}{(\hat{\mu}(z)+\hat{\nu}(z))^3}.$$

So finally our scaled equation can be written as

$$\partial_t\hat{h}(z,t) \quad = \quad -\partial_z(\hat{g}(z)\hat{h}(z)) + \partial_z(\hat{a}(z)\partial_z\hat{h}(z,t)) \tag{3.56}$$

where we have

$$\begin{aligned}\hat{g}(z) &:= \alpha\rho - \gamma z + \beta\rho\frac{\hat{\nu}(z)}{(\hat{\mu}(z)+\hat{\nu}(z))} + \frac{1}{V}\,\frac{\beta^2\rho(\hat{\nu}(z)\partial_z\hat{\mu}(z) - \hat{\mu}(z)\partial_z\hat{\nu}(z))(\hat{\mu}(z)-\hat{\nu}(z))}{(\hat{\mu}(z)+\hat{\nu}(z))^4},\\ \hat{a}(z) &:= \frac{1}{V}\,\frac{\beta^2\rho\hat{\nu}(z)\hat{\mu}(z)}{(\hat{\mu}(z)+\hat{\nu}(z))^3}.\end{aligned} \tag{3.57}$$

Scaled Limit Equation for Large Population

Since we are interested in the asymptotic behavior of the scaled limit equation for a large population we derive formally the limit $V \to \infty$. If we assume ρ to be a given parameter, $V \to \infty$ implies $N \to \infty$.

Therefore, we examine $\hat{a}(z)$ and $\hat{g}(z)$ for the formal limit case which yields

$$\begin{aligned}\lim_{V\to\infty}\hat{a}(z) &= 0,\\ \lim_{V\to\infty}\hat{g}(z) &= \alpha\rho + \beta\rho\frac{\hat{\nu}(z)}{\hat{\mu}(z)+\hat{\nu}(z)} - \gamma z := G(z).\end{aligned}$$

In the formal limit $V \to \infty$, the scaled equation (3.56) reduces to

$$\partial_t\hat{h}(z,t) \quad = \quad -\partial_z(G(z)\hat{h}(z,t)). \tag{3.58}$$

The common approach to analyze (3.58) is the method of characteristics [54] where the PDE is investigated by using the solution of ordinary differential equations along characteristic curves.

Our partial differential equation in standard form is given by

$$\partial_t\hat{h}(z,t) + G(z)\partial_x\hat{h}(z,t) = \hat{h}(z,t)\partial_z G(z)$$

with the initial condition

$$\hat{h}(z,t) = \hat{h}_0(z).$$

To apply the method of characteristics, we parameterize the initial curve C as follows,

$$z = z(\tau),\ t = 0,\ \hat{h}(z,t) = \hat{h}_0(\tau).$$

The family of characteristic curves determined by the points of C may be parameterized as $z = z(s,\tau),\ t = t(s,\tau),\ \hat{h}(z,t) = \hat{h}(z(s,\tau),t(s,\tau))$, with $s = 0$ corresponding to the initial curve C. By derivation of $\hat{h}$ along these curves we obtain

$$\frac{\partial}{\partial s}\hat{h}(z(s,\tau),t(s,\tau)) \quad = \quad \frac{\partial \hat{h}}{\partial z}\frac{\partial z}{\partial s} + \frac{\partial \hat{h}}{\partial t}\frac{\partial t}{\partial s}$$

and the characteristic equations

$$\frac{\partial z}{\partial s} = G(z(s,\tau)) \quad \text{and} \quad \frac{\partial t}{\partial s} = 1.$$

Thus, for $s = t$ the characteristic equation for $z(t)$ reads

$$\frac{\partial z(t)}{\partial t} = \alpha\rho - \gamma z(t) + \beta\rho\frac{\tilde{\nu}(z(t))}{\tilde{\mu}(z(t)) + \tilde{\nu}(z(t))}. \tag{3.59}$$

In the following we show that the fraction $\frac{\tilde{\nu}(z)}{\tilde{\mu}(z)+\tilde{\nu}(z)}$ is sigmoidal, i.e. have a non-negative first derivative and exactly one inflection point.

Proposition 3.9
Consider

$$S(z) := \frac{\tilde{\nu}(z)}{\tilde{\mu}(z) + \tilde{\nu}(z)} = \frac{\sum_{k=m_0}^{M}\left[\binom{M}{k}\left(\frac{\kappa z}{\gamma_1}\right)^k\right]}{\sum_{k=0}^{M}\left[\binom{M}{k}\left(\frac{\kappa z}{\gamma_1}\right)^k\right]}.$$

For $M \geq m_0 \geq 2$, the function $S(z)$ is sigmoidal for $z \in \mathbb{R}_+$.

Proof. First of all, let $y = \frac{\kappa z}{\gamma_1}$ and

$$s(y) := 1 - \frac{\sum_{k=0}^{m_0-1}\binom{M}{k}y^k}{(1+y)^M},$$

then $S(z) = s\left(\frac{\kappa z}{\gamma_1}\right)$. It is sufficient to prove that $s(y)$ is a sigmoidal function. Investigation of the first derivative yields

$$\begin{aligned}
s'(y) &= \frac{1}{(1+y)^{2M}}\left(M(1+y)^{M-1}\sum_{k=0}^{m_0-1}\binom{M}{k}y^k - (1+y)^M\sum_{k=0}^{m_0-1}k\binom{M}{k}y^{k-1}\right) \\
&= \frac{(1+y)^{M-1}}{(1+y)^{2M}}\left(\sum_{k=0}^{m_0-1}M\binom{M}{k}y^k - \sum_{k=0}^{m_0-1}k(1+y)\binom{M}{k}y^{k-1}\right) \\
&= \frac{(1+y)^{M-1}}{(1+y)^{2M}}\left(\sum_{k=0}^{m_0-1}\binom{M}{k}y^k(M-k) + \sum_{k=0}^{m_0-2}\binom{M}{k+1}y^k(k+1)\right)
\end{aligned}$$

Since $\binom{M}{k}(M-k) = \binom{M}{k+1}(k+1)$ we obtain

$$s'(y) = \binom{M}{m_0} m_0 \frac{y^{m_0-1}}{(1+y)^{M+1}} > 0, \qquad \forall\, y \in \mathbb{R}_+.$$

The second derivative of $s(y)$ takes the form

$$\begin{aligned} s''(y) &= \binom{M}{m_0} m_0 \frac{(1+y)^M \left[(m_0-1)y^{m_0-2}(1+y) - y^{m_0-1}(M+1)\right]}{(1+y)^{2M+2}} \\ &= \binom{M}{m_0} m_0 \frac{y^{m_0-2}}{(1+y)^{M+2}} \big(y(m_0-2-M) + (m_0-1)\big). \end{aligned}$$

Hence, we obtain, the second derivative of $s(y)$ has only one root in $\mathbb{R}_+$ at $y^* = \frac{(m_0-1)}{(M+2-m_0)}$, so that $s(y)$, respectively $S(z)$ is a sigmoidal function. □

As consequence of the sigmoidal function we find that the characteristic equation (3.59) exhibits bistable behavior and hysteresis as seen in the deterministic case, e.g. [10].

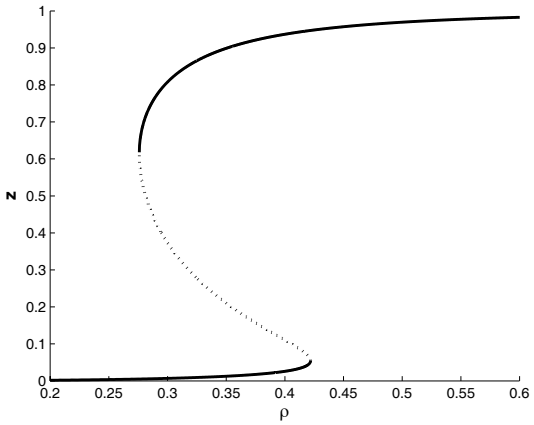

Figure 3.2.: Bifurcation diagram of the characteristic equation for $z(t)$ as a function of the parameter ρ (bold line). The solid (dotted) line represents the stable (unstable) steady states.

The stationary states of the characteristic equation (3.59) as a function of the parameter ρ was plotted in Figure 3.2. For parameter values see Appendix B.2. We see that the stationary states exhibit bistable behavior. For small values of ρ the steady state value of the AHL concentration is small whereas the steady state value is large for high values of ρ. For intermediate values of ρ we find the bistable region with three steady state solutions, where the small and large values are stable steady solutions while the intermediate solution is unstable. Moreover, in case that the parameter ρ is changed on a slow time scale, we find hysteresis.

Hence, we find that the stationary solution possesses two locally stable branches [10]. For the lower branch we call the population subcritical, where almost all cells of the population are in the resting state, whereas in the higher branch, the population is supercritical, i.e. almost all cells in the population are activated.

Biological the bistability means that for small cell densities the population is subcritical and for large cell densities it is supercritical. Moreover, it turns out that the switch between subcritical and supercritical is hysteretic, so that the population changes from subcritical to supercritical at a different cell density level than vice versa. This behavior can be interpreted as a mechanism of the Quorum Sensing system to filter noise. All in all, in the formal limit $V \to \infty$ our model corresponds to deterministic models [10, 51].

3.3.2. Stationary Solution and Asymptotic Behavior

In this subsection we analyze the stationary solution $\hat{h}_s(z)$ of the scaled limit equation (3.56) where we then obtain

$$\partial_t \hat{h}(z,t) = 0 = \partial_z(-\hat{g}(z)\hat{h}(z,t) + \hat{a}(z)\partial_z \hat{h}(z,t)).$$

Integrating with respect to z yields

$$-\hat{g}(z)\hat{h}_s(z) + \hat{a}(z)\partial_z \hat{h}_s(z) = C$$

where C is constant. This is, the flux is constant. As the flux is zero at the boundary of the interval, we obtain $C = 0$. In order to derive the stationary solution $\hat{h}_s(z)$ of the limit equation (3.56) we solve the linear differential equation of first order

$$\partial_z \hat{h}_s(z) \quad = \quad \frac{\hat{g}(z)}{\hat{a}(z)}\hat{h}_s(z). \tag{3.60}$$

This differential equation can be solved explicitly via

$$\hat{h}_s(z) \quad = \quad ce^{I(z)} \quad \text{where} \quad I(z) := \int_{z_{min}}^{z} \frac{\hat{g}(\zeta)}{\hat{a}(\zeta)} d\zeta. \tag{3.61}$$

As $\hat{h}_s(z)$ denotes the stationary solution of the marginal distribution of the AHL molecule concentration, we require $\int_{\Omega_V} \hat{h}_s(z)dz = 1$ so that the constant c is determined by

$$c := \left(\int_{\Omega_V} e^{I(\zeta)} d\zeta \right)^{-1}.$$

Simulation of the stationary solution (3.61) for different values of the density ρ reveals that the stationary marginal distribution exhibits bimodality for a certain density range, see Figure 3.3. For small densities the stationary solution exhibits one mode which is localized at the minimal AHL concentration. Thus, the population is subcritical. On the other hand, for large densities the unique mode of the stationary marginal distribution

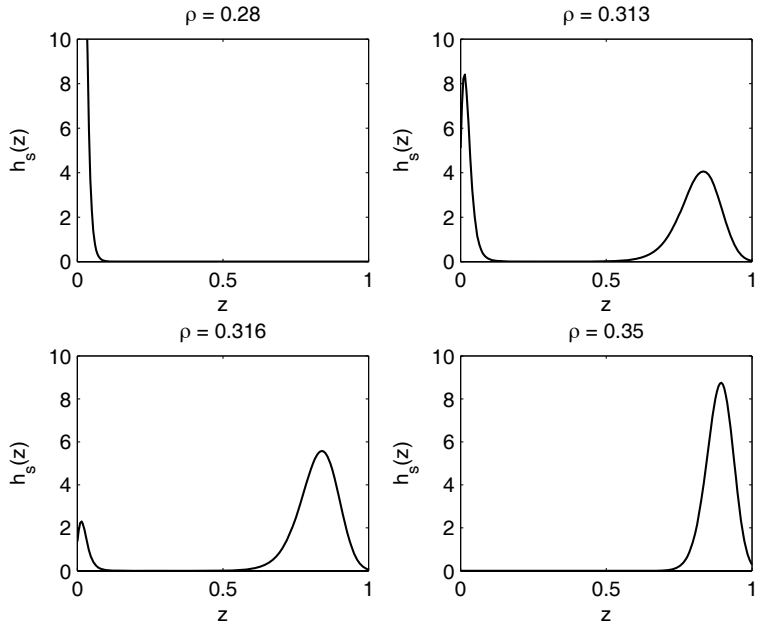

Figure 3.3.: Stationary solution (3.61) versus z for different values of the cell density ρ.

is located at the maximal concentration, i.e. the population is supercritical. For intermediate values of ρ one can find that the stationary solution is bimodal. This means that the population can either be sub- or supercritical with a certain probability, but regardless of the state of the population, the population acts in a synchronized way. Moreover, the simulation reveals that the AHL concentration dynamics does not exhibit hysteresis as the deterministic model.

By numerical simulations we show that the limit equation of the expanded model approximates the marginal distribution for the AHL concentration of the original model quite well: we simulated the marginal distribution for the AHL concentration of the original model

$$\dot{x}(t) = \alpha N + \beta n(t) - \gamma x \qquad \text{for} \qquad x \in \Omega, t \geq 0$$

three times for long time and different values of the cell density ρ, and plotted the end-concentration in Figure 3.4 (crosses). The parameters used for the simulation are in accordance to the Quorum Sensing system in *Pseudomonas putida* [11]. The exact parameter values can be found in Appendix B.2. For comparison we added a contour plot of the stationary solution of the scaled limit equation (3.61) as a function of the parameter ρ (solid line). One can see that the simulation of both models fit quite well.

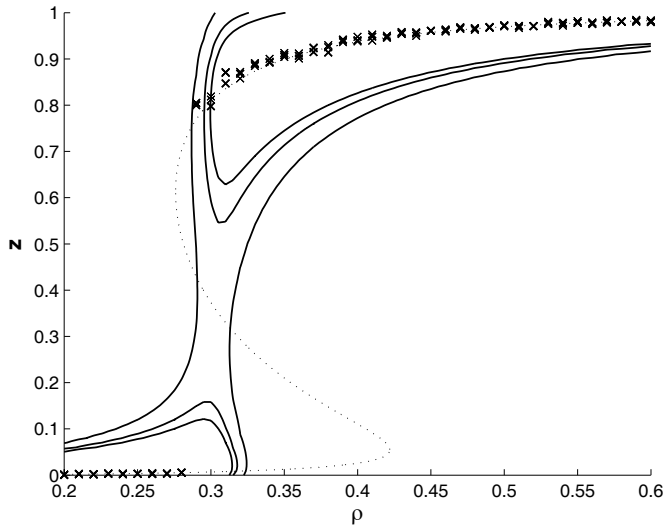

Figure 3.4.: Marginal distribution of the AHL concentration of the original model (3.10) versus ρ (crosses) and contour plot of the stationary solution of the scaled limit equation (3.61) as a function of ρ (solid lines, levels at 0.01, 0.1, 1).

Asymptotic Analysis

To derive further information about the asymptotic behavior of the stationary solution (3.61)

$$\hat{h}_s(z) = ce^{I(z)} \quad \text{where} \quad I(z) := \int_{z_{min}}^{z} \frac{\hat{g}(\zeta)}{\hat{a}(\zeta)} d\zeta$$

subject to the volume, we investigate the ratio

$$\begin{aligned} \frac{\hat{g}(z)}{\hat{a}(z)} &= V \frac{\left(\alpha\rho - \gamma z + \beta\rho \frac{\hat{\nu}(z)}{(\hat{\mu}(z)+\hat{\nu}(z))}\right)(\hat{\mu}(z)+\hat{\nu}(z))^3}{\beta^2 \rho \hat{\nu}(z)\hat{\mu}(z)} \\ &\quad + \frac{(\hat{\nu}(z)\partial_z\hat{\mu}(z) - \hat{\mu}(z)\partial_z\hat{\nu}(z))(\tilde{\nu}(x)-\tilde{\mu}(x))}{(\hat{\mu}(z)+\hat{\nu}(z))\hat{\nu}(z)\hat{\mu}(z)} =: V f_1(z) + f_2(z). \end{aligned}$$

Thus $I(z)$ can be rewritten as

$$I(z) = VI_1(z) + I_2(z), \quad \text{where} \quad I_1(z) := \int_{z_{min}}^{z} f_1(\zeta)d\zeta, \quad I_2(z) := \int_{z_{min}}^{z} f_2(\zeta)d\zeta,$$

and for the stationary solution (3.61) we obtain

$$\hat{h}_s(z) = c\left(e^{I_1(z)}\right)^V \left(e^{I_2(z)}\right). \tag{3.62}$$

Increasing the volume V, we see that the first exponential function $\left(e^{I_1(z)}\right)^V$ dominates $\left(e^{I_2(z)}\right)$. This means the interaction term only plays a role for small volumes, i.e. small

cell numbers, whereas for medium and large cell numbers the system is driven by the drift term only.

In Figure 3.5 we plotted the stationary solution of the limit equation for $\rho = 0.31$ (bimodal region) with different volumes V. As already mentioned, we find that for small values of V, i.e. small cell numbers, the interaction term of AHL production and jump process has a big influence, and the modes of the bimodal distribution are not in high gear (dash line). Increasing the volume V (dotted and solid line) we see that one mode get more and more pronounced tending to a delta peak whereas the second mode looses hight.

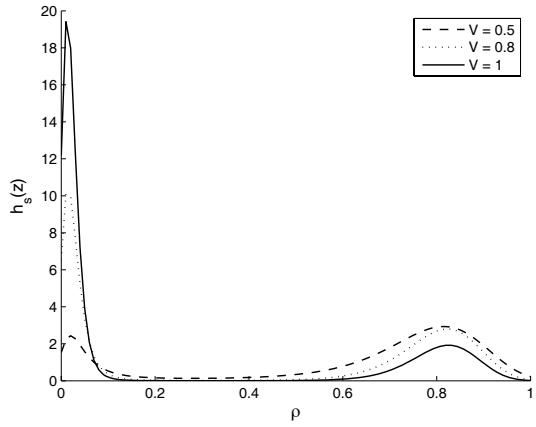

Figure 3.5.: Stationary solution of the scaled limit equation for different volume with density $\rho = 0.32$.

This behavior can be understood analytically by the following auxiliary result.

Proposition 3.10
Let $\varphi_1, \varphi_2 \in C^\infty(\Omega)$ be nonnegative functions with $\Omega \subset \mathbb{R}$ bounded. Further assume φ_1 has a unique global maximum at $z_0 \in \Omega$. Then we find

$$\psi_n(z) := \frac{\varphi_1^n(z)\varphi_2(z)}{\int_\Omega \varphi_1^n(\zeta)\varphi_2(\zeta)d\zeta}$$

is a Dirac sequence

$$\lim_{n\to\infty} \psi_n(z) = \delta_{z_0}(z).$$

Proof. Since φ_1, φ_2 are nonnegative functions we find

$$\psi_n(z) \geq 0 \qquad \text{and} \qquad \int_\Omega \psi_n(z)dz = 1 \qquad \text{for all } n.$$

It remains to show that

$$\lim_{n\to\infty} \int_{\Omega\setminus J} \psi_n = 0,$$

where $J := (z_0 - \varepsilon, z_0 + \varepsilon)$ with $z_0 := \arg\max_{z\in\Omega} \varphi_1(z)$.
We define $Z_0 := \varphi_1(z_0)$. Without loss of generality we find $\delta > 0$ so that $\varphi_1(z) \leq Z_0 - \delta$ for all $z \in \Omega\backslash J$ and rewrite

$$\int_{\Omega\backslash J} \psi_n = \frac{\int_{\Omega\backslash J} \varphi_1^n(\zeta)\varphi_2(\zeta)d\zeta}{\int_\Omega \varphi_1^n(\zeta)\varphi_2(\zeta)d\zeta} = \frac{\int_{\Omega\backslash J} \left(\frac{\varphi_1(\zeta)}{Z_0-\delta/2}\right)^n \varphi_2(\zeta)d\zeta}{\int_\Omega \left(\frac{\varphi_1(\zeta)}{Z_0-\delta/2}\right)^n \varphi_2(\zeta)d\zeta} \leq \frac{\int_{\Omega\backslash J} \left(\frac{Z_0-\delta}{Z_0-\delta/2}\right)^n \varphi_2(\zeta)d\zeta}{\int_\Omega \left(\frac{\varphi_1(\zeta)}{Z_0-\delta/2}\right)^n \varphi_2(\zeta)d\zeta}$$

Since $\frac{Z_0-\delta}{Z_0-\delta/2} < 1$ it follows

$$\int_{\Omega\backslash J} \left(\frac{Z_0-\delta}{Z_0-\delta/2}\right)^n \varphi_2(\zeta)d\zeta \xrightarrow[\infty]{n} 0.$$

To get the desired result, we further show that $\int_\Omega \left(\frac{\varphi_1(\zeta)}{Z_0-\delta/2}\right)^n \varphi_2(\zeta)d\zeta$ is bounded away from zero for $n \to \infty$. Therefore we define $J_1 \subseteq J$ with $|J_1| > 0$, so that

$$\varphi_1(z) > Z_0 - \delta/2 \qquad \text{for all } z \in J_1$$

and consequently

$$\frac{\varphi_1(z)}{Z_0 - \delta/2} \geq 1 \qquad \text{for all} z \in J_1.$$

For the integral term we now receive

$$\int_\Omega \left(\frac{\varphi_1(\zeta)}{Z_0-\delta/2}\right)^n \varphi_2(\zeta)d\zeta \geq \int_{J_1} \left(\frac{\varphi_1(\zeta)}{Z_0-\delta/2}\right)^n \varphi_2(\zeta)d\zeta > 0$$

and therefore

$$\lim_{n\to\infty} \int_{\Omega\backslash J} \psi_n = 0.$$

Hence we have shown that $\psi_n(z)$ is a Dirac sequence with $\lim_{n\to\infty} \psi_n(z) = \delta_{Z_0}(z)$. □

We want to apply Proposition 3.10 to the stationary solution $\hat{h}_s(z)$ with $\varphi_1 := e^{I_1(z)}$, and $\varphi_2 := e^{I_2(z)}$. Therefore, we need to assure that $e^{I_1(z)}$, resp. $I_1(z)$ has a unique maximum depending on the cell density ρ. There are parameter regions where $I_1(z)$ exhibits only one stationary state for all non-negative ρ. However, as depicted in Figure 3.2, for typical parameters - especially for those we are interested (appropriate for *Pseudomonas putida*) - there are two saddle-node bifurcations, leading to hysteresis. In this situation we can prove the following result.

Proposition 3.11
If there is a non-negative $\hat{\rho}$, so that $e^{I_1(z)}$ possess two local maxima, then there exists a unique ρ^* where the function $e^{I_1(z)}$ exhibits two global maxima. For all $\rho \neq \rho^*$ the function $e^{I_1(z)}$ has exactly one global maximum.

Proof. Since the exponential function is monotone, it is sufficient to investigate the extrema of $I_1(z,\rho)$ which are determined by the roots of

$$f_1(z,\rho) = \frac{\left(\alpha\rho - \gamma z + \beta\rho\frac{\hat{\nu}(z)}{(\hat{\mu}(z)+\hat{\nu}(z))}\right)(\hat{\mu}(z)+\hat{\nu}(z))^3}{\beta^2\rho\hat{\nu}(z)\hat{\mu}(z)}$$

where $f_1(z,\rho)$ is a continuous, monotone increasing function in ρ since $\gamma, z > 0$ and

$$\frac{\partial}{\partial\rho}f_1(z,\rho) = \frac{\partial}{\partial\rho}\left[\frac{\left(\alpha - \frac{\gamma z}{\rho} + \beta\frac{\hat{\nu}(z)}{(\hat{\mu}(z)+\hat{\nu}(z))}\right)(\hat{\mu}(z)+\hat{\nu}(z))^3}{\beta^2\hat{\nu}(z)\hat{\mu}(z)}\right] = \frac{\gamma z}{\rho^2} > 0.$$

Moreover, $\hat{\mu}(z), \hat{\nu}(z), \beta > 0$ so that the roots of f_1 are determined by

$$\alpha\rho - \gamma z + \beta\rho\frac{\hat{\nu}(z)}{\hat{\mu}(z)+\hat{\nu}(z)} = 0 \tag{3.63}$$

which corresponds to the stationary states of the characteristic equation (3.59). Since $\frac{\hat{\nu}(z)}{\hat{\mu}(z)+\hat{\nu}(z)}$ is a sigmoidal function (Proposition 3.9) we know that $f_1(z,\rho)$ exhibits one to three roots.

Equation (3.63) can be rewritten as

$$\frac{\gamma z}{\rho} = \alpha + \beta\frac{\hat{\nu}(z)}{\hat{\mu}(z)+\hat{\nu}(z)}. \tag{3.64}$$

Since we know that $I_1(z,\rho)$ possesses two local maxima at a certain parameter value $\hat{\rho}$, there are three roots of $f_1(z,\hat{\rho})$ present in the system (Figure 3.6, (1)). Moreover, for

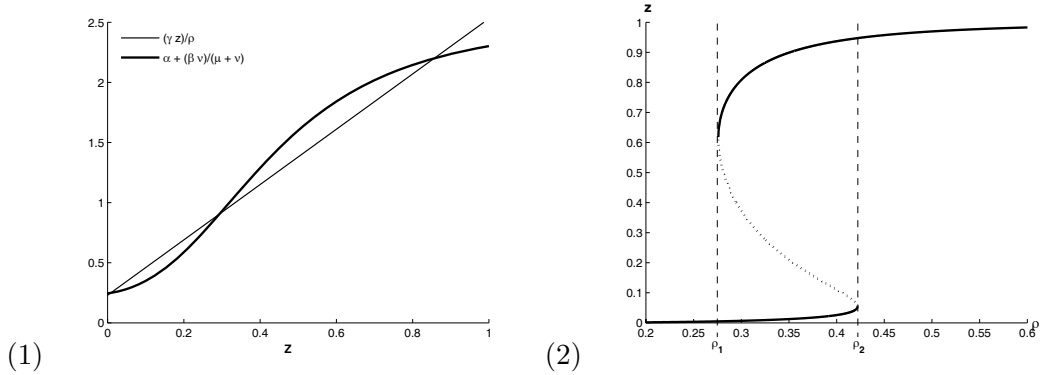

(1) (2)

Figure 3.6.: (1) Three intersection of $\alpha + \beta\frac{\hat{\nu}(z)}{\hat{\mu}(z)+\hat{\nu}(z)}$ and $\frac{\gamma z}{\hat{\rho}}$ for $\hat{\rho} = 0.32$ (2) Bifurcation diagram of (3.63)

$\rho > \hat{\rho}$ we find that there exists one unique saddle-node bifurcation at ρ_2 and for $\rho < \hat{\rho}$ we obtain one unique saddle-node bifurcation at ρ_1 (Figure 3.6, (2)). As the proof for this fact is simple and reproduced rather often (see e.g. [36, 48]), we do not reproduce the arguments here.

We consider three different cases:

$\rho < \rho_1, \rho > \rho_2$: Since $f_1(z_{min}) > 0$ and $f_1(z_{max}) < 0$ for all ρ and $f_1(z, \rho)$ exhibits only one non-negative root we obtain that $I_1(z, \rho)$ has only one maxima, which is global.

$\rho = \{\rho_1, \rho_2\}$: In this case $f_1(z, \rho)$ possesses two non-negative roots, which we denote by $z_-(\rho)$ and $z_+(\rho)$. Without loss of generality we define $z_-(\rho) < z_+(\rho)$ so that

$$\frac{\partial}{\partial z} I_1(z, \rho)\big|_{z=z_-, z_+} = 0.$$

$z_-(\rho_1)$ is a simple root of $f_1(z, \rho_1)$ and the saddle-node bifurcation happens at $z_+(\rho_1)$. Thus, $f_1(z, \rho_1) < 0$ for all $z \in (z_-(\rho_1), z_+(\rho_1))$ and

$$I_1(z_+(\rho_1), \rho_1) - I_1(z_-(\rho_1), \rho_1) = \int_{z_-(\rho_1)}^{z_+(\rho_1)} f_1(z', \rho_1) dz' < 0.$$

Similarly, for $\rho = \rho_2$ we derive $f_1(z, \rho_2) > 0$ for $z \in (z_-(\rho_2), z_+(\rho_2))$ and thus

$$I_1(z_+(\rho_2), \rho_2) - I_1(z_-(\rho_2), \rho_2) = \int_{z_-(\rho_2)}^{z_+(\rho_2)} f_1(z', \rho_2) dz' > 0.$$

Therefore, we obtain one global maximum at $z_-(\rho_1)$, resp. $z_+(\rho_2)$.

$\rho_1 < \rho < \rho_2$: In this last case $f_1(z, \rho)$ possesses three non-negative roots and we define $z_-(\rho) < z_0(\rho) < z_+(\rho)$ where

$$\frac{\partial}{\partial z} I_1(z, \rho)\big|_{z=z_-, z_0, z_+} = 0.$$

Moreover, we find

$$\begin{aligned}\frac{\partial}{\partial \rho}(I_1(z_+(\rho), \rho) - I_1(z_-(\rho), \rho)) &= \frac{\partial}{\partial \rho} \int_{z_-(\rho)}^{z_+(\rho)} f_1(z', \rho) dz' \\ &= f(z_+(\rho), \rho) z'_+(\rho) - f(z_-(\rho), \rho) z'_-(\rho) + \int_{z_-(\rho)}^{z_+(\rho)} \frac{\partial}{\partial \rho} f_1(z', \rho) dz' > 0.\end{aligned}$$

As $I_1(z_+(\rho_1), \rho_1) - I_1(z_-(\rho_1), \rho_1) < 0$, $I_1(z_+(\rho_2), \rho_2) - I_1(z_-(\rho_2), \rho_2) > 0$, and $I_1(z_+(\rho), \rho) - I_1(z_-(\rho), \rho)$ strictly increasing in ρ, there exists exactly one value $\rho^* \in (\rho_1, \rho_2)$ with

$$I_1(z_+(\rho^*), \rho^*) = I_1(z_-(\rho^*), \rho^*).$$

Otherwise, for $\rho \neq \rho^*$ the function $I_1(z, \rho)$ possesses only one global maxima. □

With Proposition 3.11 we can apply Proposition 3.10 to our stationary solution.

Corollary 3.12
For $\rho \neq \rho^*$, the stationary solution $\hat{h}_s(z) = c\left(e^{I_1(z)}\right)^V \left(e^{I_2(z)}\right)$ tends to a Dirac delta function in the limit $V \to \infty$,

$$\lim_{V \to \infty} \hat{h}_s(z) = \delta_{z_0}(z)$$

where $z_0 := \arg\max_{z \in \Omega} e^{I_1(z)}$.

In the limit $V \to \infty$, the cell density ρ^* determines a sharp threshold of the stationary solution where the population switches between sub- and supercritical, so that the system exhibits neither hysteresis nor bimodality.

Conclusion

We investigated the marginal distribution of the AHL concentration (3.51) concerning two different limits, namely $V \to \infty$ and $t \to \infty$ and found out that the result depends upon the order of the limits. When we first applied the limit $V \to \infty$ to the scaled limit equation we return to the deterministic model where the stationary solution exhibits bistability and hysteresis.
Moreover we found that for the stationary solution of the scaled limit equation the bistability of the deterministic models was translated into bimodality but the stationary solution is not determined by hysteresis. This behavior can be interpreted a "tunnel" effect, i.e. the population "tunnels" from one stationary state to the other. Only if the signal is changed fast enough, the picture changes (see Figure 3.7) and the hysteresis is present again (the tunneling effect is too slow). In Figure 3.7 we simulated the scaled limit equation for populations where the number of cells within the population increase, resp. decrease in time. Thus, the cell density changes over time and we substitute $\rho \to \rho(t) = \rho_1 + \rho_2 t$. The simulation reveals that if we change the cell density faster, the threshold, where the system switches from one state to the other, varies, i.e. we get hysteresis.

If the parameters are changed even faster, $V \to \infty$, we could prove that the solution tends to a point mass centered at the (generically unique) maximum of the stationary solution, which corresponds approximately to the locally stable stationary states of the ordinary differential equation of the first case. Hence, as expected we found the stationary states of the deterministic model. It was unexpected, though, that the bistability and hysteresis was lost in this case. This is due to the fact that the time scale separation of the change in the parameters and in the system is not given any more.

In biology the hysteresis is an important feature of the Quorum Sensing system. Usually, hysteresis is understood as a protective mechanism to filter the stochasticity of the signal. All in all, our analysis reveals that the stochasticity may destroy this hysteresis for small populations. Our results can be interpreted as the possibility of the system to "tunnel" from one, deterministic locally stable state to another. In this case, one of the stationary states generically wins. However, it takes the system rather a long time to "tunnel" from one state to the other. This aspect was found in the analysis of the stationary states. If we consider a signal that changes very slowly, the system has enough time to "tunnel" into the stationary measure. I.e., there will be a distinct jump of the system at one single given value of the signal - no matter if we decrease or increase the signal. This is true only for very slow varying signals.
If we add on top of this slow signal a (high frequent) stochastic noise, this noise may drive the system over the critical threshold. In the case of the deterministic hysteresis,

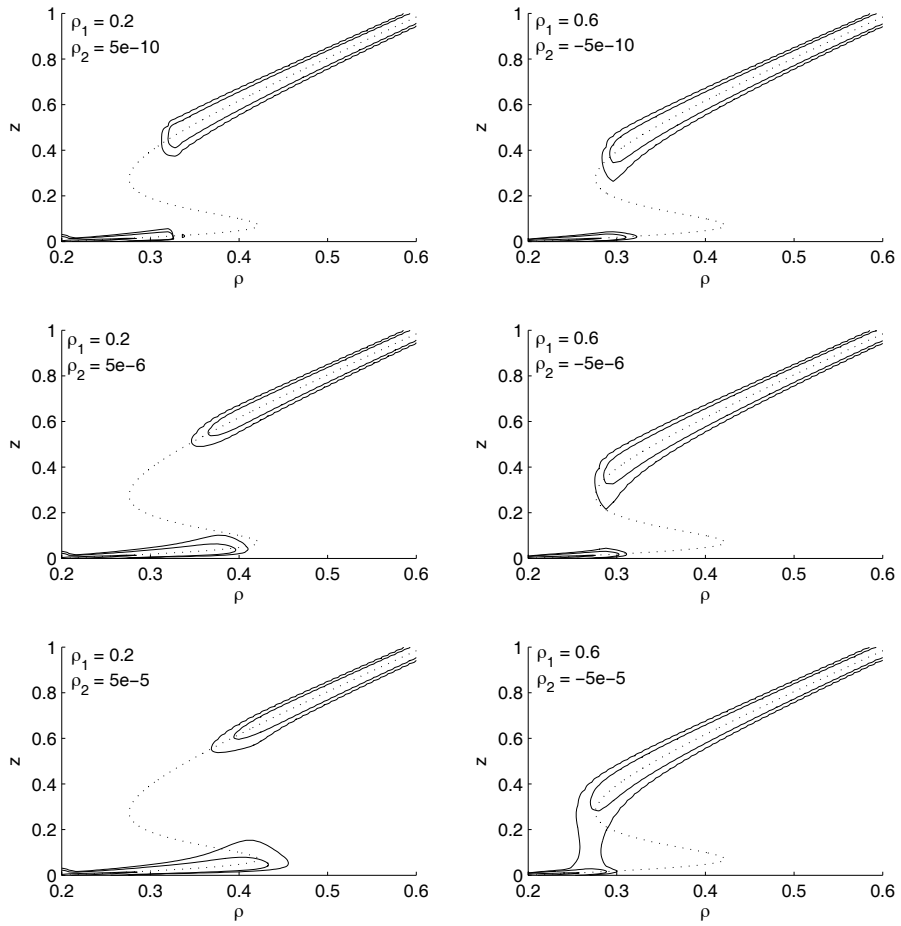

Figure 3.7.: Simulation of the scaled limit equation (3.50). Left side: initial value $\rho_1 = 0.2$, right side: $\rho_1 = 0.6$ (level lines at 0.001, 0.01, 0.25)

an arbitrary full activation/deactivation is prevented by the fact that activation and deactivation occur at different threshold values. In the present case activation and deactivation takes place at the very same signal strength. However, another mechanism prevents the system from erratic behavior: The system is very slow. The signal has to be above the threshold a long time before the "tunnel" effect allows the system to switch between sub- and supercritical. Hence, the noise is averaged out.

This is, we describe here an alternative way to filter out stochasticity in a signal. This mechanism is also based on the hysteresis in the deterministic formulation of the model, but relies on the stochastic "tunnel" effect. The advantage for a population may be,

that there is one slightly distinct threshold that determines the switch of the behavior, instead of two different thresholds (depending on the history of the systems). This may allow a more accurate response on environmental conditions.

4. Approximating the Dynamics of Active Cells in a Diffusive Medium

In order to get a better understanding of the Quorum Sensing system, experiments on single cell level are performed. Cells are tagged with reporter constructs that luminesce in different colors, and signal different states of a cell. It is hard to use classical spatially structured population models to interpret these data. These models usually describe cell densities. The data, on the other hand, express the state of single cells.

We take up the modeling approach chosen in [34] where the cells are kept as single extended objects with a spatially homogeneous interior. The model consists of a system of ordinary differential equations describing the density of the signaling molecules within the cell, coupled by a parabolic diffusion equation, governing the dispersion and absorbtion of the signaling molecules in the exterior. The cell communicate with the exterior by a spatially extended surface. This model is quite simple to develop. However, as we have a system of nonlinear ordinary differential equations coupled with a linear partial differential equation defined on a region with little holes (the cells), it is not too easy to handle this model. Analytical solutions are not available in the case of several cells, and numerical schemes require a fine discretization around the tiny holes, leading to a high computational burden.

In the stationary case, the paper [34] chooses the approach that the cell radius is shrunk to zero, leading to an homogeneous equation for the signaling substance. The interaction of the cells however appear as delta peaks on the right hand side. In case of the homogeneous space, this partial differential equation can be solved explicitly, such that the stationary points of the system can be computed as the solution of a finite dimensional algebraic equation.

The aim of this chapter is to take up the findings of the work done in [34] and present an approximative solution of the problem in the non stationary case. Therefore we investigate the model for one cell and state an approximation theorem where we can show that for long time behavior the solutions of original and approximative model are close to each other. Moreover the model for several interacting cells can be approximated by a delayed equation, where the delay represents the time needed for a signaling molecule to diffuse between the cells [44].

4.1. Mathematical Model

We apply the modeling approach of [34] and consider N cells that communicate via Quorum Sensing. In the outer space, the spatial dynamics of the signaling molecule substances is well described by a diffusion equation. Within the cells, the spatial structure is less important, and an ordinary differential equation represents appropriately the dynamics of the internal state of a cell [10]. The outer field and the internal state communicate via the in- and outflow which is determined by the boundary conditions.

The cells are described as balls $\Omega_i = \{x \in \mathbb{R}^3 : \|x - x_i\| \leq R\}$, $i = 1, ...N$, with radius R in $\mathbb{R}^3$, the total mass of the signaling substance within each cell is denoted by $a_i = a_i(t) \in \mathbb{R}$, and the exterior is denoted by $\Omega = \mathbb{R}^3 \setminus \bigcup_{i=1}^{N} \Omega_i$. The model then takes the form of an initial boundary value problem, where the exterior concentration u is described by a diffusion equation, coupled with N ordinary differential equations for a_i, $i = 1, \ldots, N$, namely

$$\begin{aligned} u_t &= D\Delta u, & u(x,0) = u_0(x), \\ -D\frac{\partial}{\partial \nu} u\big|_{\partial\Omega_i} &= d_1 u\big|_{\partial\Omega_i} - d_2 a_i(t), & \\ a_i'(t) &= f(a_i(t)) + \int_{\partial\Omega_i} (d_1 u - d_2 a_i(t))\, do, & a_i(0) = a_{i0}. \end{aligned}$$

Here $D > 0$ is the diffusion coefficient, $d_1, d_2 \geq 0$ are inflow and outflow constants, and ν denotes the outer normal of Ω.

The internal production of the autoinducer $a_i(t)$ in each cell is modeled by the function f, for instance of the form [10]

$$f(a_i) = \alpha + \frac{\beta a_i^n}{a_{\text{thresh}}^n + a_i^n} - \gamma_c a_i. \tag{4.1}$$

Thus, depending on the choice of $\alpha, \beta, a_{\text{thresh}}, \gamma_c > 0$, the problem $a_i' = f(a_i)$ may have up to three positive stationary states [10]. It is straight to use more complex ODE's where the state of a cell is described by a vector of different densities, e.g. corresponding to different Quorum Sensing systems.

This model has the disadvantage to be computational costly for numerical schemes, since cells appear as little holes in the three dimensional space, which forces a rather fine discretization around the cells leading to a high numerical effort. If $f(.)$ is monotone, the theory of monotone dynamical systems allow to draw some conclusions about stationary states and ω-limit sets [34], but the detailed time course during the intermediate phase cannot be revealed by this method.

4.2. Approximative Model

According to [34] we use the fact that cells are often scattered at large distances in comparison with their radius and investigate the limit $R \to 0$, i.e. the cell is shrunken

to a point source. Therefore we have to scale the equation suitable, where the scaling behavior of influx and efflux of a cell is of special interest.

The efflux of the mass a_i is proportional to the surface of the cell, which is $4\pi R^2$. Thus, it vanishes with order $\mathcal{O}(R^2)$ and the proportionality constant of the efflux d_2 has to be rescaled by $1/R^2$. As we expect point sources to appear in the limit $R \to 0$, close to the center x_i of a cell i the solution should behave like $u \sim 1/\|x - x_i\|$, i.e. the solution exhibits a pole of order one. The influx is also proportional to the cell surface so that we find u is proportional to $R^{-1}4\pi R^2 = 4\pi R$, and we therefore rescale the proportionality constant for the influx d_1 by $1/R$ [34]. The rescaled system thus reads

$$\begin{aligned} u_t &= D\Delta u, \qquad u(x,0) = u_0(x), && \text{(4.2a)} \\ -D\frac{\partial}{\partial \nu}u\big|_{\partial\Omega_i} &= \frac{d_1}{R}u\big|_{\partial\Omega_i} - \frac{d_2}{R^2}a_i(t), && \text{(4.2b)} \\ a_i'(t) &= f(a_i(t)) + \int_{\partial\Omega_i}\left(\frac{d_1 u}{R} - \frac{d_2 a_i(t)}{R^2}\right)do, \qquad a_i(0) = a_{i,0}. && \text{(4.2c)} \end{aligned}$$

However, in contrast to [34] we later shall also assume that the distance between cells has to be scaled, as $\|x_i - x_j\| = \mathcal{O}(R^\alpha)$ for some $0 < \alpha < 1$.

4.2.1. Case of One Cell

First, we analyze the case of one cell which is centered at the origin. Therefore, let $N = 1$, $x_1 = 0$, and write $a = a_1$. Moreover, let $a_{1,0} = a_0 = 0$ and $u_0 \equiv 0$. The latter can be seen as a compatibility condition between (4.2a,b) and (4.2c). We show that the function $a(t)$ in (4.2) can be approximated by the solution $b(t)$ of the delayed ODE

$$\begin{aligned} b'(t) &= f(b(t)) - 4\pi d_2 b + d_1 \widehat{T}_R[\hat{b}(\cdot)](t), \qquad b(0) = 0, && \text{(4.3)} \\ \hat{b}(t) &= \frac{4\pi D d_2}{d_1 + D}b(t), \quad \widehat{T}_R[\hat{b}(\cdot)](t) = 4\pi R\int_0^t \frac{1}{(4\pi D\tau)^{3/2}}e^{-R^2/4D\tau}\hat{b}(t-\tau)d\tau. && \text{(4.4)} \end{aligned}$$

In detail, we show the following theorem.

Theorem 4.1
Assume that $a(t) \in C^1$ is the solution of (4.2), and $b(t)$ the solution of (4.3). Then for all $t_1 > 0$ there exist $R_0 > 0$ and $C > 0$ such that for all $0 < R < R_0$ we have

$$\sup_{0\le t\le t_1}|a(t) - b(t)| \le CR\|a\|_{C^1}. \tag{4.5}$$

The main idea of the proof is to consider the following auxiliary problem: For given $a(t)$ we approximate solutions u of the initial boundary value problem (4.2a,b) by solutions v of the initial value problem

$$v_t = D\Delta v + b(t)\delta_0(x), \quad x \in \mathbb{R}^3, \quad v(x,0) = 0, \tag{4.6}$$

with a Dirac–delta source, and with a suitable $b(t)$. The optimal choice for b turns out to be

$$b(t) = \frac{4\pi D d_2}{d_1 + D} a(t) = \hat{a}(t).$$

Next we compare solutions of (4.2) with solutions (v, b) of

$$\begin{aligned} v_t &= D\Delta v + \hat{b}(t)\delta_0(x), \qquad v|_{t=0} = 0, && \text{(4.7a)} \\ b'(t) &= f(b(t)) + \int_{\partial\Omega} \left(\frac{d_1 v}{R} - \frac{d_2 b(t)}{R^2} \right) do, \qquad b(0) = 0. && \text{(4.7b)} \end{aligned}$$

Since (4.7a) can be solved explicitly, the ordinary differential equation (4.7b) for b can be written as

$$b'(t) = f(b(t)) - 4\pi d_2 b(t) + d_1 \widehat{T}_R[\hat{b}(\cdot)](t)$$

with $\widehat{T}_R$ defined in (4.4). Similarly, the ordinary differential equation (4.2c) can be written as

$$a'(t) = f(a(t)) - 4\pi d_2 a(t) + d_1 T_R[a(\cdot)](t),$$

where

$$T_R[a(\cdot)](t) = \int_{\partial\Omega} \frac{u(t)}{R} do,$$

with $u(t)$ the solution of (4.2a), (4.2b). The main step is to derive *a priori* estimates for the difference between $T_R[a]$ and $\widehat{T}_R[\hat{a}]$. Gronwall's inequality then yields the result.

As already explained we first want to compare solutions of (4.2a),(4.2b) with solutions of (4.6). It will turn out that $b(t) = \hat{a}(t)$ is the optimal choice for our purposes, but for now we keep b free.

Lemma 4.2
Let $w(x,t) = u(x,t) - v(x,t)$. Then $w(x,t)$ satisfies

$$\begin{aligned} w_t &= D\Delta w, \qquad x \in \Omega, \quad w(x,0) = 0, \\ -D\frac{\partial}{\partial \nu} w\big|_{\partial\Omega} &= \frac{d_1}{R} w\big|_{\partial\Omega} + g(x,t)\big|_{\partial\Omega}, \end{aligned} \tag{4.8}$$

where

$$g(x,t) = \frac{1}{R^4} \int_0^t b(\tau) \phi\left(\frac{R^2}{4D(t-\tau)} \right) d\tau - \frac{d_2 a(t)}{R^2}$$

and

$$\phi(x) = \pi^{-3/2} x^{3/2} e^{-x} (d_1 + 2Dx).$$

Proof. As $u = w + v|_\Omega$, we find

$$\begin{aligned} w_t &= D\Delta w, \quad w(x,0) = 0, \\ -D\frac{\partial}{\partial \nu} w\big|_{\partial\Omega} &= \frac{d_1}{R} u\big|_{\partial\Omega} - \frac{d_2}{R^2} a(t) + D\frac{\partial}{\partial \nu} v\big|_{\partial\Omega} = \frac{d_1}{R}(w+v)\big|_{\partial\Omega} - \frac{d_2}{R^2} a(t) + D\frac{\partial}{\partial \nu} v\big|_{\partial\Omega}, \\ &= \frac{d_1}{R} w\big|_{\partial\Omega} + g(x,t)\big|_{\partial\Omega} \end{aligned}$$

with

$$g(x,t) = \frac{d_1}{R} v\big|_{\partial\Omega} - \frac{d_2}{R^2} a(t) + D \frac{\partial}{\partial \nu} v\big|_{\partial\Omega}, \qquad x \in \partial\Omega.$$

The equation (4.6) for v can be solved explicitly. Let

$$K(x,t) = \frac{1}{(4\pi D t)^{3/2}} e^{-x^2/(4Dt)},$$

then, since $v(x,0) = 0$,

$$v(x,t) \;\; = \int_0^t \int_{\mathbb{R}^3} K(x-y, t-\tau) b(\tau) \delta_0(y) dy d\tau = \int_0^t K(x, t-\tau) b(\tau) d\tau$$

Next, $v|_{\partial\Omega} = \int_0^t K(R, t-\tau) b(\tau) d\tau$. The outer normal for $x \in \partial\Omega$ reads $\nu(x) = \frac{-x}{\|x\|}$ so that $\frac{\partial}{\partial \nu} v(x)\big|_{\partial\Omega} = \nu^T \nabla v(x) = -\int_0^t K_x(R, t-\tau) b(\tau) d\tau$, where K_x denotes the partial derivative of K with respect to x. Hence

$$g(x,t) = \frac{1}{R} \int_0^t b(\tau) \left[d_1 K(R, t-\tau) - RDK_x(R, t-\tau) \right] d\tau - \frac{d_2 a(t)}{R^2}.$$

The integral kernel reads

$$\begin{aligned} d_1 K(R,t) - DRK_x(R,t) &= \frac{1}{(4\pi D t)^{3/2}} e^{-R^2/(4Dt)} \big[d_1 + 2D \frac{R^2}{4Dt} \big] \\ &= \frac{1}{R^3 (4\pi D t / R^2)^{3/2}} e^{-R^2/(4Dt)} \big[d_1 + 2D \frac{R^2}{4Dt} \big] = \frac{1}{R^3} \phi\left(\frac{R^2}{4Dt} \right). \end{aligned}$$ □

Lemma 4.3
For solutions w of Lemma 4.8 we obtain

$$\|w\|^2_{L^2(\Omega)} \le \frac{2R}{d_1} \int_0^t \int_{\partial\Omega} g^2(x,\tau) do d\tau, \tag{4.9}$$

$$\|w\|^2_{L^2([0,t], H^1(\Omega))} \le \frac{2R}{d_1 D} \left(\int_0^t \int_{\partial\Omega} g^2(x,\tau) do d\tau + D \int_0^t \int_0^\tau \int_{\partial\Omega} g^2(x,\sigma) do d\sigma d\tau \right). \tag{4.10}$$

Proof. (see also [44]) We have the *a priori* estimate

$$\begin{aligned} D \int_\Omega |\nabla w|^2 dx + \frac{d}{dt} \frac{1}{2} \int_\Omega w^2(x,t) dx &= D \int_\Omega |\nabla w|^2 dx + D \int_\Omega w \Delta w dx \\ &= D \left[\int_\Omega |\nabla w|^2 dx - \int_\Omega |\nabla w|^2 dx + \int_{\partial\Omega} w \partial_\nu w do \right] = - \int_{\partial\Omega} w \left[\frac{d_1}{R} w + g(x,t) \right] do \\ &\le -\frac{d_1}{R} \int_{\partial\Omega} w^2 do + \frac{d_1}{R} \int_{\partial\Omega} w^2 do + \frac{R}{d_1} \int_{\partial\Omega} g^2(x,t) do = \frac{R}{d_1} \int_{\partial\Omega} g^2(x,t) do \end{aligned}$$

using (4.8), Green's first identity and the estimation

$$-wg = -\sqrt{\frac{d_1}{R}}w\sqrt{\frac{R}{d_1}}g \leq \frac{d_1}{R}w^2 + \frac{R}{d_1}g^2.$$

Thus,

$$\frac{d}{dt}\frac{1}{2}\int_\Omega w^2(x,t)dx \leq \frac{d}{dt}\frac{1}{2}\int_\Omega w^2(x,t)dx + D\int_\Omega |\nabla w|^2 dx \leq \frac{R}{d_1}\int_{\partial\Omega} g^2(x,t)do. \quad (4.11)$$

Integrating (4.11) over time we find (4.9), and integrating a second time with respect to time yields (4.10). □

The next lemma explains the choice $b(t) = \hat{a}(t) = \frac{4\pi D d_2}{d_1+D}a(t)$. It is a key step to prove Theorem 4.1. Note that the constant can be chosen in such a way that it does neither depend on R nor on t.

Lemma 4.4
Assume that $a \in C^1(\mathbb{R}_+)$ with $a(0) = 0$. For all $t_1 > 0$ there exists a $C > 0$ such that if $b(t) = \hat{a}(t)$ then, for $t \leq t_1$,

$$\int_0^t \int_{\partial\Omega} g^2(x,\tau)dod\tau \leq Ct\|a'\|_\infty (\|a\|_\infty + \|a'\|_\infty) \quad (4.12)$$

Proof. Without suitable choice of b, e.g., for $b \equiv 0$ and $a \not\equiv 0$, we obviously have $\int_0^t \int_{\partial\Omega} g^2(x,\tau)dod\tau \sim R^{-2}$. However, since $a(0) = 0$ we have, by the mean value theorem,

$$\begin{aligned}
&\int_0^t g^2(R,\tau)d\tau = \int_0^t \left[\frac{1}{R^4}\int_0^\tau \hat{a}(\tau-\sigma)\phi\left(\frac{R^2}{4D\sigma}\right)d\sigma - \frac{d_2}{R^2}a(\tau)\right]^2 d\tau \\
&= \int_0^t \left[\frac{\hat{a}(\tau)}{R^4}\int_0^\tau \phi\left(\frac{R^2}{4D\sigma}\right)d\sigma - \frac{d_2}{R^2}a(\tau) + \frac{1}{R^4}\int_0^\tau [\hat{a}(\tau-\sigma)-\hat{a}(\tau)]\phi\left(\frac{R^2}{4D\sigma}\right)d\sigma\right]^2 d\tau \\
&= \int_0^t \left[a(\tau)\left(\frac{4\pi D d_2}{R^4(d_1+D)}\int_0^\tau \phi\left(\frac{R^2}{4D\sigma}\right)d\sigma - \frac{d_2}{R^2}\right) - \frac{1}{R^4}\int_0^\tau \hat{a}'(\tilde{\theta})\sigma\phi\left(\frac{R^2}{4D\sigma}\right)d\sigma\right]^2 d\tau \\
&\leq 2\int_0^t \left[a(\tau)\left(\frac{4\pi D d_2}{R^4(d_1+D)}\int_0^\tau \phi\left(\frac{R^2}{4D\sigma}\right)d\sigma - \frac{d_2}{R^2}\right)\right]^2 d\tau \\
&\qquad + 2\int_0^t \left[\frac{1}{R^4}\int_0^\tau \hat{a}'(\tilde{\theta})\sigma\phi\left(\frac{R^2}{4D\sigma}\right)d\sigma\right]^2 d\tau = 2(I_1+I_2),
\end{aligned}$$

where $\tau - \sigma \le \tilde{\theta} \le \tau$ in I_2. Next, with $\xi = \frac{R^2}{4D\sigma}$,

$$\begin{aligned}
I_1 &= \int_0^t \left[a(\tau) \left(\frac{d_2}{R^2\sqrt{\pi}(d_1+D)} \int_{R^2/4D\tau}^{\infty} (d_1 + 2D\xi)\xi^{-1/2} e^{-\xi} d\xi - \frac{d_2}{R^2} \right) \right]^2 d\tau \\
&= \int_0^t \Bigg[a(\tau) \Bigg(\frac{d_2}{R^2\sqrt{\pi}(d_1+D)} \Bigg((d_1+D) \left\{ \Gamma(1/2) - \int_0^{R^2/4D\tau} \xi^{-1/2} e^{-\xi} d\xi \right\} \\
&\qquad\qquad + \frac{2DR}{\sqrt{4D\tau}} e^{-R^2/4D\tau} \Bigg) - \frac{d_2}{R^2} \Bigg) \Bigg]^2 d\tau \\
&= \int_0^t \left[a(\tau) \frac{d_2}{R^2\sqrt{\pi}(d_1+D)} \left(\frac{2DR}{\sqrt{4D\tau}} e^{-R^2/4D\tau} - (d_1+D) \int_0^{R^2/4D\tau} \xi^{-1/2} e^{-\xi} d\xi \right) \right]^2 d\tau \\
&\le C_1 R^{-2} \int_0^t \frac{a(\tau)^2}{\tau} \, d\tau \le C_1 R^{-2} \int_0^t \tau a'(\theta) \frac{a(\tau)}{\tau} \, d\tau \le C_1 R^{-2} \|a\|_{C_0} \|a'\|_{C_0} t,
\end{aligned}$$

where we used integration by parts and $\Gamma(1/2) = \sqrt{\pi}$. Similarly,

$$\begin{aligned}
\int_0^\tau \sigma\phi\left(\frac{R^2}{4D\sigma}\right) d\sigma =& \frac{1}{\pi^{3/2}} \left(\frac{R^2}{4D}\right)^2 \int_{R^2/4D\tau}^{\infty} \xi^{-3/2} e^{-\xi} (d_1 + 2D\xi) d\xi \\
=& \frac{R^4}{(4D)^2\pi^{3/2}} \left[4d_1 \frac{\sqrt{D\tau}}{R} e^{-R^2/4D\tau} + (2D - 2d_1) \int_{R^2/4D\tau}^{\infty} \xi^{-1/2} e^{-\xi} d\xi \right] \\
\le& \frac{R^4}{(4D)^2\pi^{3/2}} \left[4d_1 \frac{\sqrt{D\tau}}{R} e^{-R^2/4D\tau} + (2D - 2d_1)\Gamma(1/2) \right],
\end{aligned}$$

hence

$$\begin{aligned}
I_2 &= \int_0^t \left[\frac{\hat{a}'(\tilde{\theta})}{R^4} \int_0^\tau \sigma\phi\left(\frac{R^2}{4D\sigma}\right) d\sigma \right]^2 d\tau \\
&\le \left(\int_0^t \frac{16}{R^2} d_1^2 D\tau e^{-R^2/2D\tau} + (2D - 2d_1)^2 \pi d\tau \right) \|a'\|_\infty^2 \le C_2 R^{-2} \|a'\|_\infty^2 t
\end{aligned}$$

Integrating over $\partial\Omega$ now yields the result. □

To compare solutions of the full problem (4.2) and the auxiliary problem (4.7) we need to estimate the differences of the traces of u and v on $\partial\Omega$. Therefore we introduce the following operators.

Definition 4.5 Let $u \in L^2_{loc}(\mathbb{R}_+, H^1(\Omega))$ denote the solution of (4.2a),(4.2b) for given $a \in C^1(\mathbb{R}_+)$ and define

$$T_R : C^1(\mathbb{R}_+) \to L^2_{\text{loc}}(\mathbb{R}_+), \quad T_R[a(\cdot)](t) = \frac{1}{R} \int_{\partial\Omega} u(t,x) do.$$

Similarly, let v be the solution of (4.6) for $b \in C^1(\mathbb{R}_+)$, and define

$$\widehat{T}_R : C^1(\mathbb{R}_+) \to L^2_{\mathrm{loc}}(\mathbb{R}_+), \quad \widehat{T}_R[b(\cdot)](t) = \frac{1}{R}\int_{\partial\Omega} v(x,t)do.$$

Remark 4.6 Integrating (4.12) from 0 to t_1 and using (4.10) shows that the solution of (4.2a),(4.2b) for given $a \in C^1(\mathbb{R}_+)$ is in $L^2((0,t_1),H^1(\Omega))$. Therefore, the operator T_R is well defined. The well-definedness of $\widehat{T}_R$ follows by direct calculation. Obviously,

$$\begin{aligned}\widehat{T}_R[b(\cdot)](t) &= \frac{1}{R}\int_{\partial\Omega}\int_0^t \frac{1}{(4\pi D(t-\tau))^{3/2}} e^{-x^2/(4D(t-\tau))} b(\tau)d\tau do \\ &= 4\pi R\int_0^t \frac{1}{(4\pi D(t-\tau))^{3/2}} e^{-R^2/(4D(t-\tau))} b(\tau)d\tau,\end{aligned}$$

and for $b \in C^1$ we have, estimating as above, $\xi = \frac{R^2}{4D(t-\tau)}$,

$$\widehat{T}_R[b(\cdot)](t) = \frac{R^3\pi}{D}\int_{R^2/4Dt}^{\infty} (\pi R^2)^{-3/2}\xi^{-1/2}e^{-\xi} b\left(t - \frac{R^2}{(4D\xi)}\right)d\xi \to \frac{1}{D}b(t) \tag{4.13}$$

as $R \to 0$, uniformly in $t \in [t_0, t_1]$ for any $t_0 > 0$.

Finally, for $\hat{a}, \hat{b} \in C^0$ we have

$$\|\widehat{T}_R[\hat{a}(\cdot)] - \widehat{T}_R[\hat{b}(\cdot)]\|_{L^\infty(0,t_1)} \le C\|\hat{a} - \hat{b}\|_{L^\infty(0,t_1)}. \tag{4.14}$$

Setting $\zeta = \hat{a} - \hat{b}$ this follows from

$$\begin{aligned}\|[\widehat{T}_R\hat{a}](t) - [\widehat{T}_R\hat{b}](t)\|_{L^\infty(0,t_1)} &= \frac{1}{R}\sup_{t\in(0,t_1)}\int_{\partial\Omega}\int_0^t \frac{1}{(4\pi D(t-\tau))^{3/2}} e^{-x^2/(4D(t-\tau))}\zeta(\tau)d\tau do \\ \le& 4\pi\|\zeta\|_{L^\infty(0,t_1)} R\sup_{t\in(0,t_1)}\int_0^t \frac{1}{(4\pi D(t-\tau))^{3/2}} e^{-R^2/(4D(t-\tau))}d\tau \\ \le& C\|\zeta\|_{L^\infty(0,t_1)}\sup_{t\in(0,t_1)}\int_{R^2/(4t)}^{\infty}\xi^{-1/2}e^{-\xi}d\xi \le C\|\zeta\|_{L^\infty(0,t_1)}\gamma(1/2) = C\|\zeta\|_{L^\infty(0,t_1)}.\end{aligned}$$

Lemma 4.7
Let $a \in C^1(\mathbb{R}_+)$. Then

$$\|T_R[a(\cdot)] - \hat{T}_R[\hat{a}(\cdot)]\|_{L^1(0,t_1)} \le CR\int_0^{t_1}\left(\int_{\partial\Omega} g^2(x,\tau)do\right)^{1/2} d\tau \le CRt_1\|a'\|_\infty^{1/2}\|a\|_{C^1}^{1/2}.$$

Proof. We have

$$\|T_R[a(.)](t) - \hat{T}_R[\hat{a}(.)](t)\|_{L^1(0,t_1)} = \frac{1}{R}\int_0^{t_1}\left|\int_{\partial\Omega} w(t,x)do\right| dt$$

Next, reasoning like in Lemma 4.3 we have

$$\begin{aligned}
0 &\leq D\int_0^t\int_\Omega |\nabla w|^2 dx d\tau + \frac{1}{2}\int_\Omega w^2(x,t)dx \\
&= -\int_0^t \frac{d_1}{R}\int_{\partial\Omega} w^2 do - \int_{\partial\Omega}[R^{-1/2}d_1^{1/2}w][g(x,t)R^{1/2}d_1^{-1/2}]do d\tau \\
&\leq -\frac{d_1}{2R}\int_0^t\int_{\partial\Omega} w^2 do d\tau + \frac{R}{2d_1}\int_0^t\int_{\partial\Omega} g^2(x,t)do d\tau
\end{aligned}$$

and hence

$$\int_0^t\int_{\partial\Omega} w^2 do d\tau \;\leq\; \frac{R^2}{d_1^2}\int_0^t\int_{\partial\Omega} g^2 do d\tau.$$

Thus

$$\begin{aligned}
\|T_R[a(.)](t) - \hat{T}_R[\hat{a}(.)](t)\|_{L^1(0,t_1)} &= \frac{1}{R}\int_0^{t_1}\left|\int_{\partial\Omega} w(t,x)do\right| dt \\
&\leq \frac{1}{R}\int_0^{t_1}\left(\int_{\partial\Omega} 1^2 do\right)^{1/2}\left(\int_{\partial\Omega} w(t,x)^2 do\right)^{1/2} dt \leq C\int_0^{t_1}\left(\int_{\partial\Omega} w^2(x,\tau)do\right)^{1/2} d\tau \\
&\leq \sqrt{t_1}\,C\left(\int_0^{t_1}\int_{\partial\Omega} w^2(x,\tau)do\right)^{1/2} d\tau \leq CR\sqrt{t_1}\left(\int_0^{t_1}\int_{\partial\Omega} g^2(x,\tau)do d\tau\right)^{1/2}
\end{aligned}$$

and the result now follows from Lemma 4.4. □

With this auxiliary results we now prove Theorem 4.1 by comparison of the solutions of (4.2) and (4.3).

Proof. (Theorem 4.1) We write the ordinary differential equations for $a(t)$ resp. $b(t)$ as

$$\begin{aligned}
a'(t) &= f(a(t)) - 4\pi d_2 a(t) + d_1 T_R[a(.)](t), \qquad a(0) = 0, \\
b'(t) &= f(b(t)) - 4\pi d_2 b(t) + d_1 \hat{T}_R[\hat{b}(.)](t), \qquad b(0) = 0,
\end{aligned}$$

where we know that

$$\begin{aligned}
\|T_R[a(.)](t) - \hat{T}_R[\hat{a}(.)](t)\|_{L^1(0,t_1)} &\leq CRt_1\|a'\|_{C^0}^{1/2}\|a\|_{C^1}^{1/2}, \\
|\hat{T}_R[\hat{a}(.)](t) - \hat{T}_R[\hat{b}(.)](t)| &\leq C_2\|\hat{a} - \hat{b}\|_{L^\infty(0,t_1)}.
\end{aligned}$$

Let $\zeta = a - b$ and w.l.o.g assume that f is globally Lipschitz. Then,

$$\begin{aligned}
|\zeta(t)| &= \left|\zeta(0) + \int_0^t \zeta' d\tau\right| \\
&\leq \int_0^t |f(a) - f(b)| + 4\pi d_2|a-b| + d_1|T_R a - \widehat{T}_R\hat{a}| + d_1|\widehat{T}_R\hat{a} - \widehat{T}_R\hat{b}|d\tau \\
&\leq C\int_0^t \eta d\tau + d_1\|T_R a - \widehat{T}_R\hat{a}\|_{L^1} + C\int_0^t \eta d\tau \\
&\leq CRt\|a'\|_{C^0}^{1/2}\|a\|_{C^1}^{1/2} + 2C\int_0^t \eta d\tau
\end{aligned}$$

where $\eta(\tau) = \sup_{0\le\sigma\le\tau}\zeta(\sigma)$. In particular, $\eta(t) \le CRt\|a\|_{C^1} + 2C\int_0^t \eta(\tau)$, and Gronwall's inequality yields the result. □

Moreover, $\widehat{T}_R\hat{b}(t) \to \frac{1}{D}\hat{b}(t)$ as $R \to 0$, uniformly in $t \in [t_0, t_1]$ for any $t_0 > 0$, see (4.13), such that (4.3) can be approximated by

$$b'(t) = f(b(t)) - Mb, \qquad b(0) = b_0, \qquad M = 4\pi D d_2/(d_1+D). \tag{4.15}$$

Thus, for a small cell its interaction with the medium can be explicitly calculated, up to a small error. Here $M > 0$ means that the interaction of a single cell with the exterior is always damping, i.e. there is a net outflow of signaling substance out of the cell.

4.2.2. Several Cells

The picture changes if there are several cells. Apart from the net outflow we discovered in the single-cell-case, there is also a net inflow that establishes the information exchange between the cells. The basic setting parallels that of the single cell scenario. For technical reasons, however, also the distances between the cells are scaled by R^α, i.e. $\|x_i - x_j\| = \mathcal{O}(R^\alpha)$. The approximative model in this case reads

$$b_i' = f(b_i) - 4\pi d_2 b_i + \frac{1}{R}\int_{\partial\Omega_i}\left(\int_0^t \sum_j \frac{1}{(4\pi D(t-\tau))^{3/2}} e^{-|x_i-x_j|^2/4D(t-\tau)}\hat{b}_j(\tau)d\tau\right) do. \tag{4.16}$$

Again, we are able to derive an error estimate.

Theorem 4.8
Assume that $a_i \in C^1$ for the solution a of (4.2c), and b_i the solution of (4.16). Then for all $t_1 > 0$ there exist $R_0 > 0$ and $C > 0$ such that for all $0 < R < R_0$ we have

$$\sup_{0\le t\le t_1}|a_i(t) - b_i(t)| \le CR^1 \sup_{j=1,..,N}\|a_j\|_{C^1(0,t_1)}. \tag{4.17}$$

The error estimate (4.17) is now proved with obvious modifications of the analysis in section 4.2.1. The basic idea for $N \ge 2$ cells is to introduce a delta source for each cell, i.e., to consider

$$v_t = D\Delta v + \sum_{i=1}^N \hat{b}_i(t)\delta_{x_i}(x), \qquad v|_{t=0} = 0 \tag{4.18a}$$

$$b_i'(t) = f(b_i(t)) + \int_{\partial\Omega_i}\left(\frac{d_1 v}{R} - \frac{d_2 b_i(t)}{R^2}\right) do, \qquad b_i(0) = 0. \tag{4.18b}$$

The ordinary differential equations (4.18b) can then be rewritten as

$$\begin{aligned} b_i' &= f(b_i) - 4\pi d_2 b_i + \hat{T}_R^i[\vec{b}(\cdot)](t), && (4.19)\\ \hat{T}_R^i[\vec{b}(\cdot)](t) &= \frac{1}{R}\int_{\partial\Omega_i} v(t,x)do && (4.20)\\ &= \frac{1}{R}\int_{\partial\Omega_i}\left(\int_0^t \sum_j \frac{1}{(4\pi D(t-\tau))^{3/2}} e^{-|x-x_j|^2/4D(t-\tau)}\hat{b}_j(\tau)d\tau\right)do. \end{aligned}$$

The communication between different cells is represented by

$$\frac{1}{R}\int_{\partial\Omega_i}\int_0^t \sum_{j\neq i} \frac{1}{(4\pi D(t-\tau))^{3/2}} e^{-|x-x_j|^2/4D(t-\tau)}\hat{b}(\tau)d\tau do$$

As the cell surface $\partial\Omega_i$ scales with R^2, this is a first order term. However, also our error estimate shows that the error between the original model and the approximation scales with R^1. Thus, the communication is of the same order as the error and hence can be neglected. An additional scaling of the cell distance is required to reduce the order of the error resp. to increase the order of the communication terms.

For $j \neq i$ we assume $\|x_i - x_j\| := \delta_{ij} = \tilde{\delta}_{ij}R^\alpha$ to obtain

$$\begin{aligned} &R^{-(1-\alpha)}\frac{1}{R}\int_{\partial\Omega_i}\int_0^t \frac{1}{(4\pi D(t-\tau))^{3/2}} e^{-|x-x_j|^2/4D(t-\tau)}\hat{b}_j(\tau)d\tau do\\ &= R^\alpha \int_0^t (4\pi D\tau)^{-3/2} e^{-(\delta_{ij}+\mathcal{O}(R))^2/4D\tau}\hat{b}_j(t-\tau)d\tau\\ &= \frac{R^\alpha}{4D\pi^{3/2}(\delta_{ij}+\mathcal{O}(R))}\int_{\delta_{ij}/4Dt}^\infty \xi^{-1/2}e^{-\xi}\hat{b}_j(t-(\delta_{ij}+\mathcal{O}(R))^2/4D\xi)d\xi\\ &\to \frac{1}{4D\pi^{3/2}\tilde{\delta}_{ij}}\Gamma(1/2)\hat{b}_j(t) \quad \text{as } R\to 0, \end{aligned}$$

which yields the approximate system, i.e.,

$$b_i' = f_i(\vec{b}) := f(b_i(t)) - Mb_i + R^{1-\alpha}\sum_{j\neq i}\frac{4\pi d_1 d_2}{\tilde{\delta}_{ij}(d_1+1)}b_j(t). \tag{4.21}$$

The form (4.16) let us nicely recognize the diffusible character of the communication: the delay in the interaction term reflects the probability that a molecule produced at time $\tau < t$ in cell j reaches cell i at time t. However, as the random walk in three dimensions is not recurrent, the probability that a molecule of cell i hits cell j decreases if R becomes smaller, especially if the molecule already had some time to diffuse away. The scaling prevents the interaction term to become negligible, but only the molecules that are created recently (instantaneously) have a chance to influence the neighboring cells. This effect leads to the ordinary differential equation (4.21).

A. Appendix to Chapter 2

A.1. Biological Experiments

We give a short description about the procedure of the experiments analysed by the model. For more detailed information, see the experimental original papers [46, 45].

Preparation of LuxN, LuxP, LuxQ and LuxU. LuxN, LuxP, LuxQ, LuxQ and LuxU were separately overexpressed in various E. coli strains, transformed with plasmids containing the respective gene. Subsequently, LuxP and LuxU were purified in solutions. The membrane bound LuxN and LuxQ were purified and prepared in inverted vesicles, i.e. that the autoinducer binding sites were localized within the vesicles and the phosphate binding sites outside.

Phosphorylation and dephosphorylation assay. Reactions were performed in phosphorylation buffer at 25°C. Sensor kinases LuxQ and LuxN were tested in membrane vesicles. For phosphorylation assays, i.e. measurement of kinase activity, LuxN and/or LuxQ containing vesicles were mixed with purified LuxU and, if required, the respective autoinducer. AI-2 was added bound to LuxP, if required. Generally, the concentration of LuxU was more than 10 times higher than of LuxN/LuxQ. To incorporate LuxP or LuxP/AI-2 into LuxQ membrane vesicles, vesicles were treated with three cycles of freezing and thawing. The reaction was started by addition of amongst others radiolabeled ATP. At various times the reaction was terminated followed by separation of the proteins. This procedure allows to measure the amount of phosphorylated protein. All enzymatic activities were calculated as average values of at least three independent experiments. For dephosphorylation assays, i.e. to measure phosphatase activity, LuxU was first phosphorylated using LuxN. The reaction mixture contained twice the amount of LuxN and LuxU. After 10min of incubation, membrane vesicles were removed by centrifugation, and ATP was removed by gel filtration. Dephosphorylation of LuxUP was initiated by addition of amongst others membrane vesicles containing LuxQ and LuxN, respectively, with or without the cognate autoinducers.

A.2. Parameter Estimation

The fitting procedure for LuxN and LuxQ has been performed as follows:

Sensor kinase LuxN:

(1) The ratio k_1/k_{-1} can be determined from the equilibrium of the autophosphorylation reaction which can be found in [46].

(2) The time series for the phosphorylation (Fig. 2.3 (c), (d)) allows to obtain an idea about the rates k_2 and k_{-2} (delay in the onset of the phosphorylation of LuxUP) and the rate k_3.

(3) The dephosphorylation experiment targets on rates k_{-3} and, up to a certain degree also at rates k_2 and k_{-2}. These rates, however, only play a minor role in the overall dynamics (especially w.r.t. equilibrium concentrations). Higher rates of the phosphotransfer from or to LuxN can balance different values for k_2 and k_{-2}.

(4) The influence of the autoinducer on the kinase activity of LuxN has been investigated in [46]. An experiment performed in that paper shows that the phosphatase activity is not affected by autoinducer. Hence, only the phosphotransfer from ATP or that to LuxUP is modified by the autoinducer. This cannot be decided. We have chosen to modify the rate k_1 only. In order to meet the baseline experiment (no autoinducer) there, we changed the rates k_1, k_{-1}, kai_1 and kai_{-1} with a factor two resp. one half. This is acceptable, as the experiments here (especially Fig. 2.3) and the experiments in [46] have a slightly different set-up. Then, changing kai_{-1} only, the asymptotic for a large amount of AI has been determined. At the end, choosing kai_4 and kai_{-4} in an appropriate way, the half-dose of autoinducer has been adjusted.

Especially in this last step, we have a large degree of freedom. However, we assume that the reactions of autoinducers are fast. Thus, the overall system "senses" a mean of the system without autoinducer, and the system where all sensor kinase is bound to the autoinducer. As the only rate that differs between the two kinases is k_{-1}, effectively this value is replaced by a value that is a functional of the autoinducer density. As long as this functional is met appropriately, the identification problem does not play a role.

Sensor kinase LuxQ: The basic idea has been that most units of LuxQ are chemically quite similar to LuxN. Thus, the rates should be similar. Starting with the values for LuxN, the rates for LuxQ have been carefully adapted. Most rates are in the same range but one: the autoinducer reduces the ability of LuxN to accept a phosphor group to 6% of the original rate, while for LuxQ we still find 30%. This finding corresponds to the fact that LuxQ is a less potent phosphor donator, and the modification of this rate may not be crucial in the overall system.

The parameter set is by far not unique. The measured data (that consist basically of the component LuxUP only) are not sufficient to allow for an identification of the parameters. The parameter values in the model (1) for LuxN and LuxQ are chosen according to the following table.

Name	LuxN	LuxN / Fig. 2.3(e)	LuxQ
k_1	$0.1/(\min \mu M)$	$0.33/(\min \mu M)$	$0.1/(\min \mu M)$
k_{-1}	$1.1e5/(\min \mu M)$	$0.55e5/(\min \mu M)$	$1.1e5/(\min \mu M)$
kai_1	$0.0006/(\min \mu M)$	$0.00216/(\min \mu M)$	$0.03/(\min \mu M)$
kai_{-1}	$1.1e5/(\min \mu M)$	$0.308e5/(\min \mu M)$	$1.1e5/(\min \mu M)$
k_2	$35/\min$	$\rightarrow$ same	$385/\min$
k_{-2}	$0.35/\min$	$\rightarrow$ same	$3.5/\min$
k_3	$0.03825/(\min \mu M)$	$\rightarrow$ same	$0.00144/(\min \mu M)$
k_{-3}	$0.15/(\min \mu M)$	$\rightarrow$ same	$0.1/(\min \mu M)$
kai_3	$0.03825/(\min \mu M)$	$\rightarrow$ same	$0.00144/(\min \mu M)$
kai_{-3}	$0.15/(\min \mu M)$	$\rightarrow$ same	$0.1/(\min \mu M)$
kai_4	$0.6/(\min \mu M)$	$\rightarrow$ same	$0.24/(\min \mu M)$
kai_{-4}	$1.0/(\min \mu M)$	$\rightarrow$ same	$0.5/(\min \mu M)$

Please note that we have chosen slightly different parameters to reproduce the data measured for this paper on the one hand, and measured in [46] on the other hand. The data from [46] are shown in Fig. 2.3 (e), and indicated separately in the table.
The fits for the three experiments targeting on the three processes (flow of phosphor from LuxUP to ADP, the flow of phosphor from ATP to LuxU, and the influence of this flow by autoinducers) are satisfying (see Fig. 2.3) and show that the model is able to meet the data for one sensor kinase only quite well.

The values for the additional rate constants of the complete model read

Name	value
nks_3	$0.0/(\min \mu M)$
nks_{-3}	$4/(\min \mu M)$
$nksai_3$	$0.0/(\min \mu M)$
$nksai_{-3}$	$15/(\min \mu M)$
qks_3	$0.00144/(\min \mu M)$
qks_{-3}	$0.1/(\min \mu M)$
$qkai_3$	$0.00144/(\min \mu M)$
$qksai_{-3}$	$0.1/(\min \mu M)$
k_5	$2.4/(\min \mu M)$
kai_5	$500/(\min \mu M)$
k_6	$10/\min$

The simulations done in this chapter are performed with ANSITO, a simulation tool based on the programming language Python^{TM}.

B. Appendix to Chapter 3

B.1. Transition Matrix

In this section we derive some information about the tridiagonal transition matrix $L_x \in \mathbb{R}^{(N+1)\times(N+1)}$ defined in 3.1.2:

$$L_x := \begin{pmatrix} l_0(x) & l_0^+(x) & 0 & & & \cdots & 0 \\ l_1^-(x) & l_1(x) & l_1^+(x) & 0 & & & \\ 0 & l_2^-(x) & l_2(x) & l_2^+(x) & 0 & & \\ \vdots & \ddots & \ddots & \ddots & \ddots & \ddots & \vdots \\ & & 0 & l_{N-2}^-(x) & l_{N-2}(x) & l_{N-2}^+(x) & 0 \\ & & & 0 & l_{N-1}^-(x) & l_{N-1}(x) & l_{N-1}^+(x) \\ 0 & \cdots & & & 0 & l_N^-(x) & l_N(x) \end{pmatrix}.$$

where

$$\begin{array}{rcll} l_i(x) & := & -(i\mu(x) + (N-i)\nu(x)) & i = 0, ..., N \\ l_i^-(x) & := & (N-(i-1))\nu(x) & i = 1, ..., N \\ l_i^+(x) & := & (i+1)\mu(x) & i = 0, ..., N-1. \end{array}$$

We use this information during the diffusion approximation. At the moment we are only interested in the structure of the matrix, i.e. eigenvalues and eigenvectors and therefore we skip the x-dependency and analyze the matrix for a given constant AHL concentration. Thus we define

$$L_N \quad := \quad L_x \in \mathbb{R}^{(N+1)\times(N+1)}, \qquad \text{resp.} \qquad L_{N+1} := L_x \in \mathbb{R}^{(N+2)\times(N+2)} \tag{B.1}$$

In order to simplify the proofs to follow it is convenient to introduce the dimension in the notation, since the proofs are done via induction. Also μ and ν are assumed to be constant in this sections.
The first property of the transition operator matrix is, that the sum over the columns, for each column, is equal to zero. Thus we know, that the matrix has a zero left eigenvalue,

$$\mathbf{e}^T L_N \quad = \quad 0 \qquad \text{where} \qquad \mathbf{e} = (1, ..., 1),\ \dim(\mathbf{e}) = N+1 \tag{B.2}$$

Hence the matrix L_N is singular and therefore not invertible. Thus, we use a generalization of the inverse.

In the first part this section we will determine the eigenvalues λ and the corresponding eigenvectors $\mathbf{w}$ of the transition operator matrix L_N. We can give a recursive description of the eigenvectors. Further we will show that there is a normalized left Perron eigenvector $\mathbf{Y}$, resp. $\mathbf{Y}(x)$. In the second part of this section we will do some calculations concerning the generalized inverse.

B.1.1. Eigenvalues and Eigenvectors

First we investigate the eigenvalues of the transition matrix which we calculate explicit as in the following proposition.

Lemma B.1 (Eigenvalues of the transition matrix)
The transition matrix $L_N \in \mathbb{R}^{(N+1)\times(N+1)}$ has eigenvalues $\lambda_k = -k(\mu+\nu)$ for $k = 0, ..., N$.

In order to derive this proof we need the a further proposition concerning the eigenvalues of L_N. As already mentioned we determine the eigenvalues recursive. Therefore, we first state the recursive relation of eigenvectors and eigenvalues.

Lemma B.2 (Eigenvectors of the transition matrix)
Let $\lambda_k := -k(\mu+\nu)$, $k = 0, ..., N$, eigenvalues of L_N with corresponding eigenvectors $\mathbf{w}_k^N = (w_{k,0}^N, w_{k,1}^N, ..., w_{k,N}^N)^T$.
Then $\lambda_{k+1} = -(k+1)(\mu+\nu)$ are eigenvalues of L_{N+1} with eigenvectors $\mathbf{w}_{k+1}^{N+1} \in \mathbb{R}^{N+2}$ where

$$\begin{aligned} w_{k+1,0}^{N+1} &:= w_{k,0}^N \\ w_{k+1,i}^{N+1} &:= w_{k,i}^N - w_{k,i-1}^N \qquad i = 1, ..., N \\ w_{k+1,N+1}^{N+1} &:= -w_{k,N}^N \end{aligned}$$

Proof. Let $\lambda_k := -k(\mu+\nu)$ eigenvalue of L_N to the eigenvector $\mathbf{w}_k^N$. Then we show:

$$L_N \mathbf{w}_k^N = \lambda_k \mathbf{w}_k^N \;\Rightarrow\; L_{N+1}\mathbf{w}_{k+1}^{N+1} = (\lambda_k - (\mu+\nu))\mathbf{w}_{k+1}^{N+1}$$

Starting with the assumption $\lambda_k \mathbf{w}_k^N = L_N \mathbf{w}_k^N$ we find:

$$\begin{aligned} (I^*) \quad \lambda_k w_{k,0}^N &= -N\nu w_{k,0}^N + \mu w_{k+1,1}^N \\ (II^*) \quad \lambda_k w_{k+1,i}^N &= (N+1-i)\nu w_{k+1,i-1}^N - (i\mu + (N-i)\nu) w_{k+1,i}^N \\ &\quad +(i+1)\mu w_{k+1,i+1}^N \qquad \text{for} \quad i = 1, ..., N-1 \\ (III^*) \quad \lambda_k w_{k+1,N}^N &= \nu w_{k+1,N-1}^N - N\mu w_{k+1,N}^N \end{aligned}$$

Based on this we show that $(\lambda_k - (\mu+\nu))\mathbf{w}_{k+1}^{N+1} = L_{N+1}\mathbf{w}_{k+1}^{N+1}$:

$$\begin{aligned} (I) \quad (\lambda_k - (\mu+\nu)) w_{k+1,0}^{N+1} &= -(N+1)\nu w_{k+1,0}^{N+1} + \mu w_{k+1,1}^{N+1} \\ (II) \quad (\lambda_k - (\mu+\nu)) w_{k+1,i}^{N+1} &= (N+2-i)\nu w_{k+1,i-1}^{N+1} + (i+1)\mu w_{k+1,i+1}^{N+1} \\ &\quad -(i\mu + (N+1-i)\nu) w_{k+1,i}^{N+1} \\ &\quad \text{for} \quad i = 1, ..., N-1 \\ (III) \quad (\lambda_k - (\mu+\nu)) w_{k+1,N+1}^{N+1} &= \nu w_{k+1,N}^{N+1} - (N+1)\mu w_{k+1,N+1}^{N+1} \end{aligned}$$

We show the equalities $(I) - (III)$ subject to $(I^*) - (III^*)$, starting each with the right hand side.
Ad (I):

$$\begin{aligned} -(N+1)\nu w^{N+1}_{k+1,0} + \mu w^{N+1}_{k+1,1} &= -N\nu w^N_{k,0} + \mu w^N_{k+1,1} - \nu w^N_{k,0} - \mu w^N_{k,0} \\ &= \lambda_k w^N_{k,0} - (\mu+\nu) w^N_{k,0} = (\lambda_k - (\mu+\nu)) w^{N+1}_{k+1,0} \end{aligned}$$

Ad (II):

$$\begin{aligned} & (N+2-i)\nu w^{N+1}_{k+1,i-1} - (i\mu + (N+1-i)\nu) w^{N+1}_{k+1,i} + (i+1)\mu w^{N+1}_{k+1,i+1} = \\ = \; & (N+2-i)\nu (w^N_{k,i-1} - w^N_{k,i-2}) - (i\mu + (N+1-i)\nu)(w^N_{k,i} - w^N_{k,i-1}) \\ & + (i+1)\mu (w^N_{k,i+1} - w^N_{k,i}) \\ = \; & (N+1-i)\nu w^N_{k,i-1} - (i\mu + (N-i)\nu) w^N_{k,i} + (i+1)\mu w^N_{k,i+1} \\ & - \left[((N+2-i)\nu w^N_{k,i} - ((i-1)\mu + (N+1-i))\nu) w^N_{k,i-1} + i\mu w^N_{k,i} \right] \\ & + \nu w^N_{k,i-1} - \mu w^N_{k,i} + \mu w^N_{k,i-1} - \nu w^N_{k,i} \\ = \; & \lambda_k (w^N_{k,i} - w^N_{k,i-1}) - (\mu+\nu)(w^N_{k,i} - w^N_{k,i-1}) = (\lambda_k - (\mu+\nu)) w^{N+1}_{k+1,i} \end{aligned}$$

Ad (III):

$$\begin{aligned} \nu w^{N+1}_{k+1,N} - (N+1)\mu w^{N+1}_{k+1,N+1} &= -(\nu w^N_{k,N-1} - N\mu w^N_{k,N}) + (\mu+\nu) w^N_{k,N} \\ &= -(\lambda_k - (\mu+\nu)) w^N_{k,N} = (\lambda_k - (\mu+\nu)) w^{N+1}_{k+1,N+1} \end{aligned}$$

Thus we have shown the validity of the equations $(I) - (III)$ and hence proven that λ_{k+1} is a eigenvalue of L_{N+1} with eigenvector $\mathbf{w}^{N+1}_{k+1}$. □

With this proposition we can go on and proof Lemma B.1 using induction over N.

Proof. (Lemma B.1)

$N = 0$**:** $L_0 = (0)$ has eigenvalue 0.

$N = 1$**:** $L_1 = \begin{pmatrix} -\nu & \mu \\ \nu & -\mu \end{pmatrix}$ has eigenvalues $0, -(\mu+\nu)$.

$N - 1 \to N$**:** We know that $-k(\mu+\nu)$ for $k = 0, ..., N-1$ are eigenvalues of L_{N-1}. Moreover, 0 is an eigenvalue as consequence of the sum over each column. Accordingly, as L_N is the generator of a Markov chain and thus preserves the total probability mass the corresponding left eigenvector is explicitly given as $(1, 1, ..., 1)$. And from Lemma B.1 we get that L_N also has the eigenvalues $-(k+1)(\mu+\nu)$ for $k = 0, ..., N-1$.

Hence summarized we get the eigenvalues of the transition matrix L_N as:

$$\lambda_k = -k(\mu+\nu) \quad \text{for} \quad k = 0, ..., N. \qquad \square$$

Information About the Eigenvectors We do some calculations concerning the eigenvectors which are summarized in the following. Also these formulas are used in Section 3.2.

Proposition B.3 (Sums over eigenvectors of L_N)

$$\sum_{i=0}^{N} w_{0,i}^N = (\mu+\nu)^N \qquad \sum_{i=0}^{N} w_{1,i}^N = 0 \qquad \sum_{i=0}^{N} i w_{1,i}^N = -(\mu+\nu)^{N-1}$$
$$\sum_{i=0}^{N} w_{2,i}^N = 0 \qquad \sum_{i=0}^{N} i w_{2,i}^N = 0$$

Proof. To show the equations in the Proposition B.3, we do some straight forward calculations. Concerning the eigenvector w_0^N we obtain

$$\sum_{i=0}^{N} w_{0,i}^N = \sum_{i=0}^{N} \binom{N}{i} \mu^{N-i}\nu^i = (\mu+\nu)^N.$$

In order to derive the sums involving $\mathbf{w}_{1,i}^N$ and $i\mathbf{w}_{1,i}^N$ we use the recursive structure.

$$\begin{aligned}
\sum_{i=0}^{N} w_{1,i}^N &= w_{0,0}^N + \sum_{i=1}^{N-1}(w_{0,i}^{N-1} - w_{0,i-1}^{N-1}) - w_{0,N-1}^{N-1} = \sum_{i=0}^{N-1} w_{0,i}^{N-1} - \sum_{i=1}^{N} w_{0,i-1}^{N-1} \\
&= \sum_{i=0}^{N-1} w_{0,i}^{N-1} - \sum_{i=0}^{N-1} w_{0,i}^{N-1} = 0 \\
\sum_{i=0}^{N} i w_{1,i}^N &= \sum_{1}^{N-1} i(w_{0,i}^{N-1} - w_{0,i-1}^{N-1}) - N(w_{0,N-1}^{N-1}) = \sum_{i=1}^{N-1} i w_{0,i}^{N-1} - \sum_{i=1}^{N-1} i w_{0,i-1}^{N-1} - N w_{0,N-1}^{N-1} \\
&= \sum_{i=0}^{N-1} i w_{0,i}^{N-1} - \sum_{i=0}^{N-2}(i+1) w_{0,i}^{N-1} - \sum_{i=N-1}^{N-1} i w_{0,i}^{N-1} = \sum_{i=0}^{N-1} w_{0,i}^{N-1}(i-(i+1)) \\
&= -\sum_{i=0}^{N-1} w_{0,i}^{N-1} = -(\mu+\nu)^{N-1}
\end{aligned}$$

And last we analyze the sums over $w_{2,i}^N$ and $i w_{2,i}^N$ the same way:

$$\begin{aligned}
\sum_{i=0}^{N} w_{2,i}^N &= w_{1,0}^N + \sum_{i=1}^{N-1}(w_{1,i}^{N-1} - w_{1,i-1}^{N-1}) - w_{1,N-1}^{N-1} = \sum_{i=0}^{N-1} w_{1,i}^{N-1} - \sum_{i=0}^{N-1} w_{1,i}^{N-1} = 0 \\
\sum_{i=0}^{N} i w_{2,i}^N &= 0 + \sum_{1}^{N-1} i(w_{1,i}^{N-1} - w_{1,i-1}^{N-1}) + N(-w_{1,N-1}^{N-1}) \\
&= \sum_{i=0}^{N-1} i w_{1,i}^{N-1} - \sum_{i=0}^{N-1}(i+1) w_{1,i}^{N-1} = -\sum_{i=0}^{N-1} w_{1,i}^{N-1} = 0
\end{aligned}$$

□

B.1.2. Perron Eigenvector

Last we determine the eigenvector according to the zero left eigenvalue and show that this is the Perron eigenvector.

Lemma B.4 (Perron eigenvector)
Let $\mathbf{Y} = (y_0, y_1, ..., y_N)$ *where*

$$y_j := \binom{N}{j} \left(\frac{\mu}{\mu+\nu}\right)^{N-j} \left(\frac{\nu}{\mu+\nu}\right)^{j} \qquad \text{for } j = 0, ..., N$$

and $0 < \mu + \nu$. $\mathbf{Y}$ *is the Perron eigenvector, i.e. the right eigenvector for the eigenvalue zero with non-negative entities and normed to* $\|\mathbf{Y}\|_{l^1} = 1$.

Proof. First we show, that $L_N\mathbf{Y} = 0$. We do this by verifying the equality of each row:

$$\begin{array}{lll} (I) & -N\nu y_0 + \mu y_1 = 0 & \\ (II) & (N-(j-1))\nu y_{j-1} - (j\mu + (N-j)\nu)y_j + (j+1)\mu y_{j+1} = 0 & j = 1, ..., N-1 \\ (III) & \nu y_{N-1} - N\mu y_N = 0 & \end{array}$$

Ad (I): $-N\nu y_0 + \mu y_1 = \frac{1}{(\mu+\nu)^N}\left(-N\nu\mu^N + \mu N\mu^{N-1}\nu^1\right) = 0$

Ad (II): for $j = 1, ..., N-1$

$$\begin{aligned} & (N-(j-1))\nu y_{k-1} - (j\mu + (N-j)\nu)y_k + (j+1)\mu y_{k+1} = \\ = \; & \frac{1}{(\mu+\nu)^N}\left((N-(j-1))\nu\binom{N}{j-1}\mu^{N-(j-1)}\nu^{j-1} - (j\mu+(N-j)\nu)\binom{N}{j}\mu^{N-j}\nu^j\right. \\ & \left. + (j+1)\mu\binom{N}{j+1}\mu^{N-(j+1)}\nu^{j+1}\right) \\ = \; & \frac{1}{(\mu+\nu)^N}\left(\binom{N}{j}\mu^{N-j}\nu^j(j\mu - j\mu - (N-j)\nu + (N-j)\nu)\right) = 0 \end{aligned}$$

Ad (III): $\nu y_{N-1} - N\mu y_N = \frac{1}{(\mu+\nu)^N}\left(\nu N\mu^1\nu^{N-1} - N\mu\nu^N\right) = 0$

Furthermore $\sum_{n=0}^{N} y_n = 1$ so that $\mathbf{Y}$ is the corresponding normalized eigenvector to the zero left eigenvalue. As $0 < \mu + \nu$ and Lemma B.1 we know that $\lambda_0 = 0$ is simple and

$$\lambda_0 > \lambda_1 > \lambda_2 > ... > \lambda_N.$$

Therefore $\sigma(L_N) = 0$. $\mathbf{Y}$ is the so called Perron eigenvector to L_N. □

The Perron eigenvector gives us the distribution of the state behavior of the population at a certain concentration x at the stationary state. This distribution is a Binomial distribution with parameters $\left(N, \frac{\nu}{\mu+\nu}\right)$. Thus we can calculate the expectation value and the variance of the distribution depending on the concentration x as follows:

$$E(n|x) = \frac{N\nu(x)}{\mu(x)+\nu(x)} \tag{B.3}$$

$$\mathrm{Var}(n|x) = \frac{N\mu(x)\nu(x)}{(\mu(x)+\nu(x))^2} \tag{B.4}$$

To derive information about the partial derivative of the Perron eigenvector with respect to x, we have to beware of the x dependency and therefore we will denote the Perron eigenvector in the depending case by $\mathbf{Y}(x)$.

Partial Derivative of the Perron Eigenvector Anticipating our further needs, we calculate the partial derivation of the x depending Perron eigenvalue $\mathbf{Y}(x)$ with respect to x. For $n = 0, ..., N$ we find:

$$\begin{aligned}
\partial_x y_n(x) &= \binom{N}{n} \partial_x \left(\left(\frac{\mu}{\mu+\nu} \right)^{N-n} \left(\frac{\nu}{\mu+\nu} \right)^{n} \right) \\
&= \binom{N}{n} \left(\frac{\mu^{N-n}\nu^n \left((N-n)\nu - n\mu \right) \left(-\mu\partial_x\nu + \nu\partial_x\mu \right)}{(\mu+\nu)^N (\mu+\nu)\,\mu\nu} \right) \\
&= y_n(x) \left(\frac{\nu\partial_x\mu - \mu\partial_x\nu}{(\mu+\nu)\mu\nu} \right) (N\nu - n(\mu+\nu))
\end{aligned}$$

Thus we obtain

$$\partial_x \mathbf{Y}(x) = \mathbf{Y}(x) \left(\nu\partial_x\mu - \mu\partial_x\nu \right) \left(\frac{N}{(\mu+\nu)\mu} - \frac{\mathbf{n}}{\mu\nu} \right) \tag{B.5}$$

where $\mathbf{n} = (0, 1, 2, ..., N)^T$ as defined in Definition 3.5.

B.1.3. Generalized Inverse Operator

For the diffusion approximation of the velocity jump process we need to determine the inverse operator $\mathcal{L}_x^+$ of the transition operator $\mathcal{L}_x$, which is equal to calculating the inverse of the transition matrix L_x.

Definition B.5 We define a generalized inverse L^+ of the matrix L by

$$L^+ \left(\sum_{i=1}^{N} c_i \mathbf{w}_i \right) = \sum_{i=1}^{N} \frac{c_i}{\lambda_i} \mathbf{w}_i.$$

In our case we cannot determine the generalized inverse explicitly. However, the theory only requires the inverse of five distinct vectors,

$$\mathcal{L}_x^+ \left[\mathbf{Y}(x) \right], \; \mathcal{L}_x^+ \left[\left(\mathbf{n} \odot \mathbf{Y}(x) \right) \right], \; \mathcal{L}_x^+ \left[\left(\mathbf{n} \odot \mathbf{n} \odot \mathbf{Y}(x) \right) \right],$$

$$\mathcal{L}_x^+ \left[\partial_x \mathbf{Y}(x) \right] \quad \text{and} \quad \mathcal{L}_x^+ \left[\left(\mathbf{n} \odot \partial_x \mathbf{Y}(x) \right) \right].$$

Recall that $\mathbf{n} = (0, 1, ..., N)^T$ (Definition 3.5). As we see for the first expression, $\mathbf{Y}(x)$ is the normalized Perron eigenvector corresponding to the eigenvalue $\lambda_0 = 0$, so that $\mathcal{L}_x^+ \mathbf{Y}(x) = 0$. Thus we can determine the above expressions without knowing the generalized inverse, if we can express the five vectors given above in terms of the eigenvectors.

We will do this now beginning with the investigation of the vectors $\big(\mathbf{n} \odot \mathbf{Y}(x)\big)$ and $\big(\mathbf{n} \odot \mathbf{n} \odot \mathbf{Y}(x)\big)$.

Remind, $y_n^N(x) \in \mathbb{R}^{N+1}$ denotes the n-th component of the normalized Perron eigenvector $\mathbf{Y}^N(x)$ with $\dim(\mathbf{Y}^N(x)) = N+1$ and $\mathbf{n} := (0, 1, 2, ..., N)^T$ with $\dim(\mathbf{n}) = N+1$.

Investigation of the Vectors $\big(\mathbf{n} \odot (\mathbf{Y}^N)\big)$ and $\big(\mathbf{n} \odot \mathbf{n} \odot (\mathbf{Y}^N)\big)$

In this paragraph we again skip the x-dependency which means we investigate the terms for fixed x and we show that both vectors can be determined in terms of eigenvalues of the matrix L_x which is summarized in the following lemma.

Lemma B.6
The vectors $\big(\mathbf{n} \odot (\mathbf{Y}^N)\big)$ *and* $\big(\mathbf{n} \odot \mathbf{n} \odot (\mathbf{Y}^N)\big)$ *can be written in terms of eigenvectors as*

$$\begin{aligned}
\big(\mathbf{n} \odot (\mathbf{Y}^N)\big) &= \frac{N\nu(\mathbf{w}_0^N - \mu \mathbf{w}_1^N)}{(\mu+\nu)^{N+1}} \\
\big(\mathbf{n} \odot \mathbf{n} \odot (\mathbf{Y}^N)\big) &= \frac{N\nu\left[\mathbf{w}_0^N\,(\mu + N\nu) - \mathbf{w}_1^N\,(\mu(\mu+\nu(2N-1))) + \mathbf{w}_2^N(N-1)\nu\mu^2\right]}{(\mu+\nu)^{N+2}}
\end{aligned}$$

Like before $\mathbf{w}_k^N$ denotes the eigenvector corresponding to the eigenvalue $\lambda_k = -k(\mu+\nu)$ of the matrix $L_N \in \mathbb{R}^{N+1 \times N+1}$.

Before we show Lemma B.6 we proof some propositions where we investigate the terms separately.

Proposition B.7
The vector $\big(\mathbf{n} \odot (\mathbf{Y}^N)\big)$ *can be written as:*

$$\big(\mathbf{n} \odot (\mathbf{Y}^N)\big) = \frac{N\nu}{\mu+\nu} \begin{pmatrix} 0 \\ \mathbf{Y}^{N-1} \end{pmatrix}$$

Proof. For $n = 1, ..., N$:

$$n\, y_n^N = n\binom{N}{n}\frac{\mu^{N-n}\nu^n}{(\mu+\nu)^N} = \frac{N\nu}{(\mu+\nu)}\binom{N-1}{n-1}\frac{\mu^{N-n}\nu^{n-1}}{(\mu+\nu)^{N-1}} = \frac{N\nu}{(\mu+\nu)} y_{n-1}^{N-1}$$

As a special case we see that for $n = 0$ we get $0\; y_0^N = 0$. □

Proposition B.8

$$\begin{pmatrix} 0 \\ \mathbf{Y}^{N-1} \end{pmatrix} = \frac{1}{(\mu+\nu)^N}\left(\mathbf{w}_0^N - \mu \mathbf{w}_1^N\right)$$

Proof. From Lemma B.2 we know that $\mathbf{w}_1^N$ can be represented as

$$\mathbf{w}_1^N = \begin{pmatrix} w_{0,0}^{N-1} \\ w_{0,1}^{N-1} - w_{0,0}^{N-1} \\ w_{0,2}^{N-1} - w_{0,1}^{N-1} \\ \vdots \\ w_{0,N-1}^{N-1} - w_{0,N-2}^{N-1} \\ -w_{0,N-1}^{N-1} \end{pmatrix}$$

We show the desired results row by row, beginning with the first row where $n = 0$

$$\begin{aligned} \frac{1}{(\mu+\nu)^N}\left(w_{0,0}^N - \mu w_{1,0}^N\right) &= \frac{1}{(\mu+\nu)^N}\left(\binom{N}{0}\mu^N - \mu\binom{N-1}{0}\mu^{N-1}\right) \\ &= \frac{1}{(\mu+\nu)^N}(\mu^N - \mu^N) = 0 \end{aligned}$$

Before we go on we recall some identities:

$$\binom{N-1}{n} = \frac{N-n}{n}\binom{N-1}{n-1} \qquad \binom{N}{n} = \frac{N}{n}\binom{N-1}{n-1}$$

So for the rows $n = 1, ..., N-1$ we obtain:

$$\begin{aligned} &\frac{1}{(\mu+\nu)^N}\left(w_{0,n}^N - \mu w_{1,n}^N\right) = \frac{1}{(\mu+\nu)^N}\left(w_{0,n}^N - \mu(w_{0,n}^{N-1} - w_{0,n-1}^{N-1})\right) \\ = &\frac{1}{(\mu+\nu)^N}\left(\binom{N}{n}\mu^{N-n}\nu^n - \mu\left(\binom{N-1}{n}\mu^{N-n-1}\nu^n - \binom{N-1}{n-1}\mu^{N-n}\nu^{n-1}\right)\right) \\ = &\frac{(\mu+\nu)}{(\mu+\nu)^N}\binom{N-1}{n-1}\mu^{N-n}\nu^{n-1} = y_{n-1}^{N-1} \end{aligned}$$

And for the last row ($n = N$) we find:

$$\begin{aligned} \frac{1}{(\mu+\nu)^N}\left(w_{0,N}^N - \mu w_{1,N}^N\right) &= \frac{1}{(\mu+\nu)^N}\left(\binom{N}{N}\nu^N + \mu\binom{N-1}{N-1}\nu^{N-1}\right) \\ &= \frac{\nu^{N-1}}{(\mu+\nu)^N}(\nu+\mu) = \nu^{N-1} = y_{n-1}^{N-1} \end{aligned}$$

□

Proof. (Lemma B.6, first statement) Combining Proposition B.7 and B.8 we have proofed the first statement of Lemma B.6 as

$$\left(\mathbf{n} \odot (\mathbf{Y}^N)\right) = \frac{N\nu}{\mu+\nu}\begin{pmatrix} 0 \\ \mathbf{Y}^{N-1} \end{pmatrix} = \frac{N\nu}{(\mu+\nu)^{N+1}}(\mathbf{w}_0^N - \mu\mathbf{w}_1^N).$$

□

We follow the same arguments and rewrite the vector $\left(\mathbf{n} \odot \mathbf{n} \odot (\mathbf{Y}^N)\right)$ in terms of eigenvectors. Due to Proposition B.7 we find:

$$\left(\mathbf{n} \odot \mathbf{n} \odot (\mathbf{Y}^N)\right) = \frac{N\nu}{(\mu+\nu)} \left(\mathbf{n} \odot \begin{pmatrix} 0 \\ \mathbf{Y}^{N-1} \end{pmatrix}\right)$$

The vector on the right hand side can be rewrite as

$$\left(\mathbf{n} \odot \begin{pmatrix} 0 \\ \mathbf{Y}^{N-1} \end{pmatrix}\right) = \left((\mathbf{n}-1) \odot \begin{pmatrix} 0 \\ \mathbf{Y}^{N-1} \end{pmatrix}\right) + \begin{pmatrix} 0 \\ \mathbf{Y}^{N-1} \end{pmatrix}.$$

We know the second vector, as $\mathbf{Y}^{N-1} = \frac{1}{(\mu+\nu)^{N-1}}\mathbf{w}_0^{N-1}$ and thus the only thing that remains to investigate is the first vector.

Proposition B.9

$$\left((\mathbf{n}-1) \odot \begin{pmatrix} 0 \\ \mathbf{Y}^{N-1} \end{pmatrix}\right) = (N-1)\frac{\nu}{\mu+\nu} \begin{pmatrix} 0 \\ 0 \\ \mathbf{Y}^{N-2} \end{pmatrix}$$

Proof. In the first and second row we find $0 = 0$. For the remaining rows, $n = 2, ..., N$, we obtain:

$$\begin{aligned} (n-1)y_{n-1}^{N-1} &= \frac{(n-1)}{(\mu+\nu)^{N-1}}\binom{N-1}{n-1}\mu^{N-n}\nu^{n-1} \\ &= \frac{(N-1)}{(\mu+\nu)^{N-1}}\binom{N-2}{n-2}\mu^{N-n}\nu^{n-2}\nu = \frac{(N-1)\nu}{\mu+\nu}y_{n-2}^{N-2} \end{aligned}$$ □

Proposition B.10

$$\begin{pmatrix} 0 \\ 0 \\ \mathbf{Y}^{N-2} \end{pmatrix} = \frac{1}{(\mu+\nu)^N}(\mathbf{w}_0^N - 2\mu\mathbf{w}_1^N + \mu^2\mathbf{w}_2^N)$$

Proof. We show this componentwise, starting with $n = 0$:

$$\begin{aligned} \frac{1}{(\mu+\nu)^N}(w_{0,0}^N - 2\mu w_{1,0}^N + \mu^2 w_{2,0}^N) &= \frac{1}{(\mu+\nu)^N}(w_{0,0}^N - 2\mu w_{0,0}^{N-1} + \mu^2 w_{0,0}^{N-2}) \\ &= \frac{1}{(\mu+\nu)^N}(\mu^N - 2\mu^N + \mu^N) = 0 \end{aligned}$$

In the case $n = 1$:

$$\begin{aligned} &\frac{1}{(\mu+\nu)^N}(w_{0,1}^N - 2\mu w_{1,1}^N + \mu^2 w_{2,1}^N) \\ &= \frac{1}{(\mu+\nu)^N}(w_{0,1}^N - 2\mu(w_{0,1}^{N-1} - w_{0,0}^{N-1}) + \mu^2(w_{0,1}^{N-2} - 2w_{0,0}^{N-2})) \\ &= \frac{1}{(\mu+\nu)^N}(N\mu^{N-1}\nu - 2\mu((N-1)\mu^{N-2}\nu - \mu^{N-1}) + \mu^2((N-2)\mu^{N-3}\nu - \mu^{N-2})) \\ &= \frac{1}{(\mu+\nu)^N}\left(N\mu^{N-1}\nu - 2(N-1)\mu^{N-1}\nu + 2\mu^N + (N-2)\mu^{N-1} - 2\mu^N\right) = 0 \end{aligned}$$

For $n = 2, ..., N-1$ we obtain:

$$\begin{aligned}
& \frac{1}{(\mu+\nu)^N}(w_{0,n}^N - 2\mu w_{1,n}^N + \mu^2 w_{2,n}^N) \\
= \; & \frac{1}{(\mu+\nu)^N}(w_{0,n}^N - 2\mu(w_{0,n}^{N-1} - w_{0,n-1}^{N-1}) + \mu^2(w_{0,n}^{N-2} - 2w_{0,n-1}^{N-2} + w_{0,n-2}^{N-2})) \\
= \; & \frac{1}{(\mu+\nu)^N}\left[\binom{N}{n}\mu^{N-n}\nu^n - 2\mu\left(\binom{N-1}{n}\mu^{N-n-1}\nu^n - \binom{N-1}{n-1}\mu^{N-n}\nu^{n-1}\right)\right. \\
& \left. +\mu^2\left(\binom{N-2}{n}\mu^{N-n-2}\nu^n - 2\binom{N-2}{n-1}\mu^{N-n-1}\nu^{n-1} + \binom{N-2}{n-2}\mu^{N-n}\nu^{n-2}\right)\right] \\
= \; & \frac{1}{(\mu+\nu)^2} y_{n-2}^{N-2}\left(\frac{1}{n(n-1)}\left(N(N-1)\nu^2 - 2(N-1)(N-n)\nu^2\right.\right. \\
& \left.\left. + 2n(N-1)\nu\mu + (N-n)(N-n-1)\nu^2 - 2n(N-n)\mu\nu + n(n-1)\mu^2\right)\right) \\
= \; & y_{n-2}^{N-2}\frac{1}{(\mu+\nu)^2 n(n-1)}(\nu^2 n(n-1) + \mu\nu 2n(n-1) + \mu^2 n(n-1)) \\
= \; & y_{n-2}^{N-2}\frac{1}{(\mu+\nu)^2}(\nu^2 + 2\mu\nu + \mu^2) = y_{n-2}^{N-2}\frac{(\mu+\nu)^2}{(\mu+\nu)^2} = y_{n-2}^{N-2}.
\end{aligned}$$

And for $n = N$ we find:

$$\begin{aligned}
& \frac{1}{(\mu+\nu)^N}(v_{0,N}^N - 2\mu v_{1,N}^N + \mu^2 v_{2,N}^N) \\
= \; & \frac{1}{(\mu+\nu)^N}\left(\nu^N + 2\mu\nu^{N-1} + \mu^2\nu^{N-2}\right) = \frac{1}{(\mu+\nu)^N}\nu^{N-2}(\nu+\mu)^2 = y_{n-2}^{N-2}
\end{aligned}$$ □

Proof. (Lemma B.6, second statement) Combining Proposition B.9 and B.10 results in:

$$\begin{aligned}
& \left(\mathbf{n} \odot \mathbf{n} \odot (\mathbf{Y}^N)\right) = \frac{N\nu}{(\mu+\nu)}\left(\mathbf{n} \odot \begin{pmatrix} 0 \\ \mathbf{Y}^{N-1} \end{pmatrix}\right) \\
= \; & \frac{N\nu}{(\mu+\nu)}\left[\begin{pmatrix} 0 \\ \mathbf{Y}^{N-1} \end{pmatrix} + \frac{(N-1)\nu}{\mu+\nu}\begin{pmatrix} 0 \\ 0 \\ \mathbf{Y}^{N-2} \end{pmatrix}\right] \\
= \; & \frac{N\nu}{(\mu+\nu)^{N+1}}\left[(\mathbf{w}_0^N - \mu\mathbf{w}_1^N) + \frac{(N-1)\nu}{(\mu+\nu)}(\mathbf{w}_0^N - 2\mu\mathbf{w}_1^N + \mu^2\mathbf{w}_2^N)\right] \\
= \; & \frac{N\nu}{(\mu+\nu)^{N+2}}\left[\mathbf{w}_0^N(\mu + N\nu) - \mathbf{w}_1^N(\mu(\mu + \nu(2N-1))) + \mathbf{w}_2^N(N-1)\nu\mu^2\right]
\end{aligned}$$ □

Hence we have shown that we can rewrite the vectors $\left(\mathbf{n} \odot (\mathbf{Y}^N)\right)$ and $\left(\mathbf{n} \odot \mathbf{n} \odot (\mathbf{Y}^N)\right)$ in terms of the eigenvectors $\mathbf{w}_0^N, \mathbf{w}_1^N, \mathbf{w}_2^N$ of the transition matrix L_N.

B.1.4. Calculation of the Generalized Inverse

The aim of this section is to present two lemmas concerning the generalized inverse applied to the Perron eigenvector, respectively $\big(\mathbf{n}\odot\mathbf{Y}(x)\big)$ and $\big(\mathbf{n}\odot\mathbf{n}\odot\mathbf{Y}(x)\big)$ and in a second lemma we will calculate the generalized inverse applied to the partial derivative of the Perron eigenvector. Here $\dim\mathbf{Y}(x)=N+1$ and $\dim(\mathbf{w}_k)=N+1,\forall\, k\{0,1,...,N\}$.

Lets start with the first prediction of this section.

Lemma B.11
The generalized inverse (Definition B.5) applied to $\mathbf{Y}$, $\big(\mathbf{n}\odot\mathbf{Y}(x)\big)$ *and* $\big(\mathbf{n}\odot\mathbf{n}\odot\mathbf{Y}(x)\big)$ *yields:*

$$\begin{aligned}
\mathcal{L}_x^+\left[(\mathbf{Y})\right] &= 0\\
\mathcal{L}_x^+\left[\big(\mathbf{n}\odot\mathbf{Y}(x)\big)\right] &= \frac{N\nu\mu}{(\mu+\nu)^{N+2}}\mathbf{w}_1\\
\mathcal{L}_x^+\left[\big(\mathbf{n}\odot\mathbf{n}\odot\mathbf{Y}(x)\big)\right] &= \frac{N\nu\mu}{(\mu+\nu)^{N+3}}\left((\mu+\nu(2N-1))\mathbf{w}_1-\frac{1}{2}(N-1)\nu\mu\mathbf{w}_2\right)
\end{aligned}$$

Proof. $\mathbf{Y}(x)$ is the normalized eigenvector to the eigenvalue 0. Therefore

$$\mathcal{L}_x^+\left[\mathbf{Y}(x)\right]=0.$$

Let us investigate $\mathcal{L}_x^+\left[\big(\mathbf{n}\odot\mathbf{Y}(x)\big)\right]$. From the first statement in Lemma B.6 we know $\big(\mathbf{n}\odot\mathbf{Y}(x)\big)=\frac{N\nu}{(\mu+\nu)^{N+1}}(\mathbf{w}_0-\mu\mathbf{w}_1)$. As the generalized inverse is a linear operator we find:

$$\mathcal{L}_x^+\left[\big(\mathbf{n}\odot\mathbf{Y}(x)\big)\right]=\frac{N\nu}{(\mu+\nu)^{N+1}}\left(\mathcal{L}_x^+[\mathbf{w}_0]-\mu\mathcal{L}_x^+[\mathbf{w}_1]\right)$$

Further we know that $\mathcal{L}_x^+[\mathbf{w}_0]=0$ and $\mathcal{L}_x^+[\mathbf{w}_1]=-\frac{1}{(\mu+\nu)}\mathbf{w}_1$ so finally we end up with

$$\mathcal{L}_x^+\left[\big(\mathbf{n}\odot\mathbf{Y}(x)\big)\right]=\frac{N\nu\mu}{(\mu+\nu)^{N+2}}\mathbf{w}_1.$$

Then we do the same proceeding for $\mathcal{L}_x^+\left[\big(\mathbf{n}\odot\mathbf{Y}(x)\big)\right]$ where we use the second statement of Lemma B.6 and obtain:

$$\begin{aligned}
\mathcal{L}_x^+\left[\big(\mathbf{n}\odot\mathbf{n}\odot\mathbf{Y}(x)\big)\right]=\frac{N\nu}{(\mu+\nu)^{N+2}}\mathcal{L}_x^+\big[&\mathbf{w}_0\left(\mu+N\nu\right)\\
&-\mathbf{w}_1\left(\mu(\mu+\nu(2N-1))\right)+\mathbf{w}_2(N-1)\nu\mu^2\big]
\end{aligned}$$

where $\mathcal{L}_x^+[\mathbf{w}_2]=-\frac{1}{2(\mu+\nu)}\mathbf{w}_2$. Hence

$$\begin{aligned}
\mathcal{L}_x^+[\big(\mathbf{n}\odot\mathbf{n}\odot(\mathbf{Y}^N)\big)] &= \frac{N\nu}{(\mu+\nu)^{N+2}}\big(\mathcal{L}_x^+[\mathbf{w}_0]\left(\mu+N\nu\right)\\
&\quad -\mathcal{L}_x^+[\mathbf{w}_1]\left(\mu(\mu+\nu(2N-1))\right)+\mathcal{L}_x^+[\mathbf{w}_2](N-1)\nu\mu^2\big)\\
&= \frac{N\nu\mu}{(\mu+\nu)^{N+3}}\left((\mu+\nu(2N-1))\mathbf{w}_1-\frac{1}{2}(N-1)\nu\mu\mathbf{w}_2\right) \qquad \square
\end{aligned}$$

Further we calculate the generalized inverse applied to the vectors containing the partial derivative of the Perron eigenvector with respect to x.

Lemma B.12
The generalized inverse terms $\mathcal{L}_x^+ [\partial_x \mathbf{Y}(x)]$ *and* $\mathcal{L}_x^+ \left[\left(\mathbf{n} \odot \partial_x \mathbf{Y}(x)\right)\right]$ *can be written as:*

$$\begin{aligned} \mathcal{L}_x^+[\partial_x(\mathbf{Y}(x))] &= -b_1(x)\mathbf{w}_1 \\ \mathcal{L}_x^+[\left(\mathbf{n} \odot \partial_x \mathbf{Y}(x)\right)] &= b_2(x)\mathbf{w}_1^N + b_3(x)\mathbf{w}_2 \end{aligned}$$

with

$$\begin{aligned} b_1(x) &:= \frac{N(\nu(x)\partial_x\mu(x) - \mu(x)\partial_x\nu(x))}{(\mu+\nu)^{N+2}}, \\ b_2(x) &= \frac{N(\nu(x)\partial_x\mu(x) - \mu(x)\partial_x\nu(x))}{(\mu+\nu)^{N+3}} \left(N\nu - (\mu(x) + \nu(x)(2N-1))\right), \\ b_3(x) &:= \frac{N(N-1)\nu(x)\mu(x)(\nu(x)\partial_x\mu(x) - \mu(x)\partial_x\nu(x))}{2(\mu+\nu)^{N+3}}. \end{aligned}$$

Proof. As already shown in equation (B.5) the partial derivation of the Perron eigenvector with respect to x can be written as

$$\partial_x \mathbf{Y}(x) = a_1(x)\mathbf{Y}(x) - a_2(x)\left(\mathbf{n} \odot \mathbf{Y}(x)\right)$$

where $a_1(x)$ and $a_2(x)$ are scalar functions defined by

$$\begin{aligned} a_1(x) &:= \frac{N(\nu(x)\partial_x\mu(x) - \mu(x)\partial_x\nu(x))}{(\mu(x)+\nu(x))\mu(x)}, \\ a_2(x) &:= \frac{\nu(x)\partial_x\mu(x) - \mu(x)\partial_x\nu(x)}{\mu(x)\nu(x)}. \end{aligned}$$

So if we investigate the first expression, reminding that $\mathcal{L}_x^+ [\mathbf{Y}(x)] = 0$, and with the first statement of Lemma B.6, we obtain

$$\begin{aligned} \mathcal{L}_x^+[\partial_x \mathbf{Y}(x)] &= a_1(x)\mathcal{L}_x^+ [\mathbf{Y}(x)] - a_2(x)\mathcal{L}_x^+ \left[\left(\mathbf{n} \odot \mathbf{Y}(x)\right)\right] \\ &= -\frac{N(\nu(x)\partial_x\mu(x) - \mu(x)\partial_x\nu(x))}{(\mu+\nu)^{N+2}}\mathbf{w}_1 = -b_1(x)\mathbf{w}_1 \end{aligned}$$

And the same can be done for the second expression:

$$\begin{aligned} & \mathcal{L}_x^+ \left[\left(\mathbf{n} \odot \partial_x \mathbf{Y}(x)\right)\right] = \\ = \; & a_1(x)\mathcal{L}_x^+ \left[\left(\mathbf{n} \odot \mathbf{Y}(x)\right)\right] - a_2(x)\mathcal{L}_x^+ \left[\left(\mathbf{n} \odot \mathbf{n} \odot \mathbf{Y}(x)\right)\right] \\ = \; & a_1(x)\frac{N\nu\mu}{(\mu+\nu)^{N+2}}\mathbf{w}_1 - a_2(x)\frac{N\nu\mu}{(\mu+\nu)^{N+3}}\left((\mu+\nu(2N-1))\mathbf{w}_1 - \frac{1}{2}(N-1)\nu\mu\mathbf{w}_2\right) \\ = \; & \frac{N(\nu(x)\partial_x\mu(x) - \mu(x)\partial_x\nu(x))}{(\mu+\nu)^{N+3}}\left(N\nu - (\mu+\nu(2N-1))\right)\mathbf{w}_1 \\ & + \frac{N(N-1)\nu\mu(\nu(x)\partial_x\mu(x) - \mu(x)\partial_x\nu(x))}{2(\mu+\nu)^{N+3}}\mathbf{w}_2 = b_2(x)\mathbf{w}_1 + b_3(x)\mathbf{w}_2 \end{aligned}$$

□

B.2. Parameter and Simulation

The simulations throughout Chapter 3 are performed in Matlab [30]. Notice that we use the original transport equation where $\beta_1 = \beta_2 = \beta$. The parameters are chosen corresponding to the Quorum Sensing system in *Pseudomonas putida* [11]. The parameter values are described in the following table.

Name	Parameter value	Unit	Description
α	2.3e-19	mol/(cell h)	constitutive production rate
β	2.3e-18	mol/(cell h)	increased production rate
γ	0.005545	1/h	degradation rate of AHL molecules
z_t	70	nmol/l	AHL molecule threshold

From Subsection (3.1.1) we know that the transition probabilities $\mu(z)$ and $\nu(z)$ are monotone decreasing, respectively increasing, strictly positive functions. For the numerical simulations we assume the transition probabilities to be Hill functions, i.e.

$$\nu(z) = \frac{z^s}{z_t^s + z^s}, \qquad \mu(z) = 1 - \frac{z^s}{z_t^s + z^s},$$

with Hill coefficient $s = 3$ in accordance to [11].

For the simulation of the stochastic process in Figure 3.4 we assumed

$$\dot{z}(t) = \alpha N + \beta n(t) - \gamma z,$$

where $n(t)$ is governed by a Poisson process and the waiting time between jumps is exponentially distributed. The initial values are given by $t_0 = 0$, $x_0 = \frac{1}{2}(z_{max} - z_{min})$ and $n(0) = \lfloor \frac{N}{2} \rfloor$ where $N = \rho V$.

For the graphical presentation of all simulations we rescaled the AHL concentration $z \in \Omega_V$ to $\tilde{z} \in [0, 1]$.

In Figure 3.7 we simulated the marginal distribution of the AHL concentration, determined by the partial differential equation (3.50), i.e.

$$\begin{aligned} \partial_t h(z,t) &= -\partial_x(g(z,\rho)h(z,t)) + \partial_x(a(z)\partial_x h(z,t)) && z \in \Omega_V \\ 0 &= g(z,\rho)h(z,t) - a(z)\partial_x h(z,t) && z \in \partial\Omega_V \\ h(z,0) &= h_0(z). \end{aligned}$$

Since we additionally change the cell density over time we apply

$$\dot{\rho}(t) = \rho_2, \qquad \rho(t) = \rho_1 + \rho_2 t.$$

As the boundary conditions are time dependent, Galerkin like methods are not suited. Therefore we apply the method of lines (MOL) [27, Chapter 6.2]. MOL is a general procedure for the solution of time dependent partial differential equations. The basic idea

is to replace the spatial, boundary value, derivatives in the partial differential equation with algebraic approximations and return a system of ordinary differential equations that approximate the original partial differential equation.

Therefore we sample the function $h(x,t)$ at grid points

$$x_i = x_{min} + i\zeta, \qquad \zeta = \frac{x_{max} - x_{min}}{M}, \qquad i = 0, ..., M \in \mathbb{N}$$

where M are the number of sample points minus one. Let $w_i(t)$ denote the approximation of $h(x_i, t)$. Using finite differences we obtain the ordinary differential equations, for $i = 1, ..., M-1$,

$$\dot{w}_i(t) = -\frac{g_{i+1}w_{i+1} - g_{i-1}w_{i-1}}{2\zeta} + \frac{a_{i+1}(w_{i+1} - w_i) - a_i(w_i - w_{i-1})}{\zeta^2} \tag{B.6}$$

with

$$g_i := g(x_i) \qquad \text{and} \qquad a_i := a(x_i).$$

The boundary points w_0 and w_N require a more subtile handling. Usual method is to extend the number of points to virtual points w_{-1} and w_{N+1} located at $x = x_{min} - \zeta$ and $x = x_{max} + \zeta$. The boundary conditions are used to determine the value of the solution at these additional points as

$$0 = g_0 w_0 - a_0 \frac{w_1 - w_{-1}}{2h} \qquad \Rightarrow w_{-1} = -\frac{2hg_0w_0}{a_0} + w_1$$

and

$$0 = g_N w_N - a_N \frac{w_{N+1} - w_{N-1}}{2h} \qquad \Rightarrow w_{N+1} = w_{N-1} + \frac{2hg_Nw_N}{a_N}.$$

With this trick, the boundary points become inner points and can be handled like the other inner points. The ordinary differential equations (B.6) are now solved by an implicit Euler scheme combined with Newton iteration to solve for the iterative. This scheme is suited to deal with the stiffness of the problem. Note that the equations are linear and thus the equations for the iterative is a linear equation. The Newton method collapses to a solver for a linear method and is implemented by the Gauss algorithm.

Bibliography

[1] K. Anguige, J.R. King, and J.P. Ward. Modelling antibiotic- and anti-quorum sensing treatment of a spatially-structured *Pseudomonas aeruginosa* population. *Journal of Mathematical Biology*, 51(5):557–594, 2005.

[2] K. Anguige, J.R. King, J.P. Ward, and P. Williams. Mathematical modelling of therapies targeted at bacterial quorum sensing. *Mathematical Biosciences*, 192:3983, 2004.

[3] O. Arino and R. Rudnicki. Phytoplankton dynamics. *Comptes Rendus Biologies*, 327:961–969, 2004.

[4] N. Balaban. *Control of Biofilm Infections by Signal Manipulation*. Springer, 2008.

[5] J. M. Ball. Strongly continuous semigroups, weak solutions, and the variation of constants formula. *Proceedings of the Americal Mathematical Society*, 63:370–373, 1977.

[6] B. L. Bassler and R. Losick. Bacterially speaking. *Cell*, 125(2):237–246, 2006.

[7] D. L. Chopp, M. J. Kirisits, B. Moran, and M. R. Parsek. A mathematical model of quorum sensing in a growing bacterial biofilm. *Journal of Industrial Microbiology and Biotechnology*, 29(6):339–346, 2002.

[8] D. R. Demuth and R. J. Lamont. *Bacterial cell-to-cell communication*. Cambridge University Press, Cambridge, 2006.

[9] S. P. Diggle, S. A. Crusz, and M. Cámara. Quorum sensing. *Current Biology*, 17(21):907–910, 2007.

[10] J. D. Dockery and J. P. Keener. A mathematical model for quorum sensing in *Pseudomonas aeruginosa*. *Bulletin of Mathematical Biology*, 63:95–116, 2001.

[11] A. Fekete, C. Kuttler, M. Rothballer, D. Fischer, K. Buddrus-Schiemann, B. A. Hense, M. Lucio, J. Müller, P. Schmitt-Kopplin, and A. Hartmann. Dynamic regulation of N-acyl-homoserine lactone production and degradation in *Pseudomonas putida* IsoF. *submitted*.

[12] J. A. Freeman and B. L. Bassler. Sequence and function of LuxU: A two-component phosphorelay protein that regulates quorum sensing in *Vibrio harveyi*. *Journal of Bacteriology*, 181:899–906, 1999.

[13] W. C. Fuqua, S. C. Winans, and E. P. Greenberg. Quorum sensing in bacteria: The LuxR-LuxI family of cell density-responsive transcriptional regulatores. *Journal of Bacteriology*, 176:269–275, 1994.

[14] C. W. Gardiner. *Handbook of Stochastic Methods*. Springer-Verlag, 1983.

[15] A. B. Goryachev, D.-J. Toh, K. B. Wee, T. Lee, H.-B. Zhang, and L.-H. Zhang. Transition to quorum sensing in an *agrobacterium* population: A stochastic model. *PLoS Comput Biol*, 1(4):e37, 09 2005.

[16] E. Gustafsson, P. Nilsson, S. Karlsson, and S. Arvidson. Characterizing the dynamics of the quorum-sensing system in *Staphylococcus aureus*. *Journal of Molecular Microbiology and Biotechnology*, 8:232242, 2004.

[17] J. M. Henke and B. L. Bassler. Quorum sensing regulates type III secretion in *Vibrio harveyi* and *Vibrio parahaemolyticus*. *Journal of Bacteriology*, 186:3794–3805, 2004.

[18] J. M. Henke and B. L. Bassler. Three parallel quorum-sensing systems regulate gene expression in *Vibrio harveyi*. *Journal of Bacteriology*, 186:6902–6914, 2004.

[19] B. A. Hense, C. Kuttler, J. Müller, M. Rothballer, A. Hartmann, and J. Kreft. Does efficiency sensing unify diffusion and quorum sensing? *Nature Reviews Microbiology*, 5:230–239, 2007.

[20] T. Hillen and H. G. Othmer. The diffusion limit of transport equations derived from velocity-jump processes. *SIAM Journal on Applied Mathematics*, 61:751–775, 2001.

[21] J. E. M. Hornos, D. Schultz, G. C. P. Innocentini, J. Wang, A. M. Walczak, J. N. Onuchic, and P. G. Wolynes. Self-regulating gene: An exact solution. *Physical Review E*, 72(5):051907, Nov 2005.

[22] P. Jagers. *Branching Processes with Biological Applications (Probability & Mathematical Statistics)*. John Wiley and Sons Ltd, January 1975.

[23] S. James, P. Nilsson, G. J., S. Kjelleberg, and T. Fagerstrm. Luminescence control in the marine bacterium *Vibrio fischeri*: An analysis of the dynamics of lux regulation. *Journal of Molecular Biology*, 296(4):1127 – 1137, 2000.

[24] T. Kato. *Perturbation theory for linear operators*. Springer Verlag Berlin Heidelberg, 1995.

[25] T. B. Kepler and T. C. Elston. Stochasticity in transcriptional regulation: Origins, consequences, and mathematical representations. *Biophysical Journal*, 81(6):3116–3136, 2001.

[26] M. Kirkilionis and L. Sbano. An averaging principle for combined interaction graphs. Part I: Connectivity and applications to genetic switches. *WMI Preprint 5/2008. Advances in Complex Systems (submitted)*, 2008.

[27] P. Knabner and L.Angermann. *Numerik partieller Differentialgleichungen*. Springer, 2000.

[28] A.J. Koerber, J.R. King, and P. Williams. Deterministic and stochastic modelling of endosome escape by *Staphylococcus aureus*: quorum sensing by a single bacterium. *Journal of Mathematical Biology*, 50:440–488, 2005.

[29] O. A. Ladyženskaja, V. A. Solonnikov, and N. N. Ural'ceva. *Linear and Quasi-linear Equations of Parabolic Type*. American Mathematical Society, 1968.

[30] Matlab^{TM}. The Mathworks Inc., Natick, MA.

[31] M. B. Miller and B. L. Bassler. Quorum sensing in bacteria. *Annual Review of Microbiology*, 55(1):165–199, 2001.

[32] M. B. Miller, K. Skorupski, D. H. Lenz, R. K. Taylor, and B. L. Bassler. Parallel quorum sensing systems converge to regulate virulence in *Vibrio cholerae*. *Cell*, 110:303–314, 2002.

[33] K. C. Mok, N. S. Wingreen, and B. L. Bassler. *Vibrio harveyi* quorum sensing: A coincidence detector for two autoinducers controls gene expression. *Embo Journal*, 22:870–881, 203.

[34] J. Müller, C. Kuttler, B. A. Hense, M. Rothballer, and A. Hartmann. Cell-cell communication by quorum sensing and dimension-reduction. *Journal of Mathematical Biology*, 53:672–702, 2006.

[35] J. Müller, C. Kuttler, B. A. Hense, S. Zeiser, and V. Liebscher. Transcription, intercellular variability and correlated random walk. *Mathematical Biosciences*, 216:30–39, 2008.

[36] J. D. Murray. *Mathematical Biology I.* Springer, 2002.

[37] K. H. Nealson. Autoinduction of bacterial luciferase. *Archives of Microbiology*, 112:73–79, 1977.

[38] K. H. Nealson, T. Platt, and J. W. Hastings. Cellular control of the synthesis and activity of the bacterial luminescent system. *Journal of Bacteriology*, 104:313322, 1970.

[39] H. G. Othmer, S. R. Dunbar, and W. Alt. Models of dispersal in biological systems. *Journal of Mathematical Biology*, 26:263–298, 1988.

[40] H. G. Othmer and T. Hillen. The diffusion limit of transport equations II: Chemotaxis equations. *Siam Journal of Applied Mathematics*, 62:1222–1250, 2002.

[41] A. Pazy. *Semigroups of linear operators and applications to partial differential equations*. Springer Verlag New York, 1983.

[42] R. J. Redfield. Is quorum sensing a side effect of diffusion sensing? *Trends in Microbiology*, 10:365–370, 2002.

[43] L. Sbano and M. Kirkilionis. Multiscale analysis of reaction networks. *Theory in Biosciences*, 127:107–123, 2008.

[44] M. Slodička and R. Van Keer. Determination of a robin coefficient in semilinear parabolic problems by means of boundary measurements. *Inverse Problems*, 18:139152, 2002.

[45] N. Stambrau. *Der LuxP/AI-2 und LuxQ-abhängige Signaltransduktionsweg des*

Quorum Sensing Systems von Vibrio harveyi. PhD thesis, Department Biologie I, Bereich Mikrobiologie, LMU München, 2008.

[46] M. Timmen, B. L. Bassler, and K. Jung. AI-1 influences the kinase activity but not the phophatase activity of LuxN in *Vibrio harveyi*. *Journal of Biological Chemistry*, 281:24398–24404, 2006.

[47] K. C. Tu, C. M. Waters, S. L. Svenningsen, and B. L. Bassler. A small-RNA-mediated negative feedback loop controls quorum sensing dynamics in *Vibrio harveyi*. *Molecular Microbiology*, 70:896–907, 2008.

[48] J. Tyson and H. Othmer. The dynamics of feedback control circuits in biochemical pathways. *Progress in Theoretical Biology*, 5:1–62, 1978.

[49] D. L. Ulrich, D. Kojetin, B. L. Bassler, J. Cavanagh, and J. P. Loria. Solution structure and dynamics of LuxU from *Vibrio harveyi*, a phosphotransferase protein involved in bacterial quorum sensing. *Journal of Molecular Biology*, 347:205, 2005.

[50] A. M. Walczak, M. Sasai, and P. G. Wolynes. Self-consistent proteomic field theory of stochastic gene switches. *Biophysical Journal*, 88(2):828 – 850, 2005.

[51] J. P. Ward, J.R. King, A. J. Koerber, P. Williams, J. M. Croft, and R. E. Sockett. Mathematical modelling of quorum sensing in bacteria. *Mathematical Medicine and Biology*, 18(3):263–292, 2001.

[52] C. M. Waters and B. L. Bassler. The *Vibrio harveyi* quorum-sensing system uses shared regulatory components to discriminate between multiple autoinducers. *Genes & Development*, 20:2754–2767, 2006.

[53] P. Williams, K. Winzer, W. C. Chan, and M. Camara. Look who's talking: Communication and quorum sensing in the bacterial world. *Philosophical Transactions of the Royal Society*, B 362:1119–1134, 2007.

[54] E. Zauder. *Partial Differential Equations of Applied Mathematics*. John Wiley & Sons, 1989.